INAUGURAL-DISSERTATION
zur
Erlangung der Doktorwürde
der
Naturwissenschaftlich-Mathematischen
Gesamtfakultät
der
Ruprecht-Karls-Universität
Heidelberg

vorgelegt von

Dipl.-Phys. Philipp Geiger

aus Darmstadt

Tag der mündlichen Prüfung: 9. Februar 1998

Measurement of Fragmentation Functions at HERMES

Gutachter: Priv.-Doz. Dr. Antje Brüll
Prof. Dr. Otto Nachtmann

Messung der Fragmentationsfunktionen bei Hermes

Thema der vorliegenden Arbeit ist die Hadronisierung von leichten Quarks in geladene Pionen. Die hier analysierten Pionspektren wurden am Hermes Experiment, das sich am Positron-Proton Speicherring HERA am DESY befindet, aufgenommen. Während der Datennahme 1996 wurden Positronen mit einer Energie von 27.5 GeV an internen Wasserstoff-, Deuterium- und ^{3}Helium-Gastargets gestreut.

Bei der tiefinelastischen Streuung von Positronen an Nukleonen werden die Quarks aus dem Kern gestreut und fragmentieren daraufhin in Hadronen. Die Wahrscheinlichkeit, daß aus einem Quark einer gewissen Sorte ein bestimmtes Hadron entsteht, wird dabei durch Fragmentationsfunktionen beschrieben. Besondere Bedeutung hat der Vergleich der Fragmentationsfunktion, bei der das Hadron das getroffene Quark enthält, mit der Wahrscheinlichkeit, daß keine derartige Korrelation besteht. Da sich bei dem Verhältnis dieser Fragmentationsfunktionen Detektor- und Akzeptanzeffekte weitgehend aufheben, kann dieses direkt mit den Resultaten anderer Messungen und theoretischen Erwartungen verglichen werden.

Im Rahmen dieser Analyse wurden zwei verschiedene Methoden angewandt, um die Fragmentationsfunktionen in geladene Pionen aus den gemessenen Verteilungen zu bestimmen. Bei großen Werten der relativen Pionenergie z werden Abweichungen zu dem in der e^+e^--Annihilation gemessenen Verhalten beobachtet. Diese stimmen mit der einzigen anderen Messung in der tiefinelastischen Streuung überein.

Measurement of Fragmentation Functions at Hermes

The process of hadronisation of light quarks into charged pions has been investigated. The analysed pion spectra have been measured at the Hermes experiment at DESY, where 27.5 GeV positrons supplied by the HERA positron-proton collider are scattered off an internal gas target. In 1996, the target was hydrogen, deuterium and ^{3}Helium gas.

In deep-inelastic scattering, quarks are struck out of the nucleons and fragment further into hadrons. The probability to find a certain quark flavour in the measured hadron is parameterised by fragmentation functions. Special emphasis is put on the ratio of the unfavoured over the favoured fragmentation function, where the influence of the detector mostly cancels and a comparison to other results and to expectations can be performed.

The favoured and unfavoured pion fragmentation functions have been extracted from the measured pion spectra by using two different extraction methods. At high values of the fractional pion energy z, deviations are observed to the behaviour as measured in e^+e^--annihilation. However, the result is in agreement to the only other result from DIS.

Contents

1 Introduction

Deep-inelastic scattering is, 30 years after the realisation of the first experiments of this kind at the Stanford Linear Accelerator Center, one of the most important tools to understand the structur of the nucleon. The first experiments revealed the nucleon to consist of pointlike partons, which soon were identified with the earlier proposed quarks. Subsequently, the quark-parton model, which combines an intuitive simplicity with a tremendous success in the description of many static quark properties, was formulated. The discovery of the gluon, the mediator of the strong interaction between quarks, completed this picture.

The field theory of the strong interactions is Quantum Chromodynamics. It has been formulated in analogy to Quantum Electrodynamics, the theory of electroweak interactions which describes experimental data with an immense precision. The coupling constant of strong interactions was found to decrease with energy, which causes the quarks to be free in the limit of asymptotically high energies. Two consequences emerge from this behaviour known as asymptotic freedom. First, quarks and gluons are confined inside hadrons made up of two or three quarks in the case of mesons or baryons, respectively. Second, at high energies, or, equivalently, small distances, perturbation theory can be used to calculate strong interactions. This has been done with great success. One example is the predicted scaling violation of the deep-inelastic cross section which is in perfect agreement with the measurement.

At great distances, perturbation theory can no longer be applied. However, according to the factorisation theorem of Quantum Chromodynamics, the perturbatively calculable hard subprocess and the non-perturbative, soft part of the process can be separated. Additionally, the predicted universality states that the soft part is the same for various hard processes. The non-perturbative regime can only be described phenomenologically, that is, parameterised or modeled. Lattice calculations are still very limited in application.

In deep-inelastic scattering, the hard-scattering subprocess produces a highly virtual quark. This struck quark is subject to confinement and fragments, that is, it combines with other quarks to form the observable final-state hadrons. While the hard-scattering subprocess can be calculated to fixed order in perturbation theory, the fragmentation must be parameterised by phenomenological fragmentation functions. Due to universality, the fragmentation functions obtained in e^+e^--annihilation are thought to be the same as those measured in deep-inelastic scattering.

The basic properties of fragmentation are still not very well known and are difficult to access experimentally. However, the hypothesis of local parton-hadron-duality states the local conservation of the flow of quantum numbers from the parton to the hadron level. This is the basis for many models which have been created to test the picture of fragmentation by simulating the transition from partons to hadrons. The different approaches have to be compared to measurements.

The HERMES experiment at the HERA proton positron collider has been designed to study the spin structure of the nucleon. HERMES (HERa MEasurement of Spin) measures the spin-dependent deep-inelastic scattering of polarised 27.5 GeV positrons off polarised nucleons with a forward spectrometer. Besides the inclusive measurement of spin dependent structure functions of the nucleon, HERMES has been designed to probe semi-inclusive properties as well: with its good tracking and particle identification capabilities, coincident hadrons can be identified which carry information about the struck quark. The prerequisite for the latter is the validity of factorisation which has been tested within the limit of high energies. However, at the relatively low energies of HERMES non-perturbative effects may play an important rôle.

At HERMES, the main interest in the study of fragmentation properties is the comparison with results measured at higher energies. This reveals the validity of factorisation and universality at HERMES energies. The fragmentation functions are also needed as direct input for the determination of quantities like the asymmetry of the light quark sea or the polarised strange quark distribution which will be measured at HERMES. Additionally, the existing fragmentation models can be tested since no data at these energies exist so far.

This thesis is organised as follows:

In Section 2, the formalism of deep-inelastic scattering is summarised. In particular, the cross section formula for semi-inclusive deep-inelastic scattering in the framework of the quark-parton model is discussed. This is the basis for the extraction of the fragmentation functions.

Section 3 is a compilation of the definitions and properties related to the fragmentation process. Special emphasis is put on the properties of fragmentation at HERMES kinematics. In addition, the fragmentation models are described.

The experimental setup of HERMES is summarised in Section 4, while the methods used to extract the fragmentation functions are derived in Section 5.

The data analysis is outlined in Section 6. In particular, the Monte Carlo program and the corrections which are determined from such simulations are discussed. Subsequently, the systematic error sources are listed and their impact on the result is estimated.

The results for the fragmentation functions inside the HERMES acceptance, the ratio of the unfavoured over the favoured fragmentation function and the fragmentation functions corrected for the limited acceptance of the HERMES detector are presented in Section 7.

2 Formalism of Deep-Inelastic Scattering

2.1 Inclusive Deep-Inelastic Scattering

Deep-inelastic scattering (DIS) is a powerful tool to explore the structure of the nucleon by means of lepton-nucleon scattering in the limit of high lepton momenta. The process can be written

$$l + N \rightarrow l' + X \ ,$$

where an incident lepton l scatters off the nucleon N and will be detected in its final state l'. The nucleon fragments into the hadronic final state X. In inclusive DIS, only the scattered lepton l' is detected, whose kinematic distribution carries information about the structure of the nucleon. A diagram of the process can be seen in Fig. 2.1, where only the lowest order process in Quantum Electrodynamics (QED), that is the exchange of a virtual photon, is shown. The differential cross section for this process

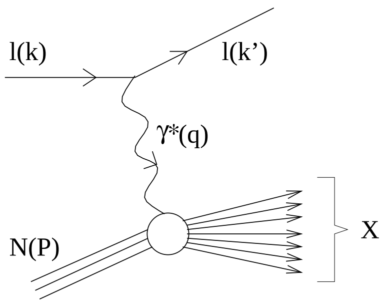

Figure 2.1: Deep-inelastic lepton-nucleon scattering in lowest order QED.

in lowest order QED can be written as the contraction of two tensors, a leptonic and a hadronic one [1],

$$\frac{\mathrm{d}^2\sigma}{\mathrm{d}\Omega \mathrm{d}E'} = \frac{\alpha^2}{Q^4}\frac{E'}{E} L_{\mu\nu} W^{\mu\nu} \ , \tag{2.1}$$

where $d\Omega$ denotes the spatial angle of the scattered lepton. The relevant kinematic variables are listed in Table 2.1. The leptonic tensor $L_{\mu\nu}$ describes the emission of the virtual gamma by the lepton and can be calculated from QED. The hadronic tensor $W^{\mu\nu}$ is not directly computable since it describes the structure of the nucleon and includes all possible hadronic final states. However the two subprocesses factorise, as shown in Fig. 2.2, and can be written as two independent processes. In the case of

Kinematic momenta vectors of the particles:

Letter		In lab. frame	Particle
$k\,(k')$	$=$	$(E,\vec{k})\ \left((E',\vec{k'})\right)$	Incident (scattered) lepton,
P	$=$	$(M,\mathbf{0})$	Incident Nucleon
q	$=$	$(\nu,\vec{q})$	Virtual gamma (γ^*)
p	$=$	$(E_h,\vec{p})$	Coincident Hadron

Inclusive variables:

Letter		Covariant		In lab. frame	
Q^2	$=$ $=$	$-q^2$ $-(k-k')^2$	$\approx$	$4EE'\sin^2(\frac{\theta}{2})$	Negative four momentum squared of the γ^*, i.e. transferred momentum squared to the nucleon
ν	$=$	$\frac{q\cdot P}{P^2}$	$=$	$E-E'$	Energy of the γ^* in the lab frame
x	$=$	$\frac{-q^2}{2P\cdot q}$	$=$	$\frac{Q^2}{2M\nu}$	Bjørken scaling variable, i.e. fraction of P carried by the parton in Breit frame
y	$=$	$\frac{q\cdot P}{k\cdot P}$	$=$	$\frac{\nu}{E'}$	Fraction of the energy of the lepton transferred to the nucleon
W^2	$=$	$(q+P)^2$	$=$	$M^2+Q^2(\frac{1}{x}-1)$	Invariant mass squared of the γ^*N system, i.e. of the final hadronic state

Semi-inclusive variables:

Letter		Covariant		In lab. frame	
z	$=$	$\frac{q\cdot p}{q\cdot P}$	$=$	$\frac{E_h}{\nu}$	Fraction of the energy of the γ^* carried by the hadron
$p_{\|\|}$ p_T	$=$ $=$	$(p\cdot q)/\|q\|$ $(p^2-p_{\|\|}^2)^{\frac{1}{2}}$			Parallel and transverse momentum of the hadron in the γ^*N CM frame with respect to the direction of the γ^*
x_F	$=$	$\frac{p_{\|\|}}{p_{\|\|max}}$	$\approx$	$\frac{2p_{\|\|}}{W}$	Fraction of the momentum of the γ^*N system held by the hadron in direction of the γ^*
η	$=$	$\frac{1}{2}\ln(\frac{E+p_{\|\|}}{E-p_{\|\|}})$	$=$	$\eta-\tanh^{-1}\beta$	Rapidity $(\beta=v/c=\|q\|/(\nu+M))$

Table 2.1: Kinematic variables in semi-inclusive deep-inelastic scattering

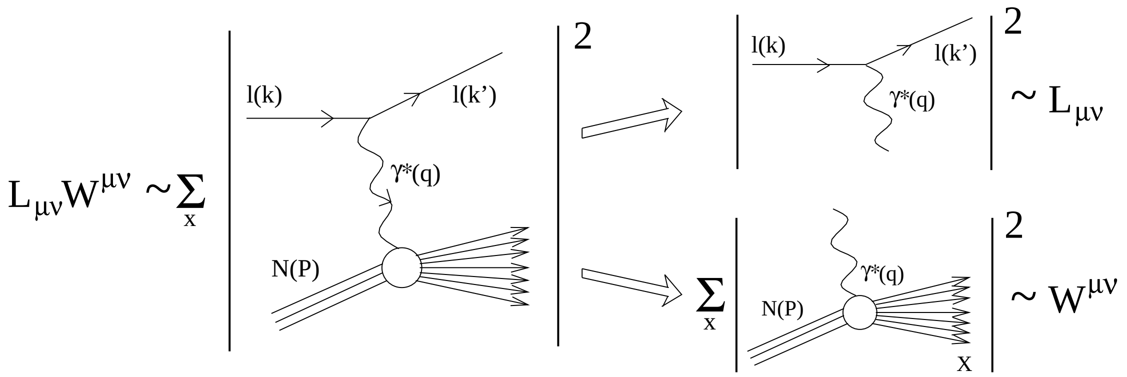

Figure 2.2: Heuristic picture for the factorisation of the leptonic and hadronic tensor which describe the deep-inelastic scattering process.

unpolarised scattering the most general form of the hadronic tensor can be simplified into two independent structure functions W_1 and W_2, considering parity conservation and time reversal invariance of the process. W_1 and W_2 depend on the transferred energy ν and on the momentum transfer Q^2. This yields the cross section formula for the elastic lepton-nucleon scattering,

$$\frac{\mathrm{d}^2\sigma}{\mathrm{d}E'\mathrm{d}\Omega} = \frac{4\alpha E'^2}{Q^4}\left[2W_1(\nu,Q^2)\sin^2\frac{\theta}{2} + W_2(\nu,Q^2)\cos^2\frac{\theta}{2}\right] . \tag{2.2}$$

The phenomenon of scaling invariance has been predicted by Bjørken: The dimensionless structure functions F_1 and F_2 are, in the limit $Q^2 \to \infty$, functions of the ratio $x \equiv x_{Bj} = Q^2/2M\nu$ only, and are therefore independent of any mass scale:

$$\begin{aligned} MW_1(\nu,Q^2) &= F_1(x,Q^2) \underset{Q^2\to\infty}{\longrightarrow} F_1(x) \\ \nu W_2(\nu,Q^2) &= F_2(x,Q^2) \underset{Q^2\to\infty}{\longrightarrow} F_2(x) \end{aligned}$$

This phenomenon arises naturally if the inelastic lepton-nucleon scattering is due to incoherent elastic scattering off pointlike constituents in the proton. This can also be seen from another argument: Q^2 defines the resolution of the scattering process, since the wavelength λ of the virtual photon can be written as

$$\lambda \propto \frac{1}{P} = \frac{1}{\sqrt{\nu^2+Q^2}} \approx \frac{2Mx}{Q^2} , \tag{2.3}$$

where P and M are the momentum and the mass of the nucleon, respectively. $1/Q^2$ is therefore proportional to the size of the resolved structure for a given x, and the observed independence of Q^2 can accordingly be interpreted in the way that nucleons consist of pointlike "partons". The partons were identified with constituent quarks which have been proposed due to group theoretical considerations.

The cross section can now be written in the well known form

$$\frac{\mathrm{d}^2\sigma}{\mathrm{d}x\mathrm{d}Q^2} = \frac{4\pi\alpha^2}{xQ^4}\left[y^2xF_1(x,Q^2) + (1-y)F_2(x,Q^2)\right] . \tag{2.4}$$

2.2 The Quark-Parton Model

The quark-parton model (QPM) is a simple model, which has been derived from the picture of quarks being pointlike constituents of the nucleon, as it is seen from scaling in DIS. In the limit of high Q^2 the time of the interaction and the size resolved by the virtual photon are considerably smaller than nucleonic distances, the distance between the partons. Therefore, the interpartonic interactions can be neglected. This together with the assumption that final state interactions act at larger space time scales means the quarks can be regarded as "quasi-free". The scattering amplitude then becomes the incoherent sum of the amplitudes of the scattering on free quarks, or equivalently, the sum of momentum distribution functions [2]. This approximation is the basis of the QPM. F_2 then becomes

$$F_2(x) = x \sum_f e_f^2 q_f(x) \ , \tag{2.5}$$

where x is the momentum fraction of the nucleon carried by the quark and $q_f(x)$ is the parton density function of a quark of flavour f with momentum fraction x and charge e_f in units of the elementary charge $|e|$.

The integration of Eq. 2.5 over x yields, however, only half of the momentum of the nucleon. The partons which are responsible for the missing momentum are thought to be the gluons, the gauge bosons of the strong interaction, which do not interact weakly or electromagnetically. In the following, quarks and gluons are collectively called "partons".

In the Breit frame, that is in the center-of-mass frame of the incoming nucleon and the virtual gamma, the momentum of the nucleon becomes large and the masses and transverse momenta of the partons can be neglected. The lepton-nucleon scattering process in such a frame according to the QPM is represented by Fig. 2.3. The model well describes the results of a series of experiments. An increased experimental precision revealed scaling violations, that is a dependence of the structure functions on Q^2. The field theory of quarks and gluons, Quantum Chromodynamics (QCD) predicts the scaling violation caused by initial and final state gluon radiaton. This is described by the *Gribov-Lipatov-Altarelli-Parisi* (GLAP) equations, where the gluon radiation of a parton and the resulting dependence of the structure functions on Q^2 can be calculated by splitting functions. With this evolution scheme, the parton distributions, whose x-dependence is known at a fixed scale Q_0^2, can be evolved to other scales. The quark-parton model enhanced by these tools is called the QCD improved quark-parton model.

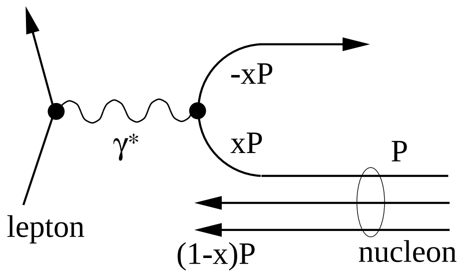

Figure 2.3: A DIS scattering process according to the QPM in the Breit-frame.

2.3 Semi-Inclusive Deep-Inelastic Scattering

In semi-inclusive deep-inelastic scattering, a hadron h is measured in coincidence with the scattered lepton l',

$$l + N \longrightarrow l' + h + X \, . \tag{2.6}$$

The relative cross section of the semi-inclusive process is given in the framework of the quark-parton model as

$$\frac{1}{\sigma_{tot}} \frac{\mathrm{d}\sigma(lN \to l'hX)}{\mathrm{d}z} = \frac{1}{N_e} \frac{\mathrm{d}N^h}{\mathrm{d}z} = \frac{\sum_f e_f^2 q_f(x, Q^2)\, D_f^h(z)}{\sum_f e_f^2 q_f(x, Q^2)} \, . \tag{2.7}$$

Here, σ_{tot} denotes the one-photon-exchange cross section, $\mathrm{d}N^h/\mathrm{d}z$ is the differential hadron rate at a certain relative hadron energy z normalised to the number of scattered DIS leptons N_e. The $D_f^h(z)$ are called fragmentation functions. According to the above equation, $D_f^h(z)$ denotes the probability to find a hadron h with momentum fraction z if a quark of flavour f has been struck in the hard-scattering subprocess.

The equation 2.7 is the central equation of semi-inclusive DIS. The assumption of factorisation in the infinite momentum approximation which leads to the simple interpretation of Eq. 2.5 is also vital for the interpretation of Eq. 2.7.

The factorisation of the hard-scattering subprocess and the "soft" hadronisation process is expressed in the independence of the fragmentation functions of x, that is the fragmentation does not depend on the momentum of the parton. This allows to separate the different processes by integrating over one variable or by performing a separation of the dependences on x and z. The tagging of the type of coincident hadron then gives access to the flavour of the struck quark via the correlation in flavour of the quark and the hadron. This is the advantage of semi-inclusive DIS, where not only the sum, as in Eq. 2.5, but the individual momentum distributions can be accessed. This is commonly done in solving the linear equation system which consists of the relative cross sections (Eq. 2.7) on different target materials. With the assumption of isospin and charge conjugation invariance of the fragmentation functions and of the quark distributions these equations can be simplified significantly and the momentum distributions can be extracted.

Similarly the fragmentation functions can be determined. This can be done in two different ways: either by using the parton distribution functions, which are available as parameterisations of the measurements of other experiments, or by restricting the measurement on an isoscalar target which further simplifies Eq. 2.7. The different methods are described in Sec. 5.

2.4 Polarised Deep-Inelastic Scattering

The spin of the nucleon can be disentangled into its various components, the polarisation of quarks $\Delta\Sigma$, gluons ΔG and a possible angular momentum contribution L_z,

$$s_z^N = \frac{1}{2} = \frac{1}{2}\Delta\Sigma + \Delta G + L_z \ . \tag{2.8}$$

The study of the spin structure of the nucleon has attracted great interest since the European Muon Collaboration (EMC) published a value for the quark spin $\Delta\Sigma$ which disagreed with the simple relativistic QPM expectations [3]. According to the model, ΔG and L_z are assumed to vanish and

$$\Delta\Sigma = \Delta u + \Delta d + \Delta s \approx 0.6 \ . \tag{2.9}$$

The measurement at following experiments instead revealed a value of $\Delta\Sigma \approx 0.3$ [4], much lower than expected. The deviation of Eq. 2.9 from unity is caused by relativistic effects.

Insights into the spin structure of the nucleon can be achieved by using polarised DIS. The cross section of unpolarised DIS has been derived in Eq. 2.4. In polarised DIS, two additional structure functions describe the polarisation of the quarks, $g_1(x,Q^2)$ and $g_2(x,Q^2)$. In the framework of the QPM, g_1 can be written as $g_1(x,Q^2) = \frac{1}{2}\sum_f e_f^2 \Delta q_f(x,Q^2)$, where f are the quark flavours, e_f is the quark charge in units of $|e|$ and $\Delta q_f(x,Q^2) = q^{\uparrow\uparrow}(x,Q^2) - q^{\uparrow\downarrow}(x,Q^2)$ are the polarised quark distributions, i.e. the difference of quarks having parallel spin with respect to the polarisation of the nucleon, to those having antiparallel spin. Thus, $g_1(x)$ is a measure of the (charge weighted) sum of the polarisation of the quarks.

From the first moment $\Gamma_1 = \int g_1(x)dx$ and the weak couplings in beta decay that can be measured with good accuracy, the quark spin content $\Delta\Sigma$ can be calculated [5]. The first moments and the weak couplings can also be compared directly [6] which leads to theoretical predictions, called sum rules. The prediction for the difference $\Gamma_1^p - \Gamma_1^n$, the Bjørken sum rule [7], has been experimentally confirmed, but the Ellis Jaffe sum rules for the moments on proton and neutron separately, Γ_1^p and Γ_1^n, disagree with the measurement [8]. Several explanations exist for this so called “spin-crisis”, the disagreement between experiment and the naïve theoretical expectation. However, the presently available inclusive measurements do not allow for an unambiguous interpretation.

More elucidating are semi-inclusive measurements which allow for the extraction of the individual quark spin distributions and thus for the discrimination between different models. This is the main goal of the HERMES experiment, where the good tracking resolution and particle identification allow the measurement of semi-inclusive processes in spin dependent DIS.

2.5 Extraction of Quark Distributions

With the combination of data on different targets like hydrogen, deuterium and ^{3}Helium, it is possible to determine the spin dependent quark distributions $\Delta u(x)$ and $\Delta d(x)$ from polarised semi-inclusive DIS [9]. This direct extraction method makes use of the cross section of semi-inclusive DIS in the framework of the QPM, Eq. 2.7, which is in the polarised case

$$d\sigma_\pi^{\uparrow\uparrow} - d\sigma_\pi^{\uparrow\downarrow} \propto \sum_{f=u,d} e_f^2 \Delta q_f \, D_f^h(z) \tag{2.10}$$

with $\Delta q \equiv \Delta q(x, Q^2)$ as defined above (Sec. 2.4) and leads to different linear combinations of Δu and Δd for different targets.

This determination of the polarised quark distribution Δq is based on several assumptions:

- Factorisation of the hard-scattering subprocess and the long distance fragmentation process is assumed to hold at the relatively low energies of Hermes. This allows to separate the quark distributions and the fragmentation functions.
- Isospin and charge conjugation invariance of the fragmentation functions $D_f^h(z)$ are necessary assumptions to reduce the number of unknown quantities. It leads to two pion fragmentation functions $D^+ \equiv D_u^{\pi^+} = D_d^{\pi^-} = D_{\bar{u}}^{\pi^-} = D_{\bar{d}}^{\pi^+}$ and $D^- \equiv D_u^{\pi^-} = D_d^{\pi^+} = D_{\bar{u}}^{\pi^+} = D_{\bar{d}}^{\pi^-}$ (see Sec. 3.4.3).

Using these assumptions, the charge pion difference $\mathrm{d}\sigma_{\pi^+-\pi^-} \equiv (\mathrm{d}\sigma_{\pi^+} - \mathrm{d}\sigma_{\pi^-})$ can be expressed in the following way for different targets:

$$\text{Proton: } \left(d\sigma_{\pi^+-\pi^-}^{\uparrow\uparrow} - d\sigma_{\pi^+-\pi^-}^{\uparrow\downarrow}\right) \propto \left(4\Delta u(x) - \Delta d(x)\right) \cdot \left(D^+(z) - D^-(z)\right) \tag{2.11}$$

$$\text{Deuterium: } \left(d\sigma_{\pi^+-\pi^-}^{\uparrow\uparrow} - d\sigma_{\pi^+-\pi^-}^{\uparrow\downarrow}\right) \propto \left(\Delta u(x) - \Delta d(x)\right) \cdot \left(D^+(z) - D^-(z)\right) . \tag{2.12}$$

Measuring the asymmetry

$$A_\pi(x) = \frac{d\sigma_{\pi^+-\pi^-}^{\uparrow\uparrow} - d\sigma_{\pi^+-\pi^-}^{\uparrow\downarrow}}{d\sigma_{\pi^+-\pi^-}^{\uparrow\uparrow} + d\sigma_{\pi^+-\pi^-}^{\uparrow\downarrow}} \tag{2.13}$$

on different targets allows to extract Δu and Δd.

It is interesting to extract fragmentation functions in order to check the validity of the QPM assumptions at Hermes energies, which are well below the energies of existing data. These assumptions are the prerequisite to extract the polarised quark distributions.

The knowledge of the fragmentation functions is also needed for the determination of quantities like the polarised strange quark distribution [10] or the flavour asymmetry of the (unpolarised) light quark sea [9], $[\bar{d}(x) - \bar{u}(x)]/[u(x) - d(x)]$: Actually, the QPM assumes a flavour symmetric quark sea, i.e. $\bar{u} = \bar{d}$. However, the measurement of the

New Muon Collaboration (NMC) [11] of the violation of the Gottfried Sum Rule can be interpreted as an excess of $d\bar{d}$ pairs over $u\bar{u}$ pairs in the proton [12, 13].

The extraction method of this light quark sea flavour asymmetry is based on the QPM formula of semi-inclusive DIS, Eq. 2.7:

$$\frac{\bar{d}(x)-\bar{u}(x)}{u(x)-d(x)} = \int \frac{\frac{3}{5}\left(\frac{1+D^-/D^+}{1-D^-/D^+}\right)\Big(1-r(x,z)\Big) - \Big(1+r(x,z)\Big)}{\frac{3}{5}\left(\frac{1+D^-/D^+}{1-D^-/D^+}\right)\Big(1-r(x,z)\Big) + \Big(1+r(x,z)\Big)}\,\mathrm{d}z\ , \quad (2.14)$$

$$\text{where} \qquad r(x,z) = \frac{N_p^{\pi^-}(x,z)-N_p^{\pi^+}(x,z)}{N_n^{\pi^-}(x,z)-N_n^{\pi^+}(x,z)}\ . \quad (2.15)$$

$N^{\pi^\pm}(x,z)$ are the measured pion distributions and $D^-/D^+ \equiv D^-(z)/D^+(z)$ is the ratio of the unfavoured over the favoured fragmentation function, which will be defined in Sec. 3.4.3 and extracted in this analysis. If the fragmentation is understood and factorisation holds, then the usage of the measured ratio $D^-(z)/D^+(z)$ should lead to the z-independence of the light quark sea asymmetry.

3 Fragmentation

3.1 The Fragmentation Process: from Partons to Hadrons

According to the factorisation theorem of QCD, the region in space-time after the occurrence of the hard-scattering subprocess can be subdivided into a short distance and a long distance region. In the short distance region the strong coupling constant α_s is small and perturbative calculations can be performed. Partons emerge from the highly virtual initial partons by subsequent gluon radiation and quark-antiquark creation processes. This is briefly outlined in the next section.

However, the long distance region is the non-perturbative regime where the strong coupling constant is becoming large. After the coloured partons have radiated most of their energy they combine to form colourless hadrons, i.e. mesons and baryons. This is the hadronisation or fragmentation process, which cannot be described by perturbation theory and is therefore difficult to access theoretically. The fragmentation process is briefly discussed in Sec. 3.1.2, while the phenomenologic approach is treated in Sec. 3.2-Sec. 3.4.

3.1.1 Parton Evolution

The leading order process at the parton level is the coupling of the vector boson, that is the virtual photon[1], to the quark, $\gamma q \to q$, which can be calculated in leading order QCD by the evaluation of the corresponding matrix element. In addition, the first order QCD processes of gluon radiation $q \to qg$ and boson-gluon fusion $\gamma g \to q\bar{q}$ are also calculable from matrix elements.

During the further development of the struck parton, a parton cascade or parton shower emerges via the consecutive radiation of gluons which further radiate into $q\bar{q}$ pairs. In the case of parton radiation at low energies or small angles, the matrix elements become divergent. A possibility to overcome these soft and collinear singularities is a summation over all leading terms in all orders in α_s. This leading logarithmic approximation of QCD (LLA) [14], as opposed to the exact treatment in fixed order by matrix elements, is described by the *Gribov-Lipatov-Altarelli-Parisi* (GLAP) formalism [14].

[1] In principal, any of the γ, Z^0 or $W^{\pm}$ bosons may be transferred. At HERMES, only the γ is significant, the Z^0 and the $W^{\pm}$ exchange are suppressed due to their large masses.

3.1.2 Fragmentation

Experimentally, the existance of isolated partons has never been observed. Partons are presumed to exist only inside colourless hadrons and are bound by the attracting interactions due their colour charges. This property known as "confinement" is predicted by QCD [15] and characterises the long distance part of the scattering process where the coloured partons form colourless hadrons. This process is called fragmentation and cannot be calculated perturbatively. QCD also predicts the already mentioned factorisation of the hard-scattering subprocess which has been proven to hold at all orders perturbation theory.

In order to get experimental access to the fragmentation process, measurable quantities have to be defined. This is not simple, because the experimental access to the complex process is poor, since neither the origin of the hadron nor the time of its production can be measured.

A successful approach is the design of fragmentation models which simulate the above quantities on a statistical basis, i.e. with a Monte Carlo technique. The output of the models can be directly compared with experimentally accessible quantities like hadron distributions or multiplicities. There exists a variety of such models [16] of which the most important ones will be briefly summarised below. This is an indirect but nevertheless powerful technique, since many phenomenological features can be implemented and comparisons to data easily performed. That way, the underlying picture of fragmentation can be tested. The fragmentation process is predicted by the models to depend on the fractional energy z, but to scale with energy, cf. Sec. 3.2.2. Therefore hadron distributions and fragmentation functions are investigated as a function of z.

Apart from this, the predicted feature of scaling violations, i.e. the dependence on Q^2, can be verified by applying the GLAP formalism to fragmentation functions [17]. This appears as a natural supplement to the above indirect method and provides a useful tool to compare data of different scales. It will be discussed in more detail in Sec. 3.4.2.

3.2 Fragmentation Models

Since the fragmentation process cannot yet be calculated from first principles, fragmentation models have been created in order to provide a general framework in which the properties of hadroproduction can be studied phenomenologically [18]. In particular, the models have been designed to be used in Monte Carlo programs.

The models are based on the quark-parton model. In addition, the hypothesis of local parton-hadron-duality (LPHD) is made, which states that the flow of the quantum numbers from the partonic to the hadronic state during the fragmentation process is locally conserved [19]. This important hypothesis is the prerequisite of all analyses which draw conclusions on partons from the observations of hadronic properties. There are various indications that LPHD is valid [14, 19].

3.2.1 Independent Fragmentation

The independent fragmentation model was developed in the early 1970s by Field and Feynman [20] to reproduce the limited transverse momenta and approximate scaling of energy fraction distributions observed in quark jets produced in e^+e^--annihilation. It is based on the simple assumption that every parton fragments independently. In the model, the struck quark q_0 combines with the antiquark $\bar{q}_1$ of a quark-antiquark pair $q_1\bar{q}_1$ which is created out of the vacuum, to create the first rank primary meson with energy fraction z_0, see Fig. 3.1.

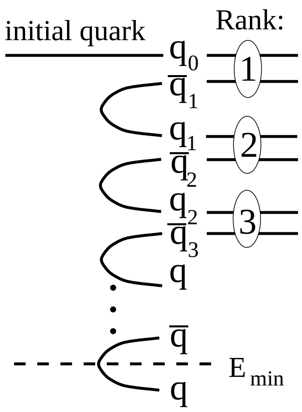

Figure 3.1: Diagram of independent fragmentation.

In the model, the "rank" of a specific hadron is the ordering in production time in the center-of-mass system, starting with the hadron containing the struck quark. These produced hadrons are the "primary" hadrons since they directly descend from parton fragmentation. If they decay further, the decay products are called secondary, tertiary, etc. mesons.

The left over energy fraction $(1 - z_0) = z_1$ of the first-rank primary meson $q_0\bar{q}_1$ is assigned to the remaining quark q_1. This process is iterated down to a certain energy cutoff E_{min}, when the last, remaining quark is neglected. This way, quark-antiquark pairs $q_i\bar{q}_i$ are created with energy fraction $(1 - z_i)$. The energy is assigned randomly according to an universal distribution $f(z)$ which causes the fragmentation to scale with energy. The antiquark $\bar{q}_i$ then combines with the quark of the former rank q_{i-1} to form a meson with quark content $q_{i-1}\bar{q}_i$.

The basis of independent fragmentation is an integral equation which describes the probability to find a primary meson with energy z within dz in a jet of hadrons [20],

$$F(z)\mathrm{d}z = f(1-z)\mathrm{d}z + \int_z^1 f(\eta)\mathrm{d}\eta\, F(z/\eta)\mathrm{d}z/\eta \tag{3.1}$$

where $f(1-z)\mathrm{d}z$ is the probability that this particular meson is of first rank. If this is not the case, then this first rank primary meson has left a momentum fraction η with probability $f(\eta)\mathrm{d}\eta$. The probability to find the meson with energy z in dz within this remaining cascade is equal to $F(z/\eta)\mathrm{d}z/\eta$, since $F(z)$ scales with energy.

A simple solution for Eq. 3.1 is the ansatz $f(z) \propto z^d$, or

$$f(z) = 1 - a + 3a(1-z)^2\,, \tag{3.2}$$

with $a = 0.77$ determined from fits to data [20]. The function $f(z)$ parameterises the probability that a energy fraction z is left to the remaining cascade. With this choice, $zF(z) = f(1-z)$.

If different flavours are regarded, the probability γ_u to create a $u\bar{u}$ or γ_d to create a $d\bar{d}$ is introduced, where $\gamma_u + \gamma_d + \gamma_s = 1$ and $\gamma \equiv \gamma_u = \gamma_d$. The probability to create a $s\bar{s}$

is $\gamma_s = 0.3\gamma$, according to the measured K/π-ratio [21]. In the case of three flavours, this leads to $\gamma = 0.435$ due to the normalisation requirement. Pseudoscalar and vector mesons are formed with equal probability. The transverse energy is distributed as a Gaussian with $\langle p_\perp^2 \rangle = 0.35$ (GeV/c)^2, where the quark and antiquark of a $q\bar{q}$ pair have opposite $p_\perp$. Independent fragmentation does not predict an ordering according to momenta of the produced hadrons. It is likely, however, that the first-rank hadron possesses the highest momentum and the hadrons of higher rank accordingly lower momenta.

If the probability to find the struck quark in the detected meson is called the favoured fragmentation function, i.e. $D^+(z) = [(1-\gamma)f(1-z) + \gamma F(z)]\mathrm{d}z$, and the probability that the meson does not contain this quark the unfavoured fragmentation function[2], $D^-(z) = \gamma[F(z) - f(1-z)]\mathrm{d}z$, then the ratio of unfavoured over favoured fragmentation functions yields

$$\frac{D^-(z)}{D^+(z)} = \frac{\gamma\,(1-z)}{z + \gamma\,(1-z)}\,. \tag{3.3}$$

Two remarkable predictions can be derived: First, the ratio is expected to tend to one for $z \to 0$ and to zero for $z \to 1$, independent on γ. Hence, for $z = 1$ only the first rank primary hadron is produced, as expected. Second, if the strange quarks are neglected, i.e. $\gamma = 0.5$, then the simple expression $D^-/D^+ = (1-z)/(1+z)$ follows.

Many properties of hadronic jets are described quite successfully by independent fragmentation. Some inherent weaknesses however lead to the development of other models. For example, in independent fragmentation, the Lorentz transformation into another reference frame causes the violation of momentum conservation. Also, the particle multiplicities depend on the reference frame. Through the neglect of the quark of highest rank in a jet, the colour and flavour quantum numbers are not conserved either.

The later developped LUND string model is used today instead of the independent fragmentation model, while the latter still serves for comparisons. Independent fragmentation is realised as a Monte Carlo program in the JETSET [22] program library.

3.2.2 The LUND String Model

The LUND string model of hadronisation [23] is based on the QCD prediction of confinement, which causes the potential energy of the colour field stretched between the quarks to increase with length, i.e. with the distance between the quarks. It is the most successful model nowadays, since it combines a consistent, covariant picture of the fragmentation of quarks and gluons and matches the data very well [24].

The model is best explained in e^+e^--annihilation: The quark-antiquark pair $q_0\bar{q}_0$, moving apart from each other, is connected by a colour field stretched between them. At a certain field length the potential field energy is sufficient to produce a quark-antiquark pair $q_1\bar{q}_1$, which may take place at any point on the hyperbola $x^2 - t^2 = m^2/\kappa^2$ between the quarks, κ being the field energy per unit length and x and t the space-time

[2] Later in this work, "favoured" and "unfavoured" will be defined slightly differently.

distance between q_0 and $\bar{q}_0$. The field between the newly created quark and antiquark $q_1\bar{q}_1$, which are pulled apart from each other, will be cancelled by the new field. Two

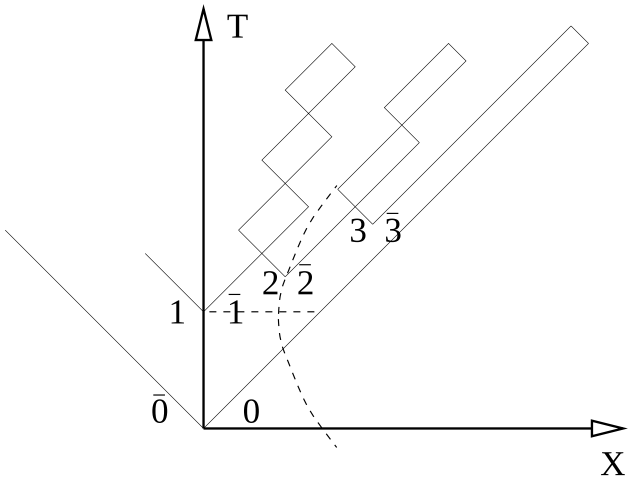

Figure 3.2: Hadroproduction in e^+e^--annihilation according to the LUND string model. The initially produced quarks $q_0\bar{q}_0$, denoted here by **0** and $\bar{\mathbf{0}}$, are moving away in opposite directions. Quark-antiquark pairs are produced in the field. The production point of a $q\bar{q}$ pair is lying on a hyperbola given by $(\Delta x)^2 - (\Delta t)^2 = const.$

strings are now moving in opposite directions, one of fractional energy z, the other of energy $(1-z)$. For each string, this iterative process continues until a string-connected quark-antiquark is close to the mass shell of a hadron. The decision which final state hadron type is chosen is made according to random decisions, based on three parameters, the flavour production ratios $u\bar{u} : d\bar{d} : s\bar{s} = 1 : 1 : 0.3$, the ratio between vector- and pseudoscalar meson production $(1 : 1)$ and the ratio between quark- and diquark production, which controls the ratio between mesons and baryons.

This fragmentation process continues until energy, momentum and quantum numbers have been distributed among the primary hadrons. This hadron creation process conserves energy, momentum and all internal quantum numbers. The distribution function of the fractional longitudinal energy assigned to a string is the so called LUND symmetric fragmentation function,

$$f(z) = \frac{(1-z)^a}{z} \cdot \exp(\frac{-bm_\perp^2}{z}) \,, \tag{3.4}$$

where the transverse mass squared $m_\perp^2 = m + p_\perp^2$, a and b have to be determined from data. The equation 3.4 is the simplest non-trivial function which remains invariant under symmetric, that is oppositely directed, Lorentz boosts.

The transverse momenta of the produced quarks arise from a tunneling mechanism for the $q\bar{q}$-pair production and are locally, i.e. for each $q\bar{q}$-pair, compensated. Classically, massless partons can be created at one point and then pulled apart by the field, but massive partons or partons with transverse momentum cannot. The $q\bar{q}$ can however be produced quantum mechanically at one point and then tunnel out to the classically allowed region, with a tunnel probability equal to $\exp(-\pi m_\perp/\kappa)$. A hadron on the mass shell then obtains the sum of the $p_\perp$ of its constituent quarks. The width of the $p_\perp^2$ distribution of the quarks has to be determined from data.

The process looks very similar to independent fragmentation, as it is based on an iterative production of quark-antiquark pairs, too. Independent fragmentation however does not give any dynamical picture of the actual fragmentation process, whereas the string model is formulated with relativistic kinematics of the strings. It has been developed by taking the 1+1 dimensional Schwinger model as a guide line. The Schwinger model is an exactly solvable model of a linear force field, formulated in massless QED, with the feature of confinement.

An important prediction of the LUND model thus concerns gluon fragmentation. The so called string effect [25] occurs if a gluon is radiated off a string and decays into a $q\bar{q}$. This leads to the separation of the original string into two strings which fragment separately and produce a "kink" in the spectra. This "kink" has been successfully measured. Another difference from independent fragmentation concerns the ordering of the hadrons. The LUND model possesses an explicit "inside-out" momentum ordering structure in time, i.e. the slowest hadrons are produced first. This ordering is Lorentz invariant because q_0 and $\bar{q}_0$ are treated as a system instead of being independent, and the string is fragmenting rather than the individual partons [26]. It is a direct consequence of the condition of the $q\bar{q}$ pairs to be produced on a hyperbola in space-time.

It is important to note that the particular ordering of the produced hadrons is frame dependent, cf. Fig. 3.2: A hadron which is fastest in one frame (and thus being produced last in that particular frame) is not necessarily produced last in another. But, as it has been pointed out above, in every frame the "inside-out" structure of the momentum ordering is given.

The LUND model as realized in the JETSET [22] program library has been the underlying model for most of the Monte Carlo studies in this work.

3.2.3 Cluster Fragmentation

The fragmentation process according to the cluster fragmentation model is characterised by cluster formation through preconfinement and phase space guided cluster decay, instead of providing complex fragmentation functions.

The parton showering process after the hard-scattering subprocess is followed by the formation of highly virtual partons into colour-singlet clusters with low virtuality, see Fig. 3.3 for a scheme. This cluster formation is called "preconfinement". In other words, the cluster fragmentation model describes the evolution of partons with large virtual mass into low-mass clusters using perturbation theory, in contrast to string or independent fragmentation, which parameterise this evolution. In this phase, heavy quarks are decaying weakly and the clusters consist of the light quarks u, d and s only. The perturbative method used to split the highly virtual partons is performed by the leading logarithmic approximation (LLA).

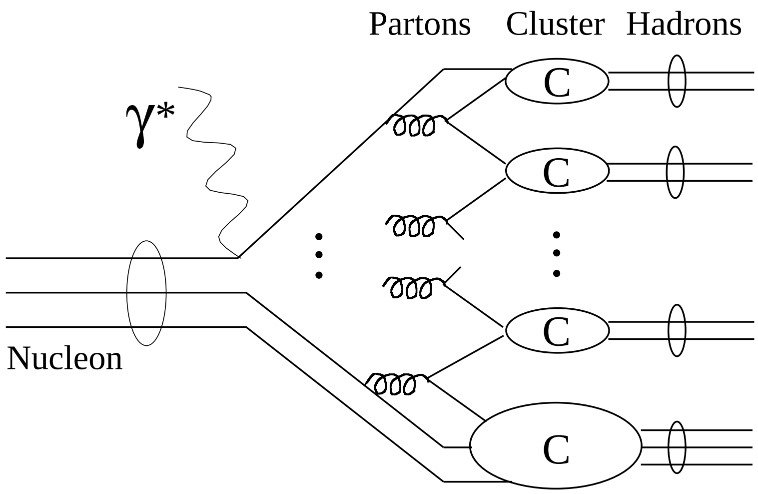

Figure 3.3: Scheme of the Cluster Fragmentation Model.

The colourless clusters then decay into hadrons from simple phase space arguments. This leads to a picture of the hadronisation process where no phenomenological parameters have to be adjusted like in the case of the LUND model. For example, baryon or s quark production is naturally suppressed due to its higher masses. The adjustable parameters of the model are the QCD scale parameter Λ_{QCD}, the parton masses and the maximal cluster mass $M^{max}_{Cluster}$.

Hadrons are produced according to the "inside-out" momentum ordering with time, that is low momenta are produced first. This appears as a consequence of soft gluon emission in an earlier stage caused by colour interference effects in the parton shower. In summary, hadronisation according to the cluster fragmentation model is described by low energy dynamics.

The HERWIG [27, 28] Monte Carlo generator incorporates the cluster fragmentation model. It has been used in comparison to the LUND model, see Sec. 6.4.1.

3.3 Definition of Fragmentation Functions

The fragmentation functions $D^h_f(z)$ in Eq. 2.7 are defined as the probability of the formation of a hadron h after a quark of flavour f is struck in the interaction. This is a very general definition which shall be discussed in more detail now.

3.3.1 Forward and Backward Hemisphere

The ideal measurement for the fragmentation process would be a perfect detection of all hadrons, their energies and their rank with respect to the time of production. As it has been seen, this is principally not possible, since the ordering of the fragmentation process is frame dependent. In addition, the experimental apparatus constrains the accessible information.

The hypothesis of local parton-hadron-duality predicts a correlation between the partons and the hadrons [19]. Therefore, the correlation to the struck quark can be measured, if those hadrons can be selected, which have been produced in space-time neighbourhood of the struck quark.

In deep-inelastic scattering, in the center-of-mass system of the virtual photon and the target nucleon, the struck quark and the remnant diquark will move away from each other in opposite directions, see Fig. 2.3, and stretch a colour field between them. The quark-antiquark pairs will be created along this field and the correlation of the hadron with the struck quark will decrease with the distance between them. Therefore, the measured hadrons are often divided into those coming from the forward and those coming from the backward hemisphere, where the hemispheres are defined with respect to the direction of the virtual photon in the center-of-mass of the nucleon-photon system.

The forward hemisphere is characterised by a positive x_F, the fraction of the energy of the nucleon-photon system held by the hadron in direction of the virtual photon (see Table 2.1) and is also called the current fragmentation region. The restriction of the origin of the selected hadrons to the current fragmentation region will lead to an enhancement of the correlation to the struck quark. Hadrons from the target fragmentation region dilute the correlation.

So defined, the fragmentation functions are the correlation in flavour of the measured forward hadrons to the struck quark and can be measured according to Eq. 2.7 by restricting the measurement to the forward hemisphere.

The measurement of "forwardness" is however difficult, too. There exist several possibilities [29], which are not equivalent:

Frame:	Criterion for Forwardness
Laboratory	$z > z_{min} > 0$
Center-of-Mass	$x_F > 0$
"	Rapidity $\eta > \eta_{min} > 0$

with z_{min} and η_{min} being lower limits on the fractional energy and rapidity, respectively, for the target suppression for a particular kinematic and detector acceptance.

No unique method is used in literature. It is however important to suppress hadrons from the target fragmentation region efficiently. Thus, a good measure for the forwardness of the hadrons has to be chosen where a simple cut can be applied.

In order to obtain a measure for the quality of the ordering, the "distance" of the different variables to each other has been studied [30]. This was done by analyzing how many permutations are needed to convert the ordering according to one variable into the ordering according to another variable. It turned out, that the distances of the orderings in x_F, rapidity and longitudinal momentum are significantly smaller than the distances of each of them towards z.

An appropriate variable to select the current fragmentation region is x_F or the rapidity η due to its natural relation to the direction of the photon. They give a good description of the forwardness of the hadrons. The criterion $x_F > x_{F\,min}$ with $x_{F\,min} = 0.1$ has been used in this work.

3.3.2 Decay Products

The fragmentation process discussed above deals with the fragmentation of partons into primary hadrons. Decay products, that is secondary, tertiary, etc. hadrons are not discussed, since their dynamic behaviour differs significantly from partonic fragmentation. In Fig. 3.4, a Monte Carlo study shows the influence of the pions coming

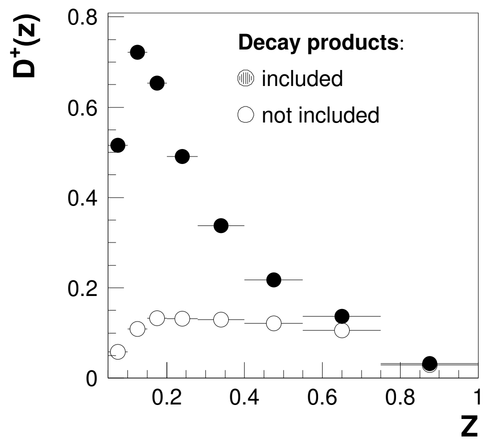

Figure 3.4: The fragmentation functions from the Monte Carlo, where the impact of the pions from particle decays can be seen. For smaller values of z this contribution is dominating.

from decays on the favoured valence quark fragmentation function $D^+(z)$. As a lookahead, the favoured fragmentation function is the probability that the flavour of the struck quark is also found in the final-state hadron, depending on the fractional energy z. The contribution from decay products is dominant for $z < 0.4$ and becomes less important for large z.

It is difficult or even impossible to suppress decay products experimentally, since either all decay products must be detected in order to reconstruct the invariant mass of the primary hadron, or the secondary decay vertices[3]must be resolved, that is precisely distuingished from the primary vertices.

In the case of HERMES, the acceptance is not large enough to capture every decay product. In addition, the strong decay of particles like the ρ^0 does not allow for an experimentally accessible separation of the spacepoints of the hard-scattering subprocess and the occurrence of the decay. A longitudinal track resolution in the order of 1 cm, as for HERMES, makes this impossible for weakly decaying particles as well. The measured fragmentation functions are therefore called "effective" fragmentation functions and contain all hadrons of a particular type, including those from decays.

[3]A vertex is the spacepoint of nearest approach of two tracks. The secondary vertex is the spacepoint of the decay of an instable particle, the primary vertex is its production point.

3.3.3 Acceptance

The measured fragmentation functions are extracted from the measured hadron spectra. Especially in DIS experiments where the detectors usually covers only the forward hemisphere the hadron spectra strongly depend on the acceptance of the detector.

In order to get an impression of the impact of the acceptance on the fragmentation functions, the favoured and unfavoured fragmentation functions as realised in the LUND model are shown in Fig. 3.5, where the fragmentation functions as seen by a detector with 4π, i.e. unlimited acceptance and as seen by the HERMES detector are opposed. The HERMES detector will be described in detail in Sec. 4.

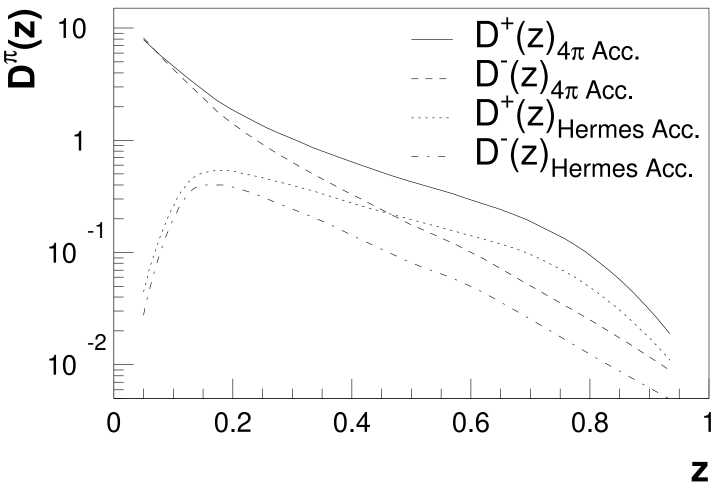

Figure 3.5: Favoured fragmentation function $D^{+}(z)$ and unfavoured fragmentation function $D^{-}(z)$ as simulated with the LUND model. The pion spectra are generated in an unlimited (4π) and inside the HERMES acceptance.

In order to compare the results from different experiments, either ratios of fragmentation functions have to be compared where the influence of the acceptance mostly cancels, or the fragmentation functions have to be corrected for the limited acceptance. This correction, which will be discussed in Sec. 6.4, is large however. Since fragmentation functions are also needed as direct input for other quantities, like the strange polarized quark distributions, three approaches will be undertaken here. First, the fragmentation functions will be extracted as measured inside the HERMES acceptance without corrections which account for the restricted acceptance. Second, the ratio is extracted where no such corrections are needed. Third, the fragmentation functions are extracted from spectra which are corrected for the limited acceptance. These fragmentation functions have hence larger systematic error due to the larger corrections but can be compared to results from other experiments.

3.3.4 Particle Type

In principle, the fragmentation functions of any parton into any hadron type or even into combinations of hadron types can be defined. However, in the latter case the general properties of fragmentation will be hidden behind the different fragmentation behaviours of the different particle species.

With the HERMES spectrometer, only pions between 4 and 13.5 GeV can be identified unambigously (described later in Sec. 4). Protons and kaons cannot be separated from each other due to their high Čerenkov thresholds. Therefore this work concentrates on pion fragmentation only. With the Ring Imaging Čerenkov Counter (RICH) which will replace the threshold Čerenkov counter of HERMES in 1998, a good separation of pions, kaons and protons will be possible and the different fragmentation functions can be measured in the future.

Now the definition of the fragmentation functions can be given. The fragmentation function $D_f^h(z)$ is defined as the parameterisation of the correlation of the flavour f of either quark of the measured forward hadron of a specific type h with the struck quark within a given experimental acceptance, including decay products.

The favoured fragmentation function $D^+(z)$ is the fragmentation function $D_f^h(z)$ if the flavour of the struck quark and the flavour of either quark of the measured hadron are in agreement. In the case of the unfavoured fragmentation function $D^-(z)$, the flavours do not agree. The average pion fragmentation function $D^\pi(z)$ is introduced as well, since it will be used in this analysis. It is is just the average of $D^+(z)$ and $D^-(z)$ in the case of pions.

3.4 Properties of Fragmentation Functions

The properties of the fragmentation functions, as far as predicted by QCD and already mentioned in the preceding sections, are summarised below. The limits are outlined and the model predictions and assumptions are confronted with experimental data or Monte Carlo studies.

3.4.1 Factorisation

The assumption of factorisation leads to the definition of fragmentation functions and to the possibility of their measurement, because otherwise no separation between the scattering and the fragmentation subprocess would be possible. Factorisation implies that the fragmentation of the quarks should be independent of their formation. This has been verified by comparing data on hadron production in e^+e^--annihilation experiments with similar data in deep-inelastic muon scattering [31]. Good agreement was found, but only the integral of the fragmentation functions, i.e. the dependence of the multiplicity versus W^2 has been measured.

A factorisation breaking was later investigated in more detail [32]. A slight dependence of the normalised, differential hadron multiplicities in deep-inelastic muon scattering, $(1/N_\mu)\mathrm{d}N^h/\mathrm{d}z$ on x has been found, mostly at high fractional energies z. This is not described by the QPM, but can be derived from next-to-leading order (NLO) QCD calculations [33]. In particular, vertex corrections from gluon graphs connecting the initial with the final state of the struck quark are thought to be responsible for this small effect.

3.4.2 Scaling and Evolution

The QPM predicts scaling of the fragmentation functions, that is the independence of the fragmentation process of the momentum transfer Q^2. However, gluon radiation plays a rôle in the fragmentation process which introduces a dependence of the fragmentation functions on Q^2.

This dependence can be calculated by performing a GLAP evolution of the fragmentation functions in Q^2 [34]. The various fragmentation functions are assumed to evolve in a similar way. For example, the evolution of the fit to the average pion fragmentation function $D^\pi(z)$ has been performed [35]. In that case, data from e^+e^--annihilation experiments [36, 37] were fitted. In e^+e^--annihilation, quarks and their antiquarks are created simultaneously and thus only the average fragmentation function $D^\pi(z) = \frac{1}{2}(D^+(z) + D^-(z))$ is accessible.

The evolution is performed as follows: Measured at a certain scale Q_0^2, the z-dependence of $D^\pi(z)$ is fitted according to the commonly used ansatz

$$D^\pi(z)|_{Q^2=Q_0^2} = N z^\alpha (1-z)^\beta \ . \tag{3.5}$$

The change with Q^2 of a general fragmentation function $D_a^h(z)$, where a is the initial quark or gluon, can be calculated via the GLAP equations [38, 39, 40],

$$\frac{\mathrm{d}}{\mathrm{d}\ln Q^2} D_a^h(z, Q^2) = \frac{\alpha_S(Q^2)}{2\pi} \sum_b \int_z^1 \frac{\mathrm{d}y}{y} \, P_{ab}^T(y, \alpha_S(Q^2)) \, D_b^h(z/y, Q^2) \ . \tag{3.6}$$

The P_{ab} are so called splitting functions which parameterise the splitting of parton a with momentum fraction z into parton a and b, where the momentum of a reduces to y. This integro-differential equation is solved using the Mellin transformation technique, which renders convolutions (here: $\int P_{ab}^T \, D_b^h$) into products. The products can then be evolved analytically by applying an evolution operator. This evolved products are retransformed numerically by applying the inverse Mellin transformation, which yields the evolved fragmentation functions. The results depend on Q^2 via the normalisation constant and the exponents of Eq. 3.5, which now depend on the scaling variable $\bar{s}$,

$$\bar{s} \equiv \bar{s}\,(Q^2, Q_0^2) = \ln \frac{\ln(Q^2/\Lambda^2)}{\ln(Q_0^2/\Lambda^2)} \ . \tag{3.7}$$

The parameterisation (Eq. 3.5) then transforms to

$$D^\pi(z, Q^2) = N(\bar{s}) \, z^{\alpha(\bar{s})} \, (1-z)^{\beta(\bar{s})} \ . \tag{3.8}$$

In Fig. 3.6, the parameterisation of the average pion fragmentation function D^π for different values of Q^2, evolved using a recent calculation [41], is shown. The data points have been measured by the EMC [42] and show good agreement in the z range $0.15 < z < 0.7$ with the parameterisation at $Q^2 = 25$ GeV^2, which is the average Q^2 value of the EMC measurement. The deviation at low Q^2 can be accounted for by acceptance affects or by an influence from target fragmentation. The disagreement at high z can be partly due to the deviation of the measured average Q^2 at high z from the quoted overall average Q^2, which is 25 GeV^2. In particular, an earlier analysis of the EMC [43] states lower Q^2 at high z.

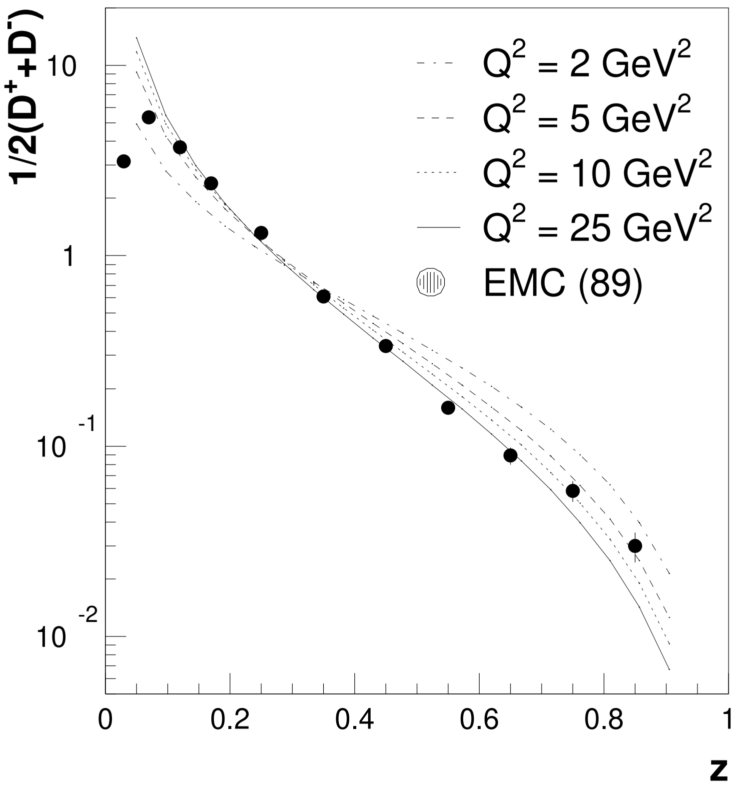

Figure 3.6: Evolution of the average fragmentation function $D^\pi = \frac{1}{2}(D^+ + D^-)$ with Q^2 according to [41]. The data of the EM Collaboration [42] at $Q^2 = 25\ \mathrm{GeV}^2$ have been overlaid.

3.4.3 Charge and Isospin Conjugation Invariance

As far as pion fragmentation is concerned, there exist 18 different fragmentation functions, since 6 quarks (u, d, s and their antiquarks) can fragment into three types of pions (π^+, π^- and π^0). For charged pions (neutral pions are difficult to detect experimentally) 12 fragmentation functions remain. Since only three differential pion cross sections on hydrogen, deuterium and ^{3}Helium have been measured at HERMES, an analysis of pion fragmentation has to reduce the number of different fragmentation functions in order to determine them from data.

The basic assumption of fragmentation in the framework of the QPM is charge and isospin invariance, that is the fragmentation of a u quark into a positively charged pion is supposed to be equal to the fragmentation of a d quark into a negatively charged pion, since in both cases the quark is a constituent of the pion. Additionally, charge symmetry relates the fragmentation of a quark/antiquark of a certain flavour into a π^+/π^-:

$$\begin{array}{lcl} q \leftrightarrow \bar{q} & : & D_q^{\pi^+} = D_{\bar{q}}^{\pi^-} \quad \text{(Charge)} \\ u \leftrightarrow d & : & D_u^{\pi^+} = D_d^{\pi^-} \\ n \leftrightarrow p & : & u_p = d_n \end{array} \left.\vphantom{\begin{array}{l} a \\ b \end{array}}\right\} \text{(Isospin)}\ . \tag{3.9}$$

Here and in the following, $D_f^h \equiv D_f^h(z)$.

The symmetry listed in the last row is not directly related to fragmentation but further simplifies the cross section formulas in the case of targets with mass $A > 1$. It does not influence the fragmentation functions if the target mass is considered in the normalization of the pion yields.

These symmetries lead to the definition of favoured (D^+) and unfavoured (D^-) fragmentation functions as already discussed in Sec. 3.3.4:

$$D^+ \equiv D_u^{\pi^+} = D_d^{\pi^-} = D_{\bar{u}}^{\pi^-} = D_{\bar{d}}^{\pi^+} \tag{3.10}$$

$$D^- \equiv D_u^{\pi^-} = D_d^{\pi^+} = D_{\bar{u}}^{\pi^+} = D_{\bar{d}}^{\pi^-} . \tag{3.11}$$

Additionally, a fragmentation function for the strange quark fragmentation has to be defined. Strange quarks are supposed to fragment differently compared to u and d quarks, but all strange fragmentation functions are assumed to be similar, that is $D_s \equiv D_s^{\pi^+} = D_s^{\pi^-} = D_{\bar{s}}^{\pi^+} = D_{\bar{s}}^{\pi^-}$.

The validity of the isospin and charge invariance as realised in the LUND Monte Carlo generator has been studied. The LUND model describes the data of many different processes in various experiments very well.

To extract fragmentation functions from the Monte Carlo, the flavour of the struck quark has to be tagged and the generated hadron distributions have to be normalized appropriately,

$$\left.\frac{1}{N_e}\frac{dN^h}{dz}\right|_{f=f'} = \left.\frac{\sum_f e_f^2 q_f(x) D_f^h(z)}{\sum_f e_f^2 q_f(x)}\right|_{f=f'} = D_{f'}^h(z) . \tag{3.12}$$

The isospin and charge invariance are studied as ratios of fragmentation functions, where charge and/or isospin are interchanged. Fig. 3.7-Fig. 3.9 show the results of the study for valence quarks, sea quarks and the ratio of valence over sea quarks. On the left side, the ratios of the favoured, and on the right, the ratios of the unfavoured fragmentation functions are shown. As it is seen, charge and isospin invariance holds for valence and for sea quarks. However, a significant difference between valence and sea quark fragmentation is observed.

3.4.4 Target and Polarisation Dependence

From the QPM assumptions, fragmentation should only depend on the intial quark and the final hadron, not on the target mass. This is certainly true as long as no nuclear effects are involved. For the targets of the HERMES experiment, hydrogen, deuterium and ^{3}Helium, nuclear effects are playing a minor rôle [44] and are neglected. Besides, the statistics of the measurement will not allow for a clear determination of those effects.

A possible dependence on the target mass can by studied by using data which has been measured with a nitrogene gas target during two weeks of data taking in 1997. An analysis is underway [45] to extract fragmentation functions from this data.

As far as polarisation is concerned, no impact on the pion fragmentation is expected from the fact that pions have no spin and zero angular momentum. For that reason, their spectrum cannot depend on the spin of the initial parton q of flavour f and

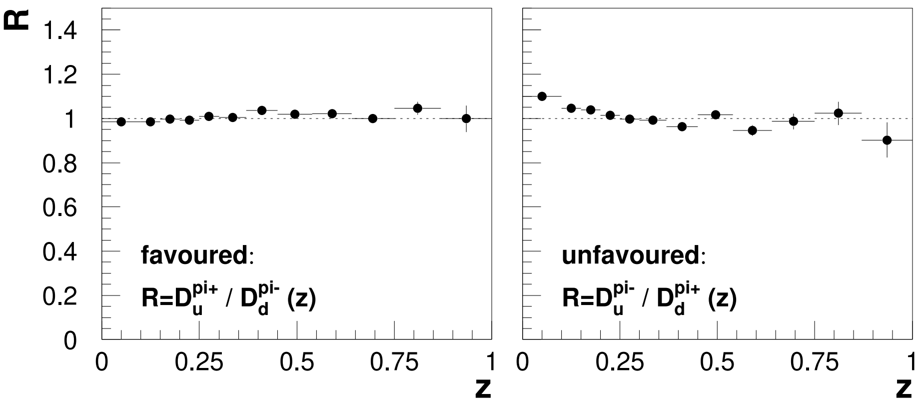

Figure 3.7: Ratio of the fragmentation functions of u- over d valence quarks into charged pions, for the favoured (left) and unfavoured (right) case.

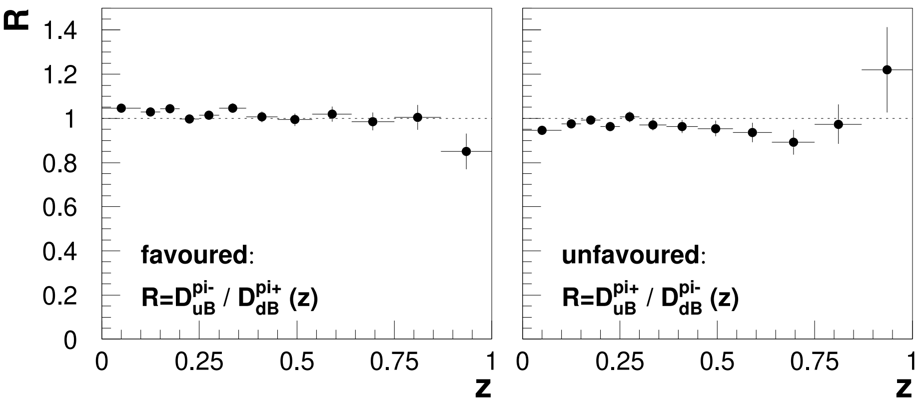

Figure 3.8: Ratio of the fragmentation functions of u- over d sea quarks into charged pions, for the favoured (left) and unfavoured (right) case.

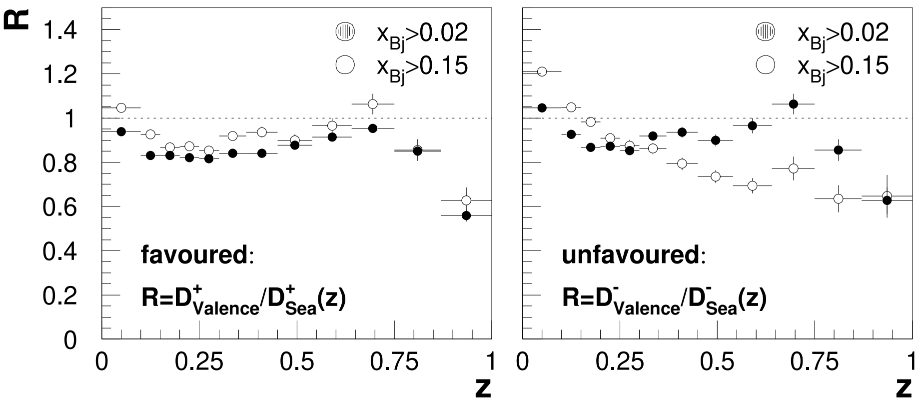

Figure 3.9: Ratio of the fragmentation functions of valence over sea quarks into charged pions, for the favoured (left) and unfavoured (right) case and two different values of the lower limit in x.

the spin dependent fragmentation function $\Delta D_f^\pi(z) = (D_{f\uparrow\uparrow}^\pi(z) - D_{f\uparrow\downarrow}^\pi(z))$ is zero. Spin dependent effects of second order like via decaying particles or via acceptance effects could play a small rôle. Since the data analysed in this work are taken with an unpolarized target, this possibility can be excluded.

3.5 The Fragmentation Function Ratio

The ratio $D^-(z)/D^+(z)$ is an interesting quantity because many influences like detector effects cancel and thus a direct comparison with other experiments or theoretical expectations can be performed. The Field and Feynman prediction [20] for the ratio of unfavoured over favoured fragmentation for independent parton fragmentation in the high energy limit has been given in Sec. 3.2.1. If the strange quarks are neglected in this model the ratio is expected to behave like

$$\frac{D^-(z)}{D^+(z)} = \frac{1-z}{1+z} \,. \tag{3.13}$$

The low and high z limits follow from simple energy conservation considerations: at $z \approx 0$, enough energy is available for $q\bar{q}$-pairs to be produced, and thus unfavoured fragmentation appears to be equally probable than favoured fragmentation, i.e. $D^-/D^+(z \to 0) = 1$. On the contrary, as $z \to 1$ no energy is left to produce such a quark pair and thus only favoured fragmentation should take place, i.e. $D^-/D^+(z \to 0) = 1$.

It should be mentioned, that this behaviour of D^-/D^+ at very low and very high z does not depend on neglecting the strange quarks. In general, this behaviour does not depend on the creation probability of a quark-antiquark pair of flavour u, d or s (denoted by the symbol γ in Eq. 3.3).

In Fig. 3.10, the ratios of unfavoured over favoured fragmentation function as realised in a Monte Carlo simulation using the LUND model, a Monte Carlo using independent fragmentation and as naïvely expected from independent fragmentation (Eq. 3.13) is shown. The models are implemented in the same software package JETSET [22], where they can be chosen by a program switch. The decay mechanism is the same in both cases, as well as the program "frame" which chooses the kinematics and calculates the event weights, etc. In the case of the LUND model, the symmetric LUND distribution function has been used. The parameters of the LUND model (describing the string breaking properties) were adjusted to the hadron spectra measured at HERMES (see Sec. 6.4.2). The impact on the ratio of the difference between the default and the so "tuned" parameters has been determined to be less than 5%. In the case of independent fragmentation, the Field and Feynman fragmentation distribution function (Eq. 3.2) has been chosen with the default parameter (see Sec. 3.2.1). This leads to a consistent comparison between the two models.

Remarkable differences between the ratio as simulated by the LUND model and by independent fragmentation exist. The behaviour of the simulated ratio at small z indicates a limitation in the number of string breakings at the relatively low HERMES

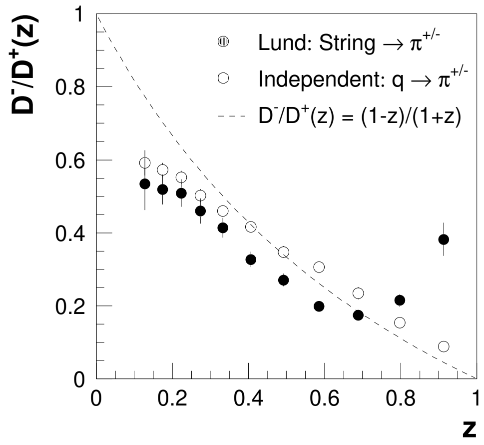

Figure 3.10: The ratio $D^-(z)/D^+(z)$ for pion fragmentation, from the LUND and the independent fragmentation model No decays products are included.

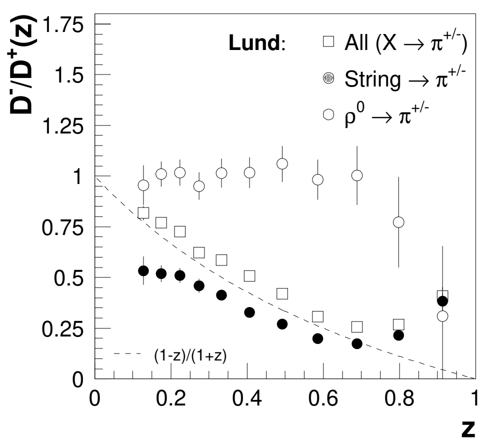

Figure 3.11: The fragmentation function ratio, simulated with the LUND model. The different behaviour for different origins of the pions can be seen, see text.

energies. This causes to limit the ratio as well. At high z, the ratio of the simulation of independent fragmentation generates follows the expected trend to zero for $z \to 1$ while the ratio which is generated by the LUND model increases at high z. This behaviour is not yet understood.

In Fig. 3.11, the impact of the origin of the pions can be seen. If the pions are directly produced from fragmentation, the ratio follows the naïvely expected trend, at least for $z < 0.8$. However, as soon as a ρ^0 is produced which then decays further into pions, the unfavoured and favoured fragmentation functions of those pions are approximately equal. Since the fraction of pions from ρ^0 decays is not negligible this influences the ratio significantly. In the case of HERMES, the fraction of charged pions from ρ^0 decay accounts to approximately 15%.

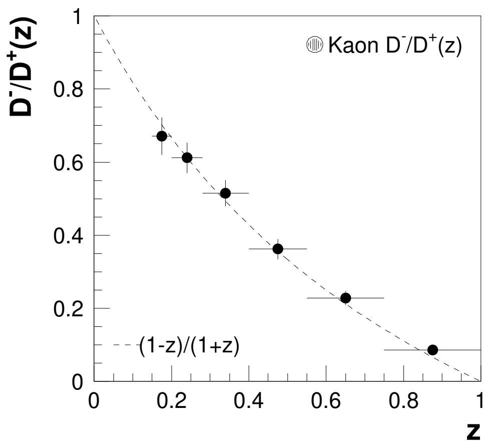

Figure 3.12: The ratio of unfavoured over favoured Kaon fragmentation simulated with the LUND model. Overlaying is the naïve expectation for independent fragmentation (dashed line).

For comparison the fragmentation behaviour of kaons in the present Monte Carlo simulation can be studied. Only a small fraction of kaons are decay products. The result of the study can be seen in Fig. 3.12. The steady decrease of the ratio of unfavoured over favoured kaon fragmentation to zero as $z \to 1$ is the expected behaviour for the ratio in the case of independent parton fragmentation.

3.6 Existing Measurements

A very good tool to probe the fragmentation process is e^+e^--annihilation, since the $q\bar{q}$-pair is created without additional effects from spectator processes, target remnant interactions or nuclear matter dependences. As already pointed out only the average fragmentation function can be measured.

In Fig. 3.13, the normalised charged hadron production cross-sections which are just the average fragmentation functions are plotted as a function of the relative jet energy z. Fig. 3.13 is a compilation of measured charged hadron spectra from LEP and other e^+e^--annihilation experiments at lower energies like the TPC [36] or TASSO [47] collaboration. The figure is originating from an analysis of scaling violations in e^+e^--fragmentation functions [46]. As it is seen, a fit on data measured at LEP energies ($\sqrt{s}$ = 91.2 GeV) successfully describes data at other energies when evolved to that particular scale.

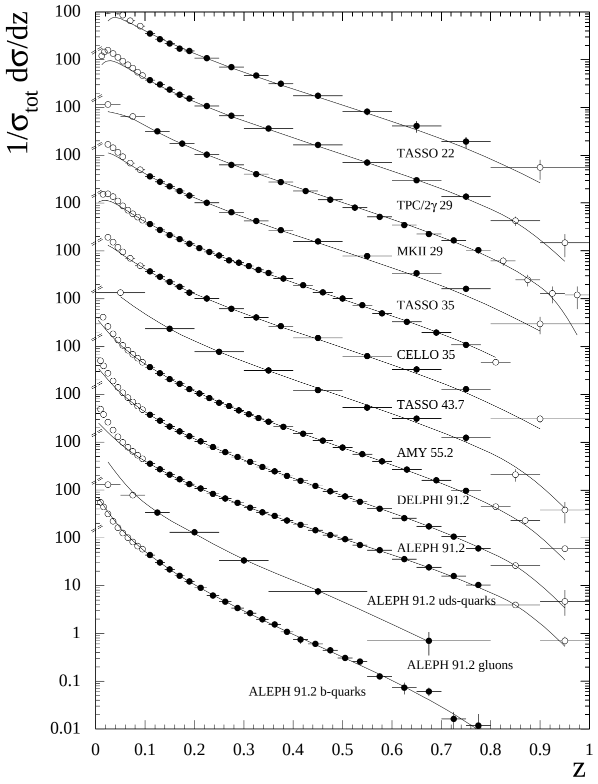

Figure 3.13: Fragmentation function analysis by the ALEPH Collaboration [46]

The only measurement of fragmentation functions in DIS has been performed by the EMC. In Fig. 3.14, the favoured and unfavoured extracted pion fragmentation functions from [43] (1985) and from [42] (1989) are shown. The two measurements, which agree very well, correspond to two different extraction methods which are also applied in this analysis (Sec. 5). In Fig. 3.15, the favoured and unfavoured kaon fragmentation functions are shown [42]. The D^K/D^π ratio raises from ≈ 0.15 at $z = 0.2$ to 0.4 at $z = 0.8$.

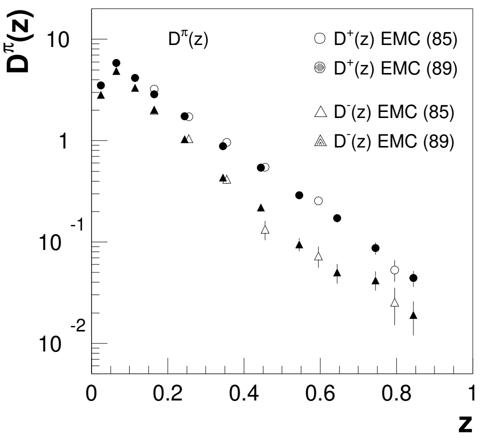

Figure 3.14: Favoured ($D^{+}(z)$) and unfavoured ($D^{-}(z)$) pion fragmentation functions as measured by the EMC.

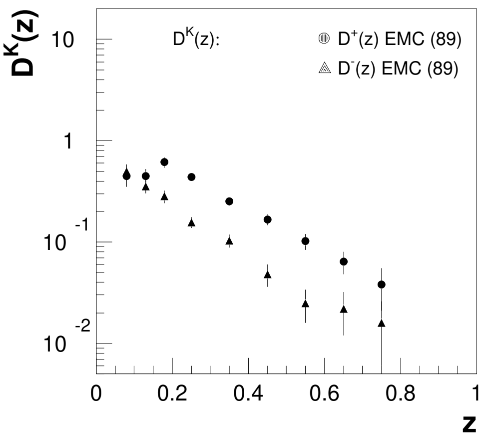

Figure 3.15: Favoured and unfavoured kaon fragmentation functions extracted by the EMC.

4 The Experimental Setup of HERMES

The HERMES experiment at the HERA proton positron collider has been designed to study the spin structure of the nucleon. HERMES measures the inclusive and semi-inclusive spin dependent deep-inelastic scattering of polarised 27.5 GeV positrons off polarised nucleons with a forward spectrometer. Two novel techniques are employed, the spin rotation of the transversely polarised positrons in the HERA positron storage ring into longitudinal polarisation at the HERMES experimental site and the usage of internal polarised gas targets in the positron beam. The spectrometer is described in detail in [48]. First results on the spin structure function of the neutron $g_1^n(x)$ have recently been published [49].

Additionally, the HERMES detector allows to study diffractive vector meson production, to test SU(3) flavour symmetry by measuring the spin transfer to the self analysing Λ [50] and to do several measurements with unpolarised targets. In particular, the latter covers a determination of the flavour symmetry of the light quark sea.

4.1 The Beam

HERMES utilises the 27.5 GeV positron beam of the HERA proton positron collider. The apparatus is installed in the east straight section of HERA, three other experiments are located in the north (H1), south (ZEUS) and west (HERA-B) sections, see Fig. 4.1.

The positrons in the HERA positron beam are transversely polarised due to the Sokolov-Ternov effect. In order to obtain longitudinal polarisation, spin rotators have been installed before and after the HERMES experimental area. The polarisation is measured by Compton backscattering of circularly polarised laser light off the beam positrons. The average polarisation in 1995 and 1996 was $\approx 55\%$ with an overall relative systematic error of 5.4%.

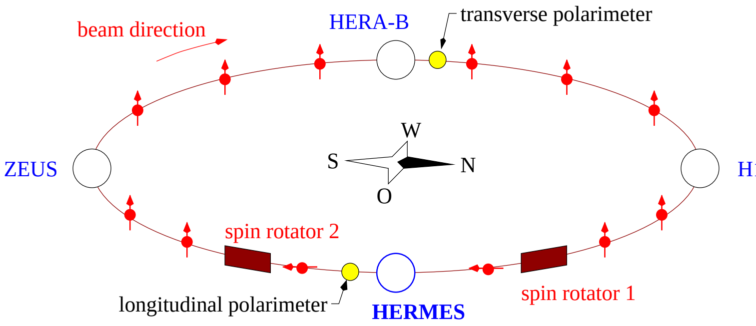

Figure 4.1: The HERA proton positron collider at DESY. Shown are the sites of the four experiments and the direction and polarisation of the positrons. Two polarimeters are measuring the beam polarisation.

4.2 The Internal Gas Target

The internal polarised gas target consists of a T-shaped storage cell [51]. The gas enters the pipe from the middle and diffuses to the ends where pumps are exhausting, see Fig. 4.2. The advantages of this concept are high density, no target window, and no dilution due to pure atomic species. In 1995, the target gas was ^{3}Helium in order to measure the spin structure function $g_1^n(x)$. The ^{3}Helium ground state atoms were polarised by spin exchange collisions with the metastable ^{3}S state, which in turn was produced via optical pumping. Metastability exchange collisions transfer the polarisation to the nucleus. The target areal density of 10^{15}nucl/cm^2 had to be limited in order not to reduce the beam lifetime significantly. Two polarisation measurements have been performed, in the pumping cell and in the storage cell. The average polarisation was 46% with a fractional error of 5% and reversed every 10 minutes to minimise systematic influences.

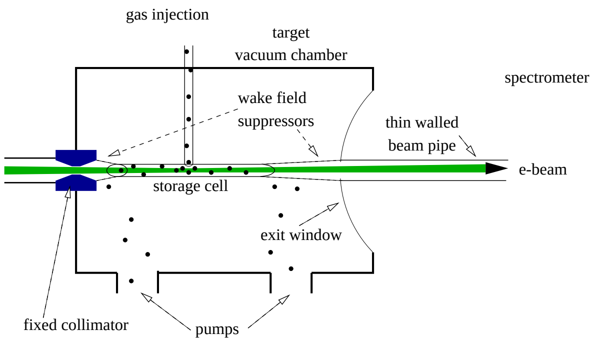

Figure 4.2: The internal storage cell target of HERMES.

In 1996, the target was replaced by a hydrogen atomic beam source (ABS) in conjunction with a Breit Rabi polarimeter [52]. With this setup, a target density of $7 \cdot 10^{13}$nucl/cm^2 and an average polarisation of 90% could be reached. The target polarisation was reversed every 45 seconds.

This thesis is based on the data taken in 1996 on unpolarised hydrogen, deuterium and ^{3}Helium. The target thickness was 10^{15}nucl/cm^2, again limited by the influence in the beam lifetime.

4.3 The Spectrometer

The HERMES apparatus is a forward spectrometer, equipped with a dipole magnet with an integrated field strength of 1.3 Tm and 36 Planes of microstrip gas and drift tracking chambers, see Fig. 4.3. The angular acceptance ranges between 40 and 220 mrad. With a fast track reconstruction algorithm [53] the momentum resolution was $\Delta P/P \approx 1-2\%$ and the angular resolution was $\Delta\theta \approx 0.6$ mrad. For particle identification

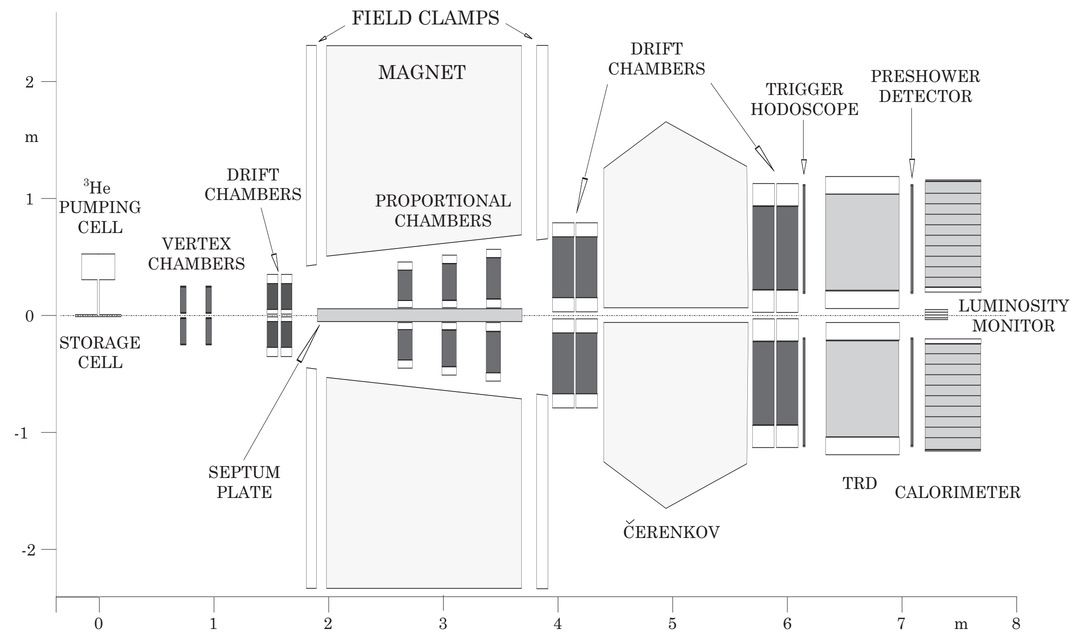

Figure 4.3: Schematic drawing of the HERMES spectrometer, side view

(PID) purposes four detectors are used:

- a threshold Čerenkov counter, filled with nitrogen and C_4F_{10} gas. In order to emit Čerenkov radiation, particles must have a relativistic γ above the threshold $\gamma_t = (\sqrt{1-n^{-2}})^{-1}$, where n is the refraction index of the gas. This corresponds to a momentum of 15 MeV for electrons, 4 GeV for pions and 14.13 GeV for kaons.
- a transition radiation detector (TRD), based on the photon emission from particles with high relativistic γ, i.e. electrons, when traversing layers with different refraction index,
- a preshower counter, consisting of a thin lead shield in front of a hodoscope to separate photons from electrons, which produce an electromagnetic shower,
- and an electromagnetic calorimeter, build from 840 lead glass blocks of 18 radiation lengths each, to separate electrons from hadrons by their deposited energy.

The configuration is optimised to discriminate hadrons against electrons. Combining the responses of the different PID detectors with a likelihood method yields a positron efficiency $> 99\%$ and a hadron contamination $< 1\%$. In the momentum window between 4 and 14 GeV, pions can be separated from protons and kaons.

A detailed description of the components of the spectrometer is given in [54] and [55].

4.4 Acceptance and DIS Kinematics

The geometric acceptance of HERMES is primarily constrained by the septum plate, which shields the positron and proton beams of HERA from the magnetic field, as shown in Fig. 4.3. This leads to a lower limit on the acceptance for the scattering angle of $\theta_{min} = 40$ mrad and limits the kinematics. With the incident positron energy of 27.5 GeV, the range of the accessible DIS kinematics is constrained as summarised below:

scattering angle	θ_{min}	=	40 mrad	θ_{max}	=	220 mrad
Q^2	Q^2_{min}	=	0.2 GeV^2	Q^2_{max}	=	20 GeV^2
x_{Bj}	$x_{Bj\,\mathrm{min}}$	=	0.01			
W^2	W^2_{max}	=	45 GeV^2			

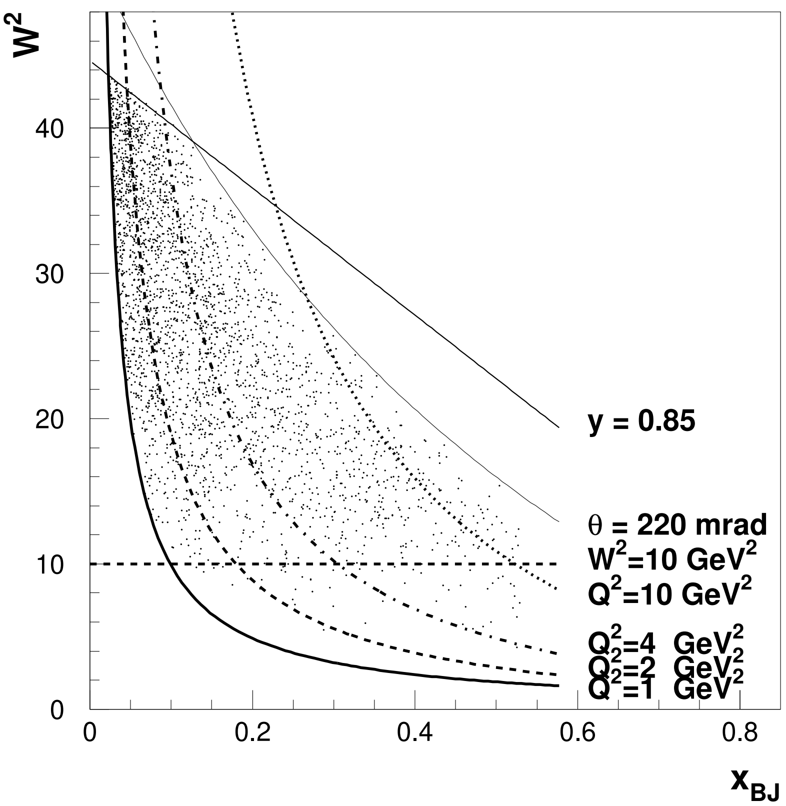

Figure 4.4: The kinematc acceptance of HERMES in the $x_{Bj} - W^2$ plane with iso-Q^2 lines. The $y = 0.85$ line denotes the lower limit of the positron energy, the horizontal, dashed $W^2 = 10$ GeV^2 line is the cut applied to the events during this analysis and the maximal scattering angle is illustrated by the $\theta_{\mathrm{max}} = 220$ mrad curve.

The acceptance in the event kinematics is shown in Fig. 4.4. Shown are events in the plane of x versus W^2, where the lines of constant Q^2 are superimposed.

5 Extraction Methods for the Fragmentation Functions

In this section, the expressions for the determination of the fragmentation functions from the hadronic differential cross section for different targets will be given. Two different equations for the favoured and unfavoured fragmentation functions are deduced, corresponding to two different methods for the extraction of the fragmentation functions from measured hadron distributions.

The first method, denoted "extraction method (I)" in this thesis, corresponds to a method used in the first of two publications from the EMC [43]. In the case of a deuterium target, the fragmentation function formula simplifies and becomes independent of x. The favoured and the unfavoured fragmentation functions can then be extracted without further assumptions on the quark distributions. However, as this method neglects any contribution from the sea quarks, the result is only valid for high values of x or has to be corrected for the influence of the sea.

The second method, labeled "extraction method (II)", is based on the second publication from the EMC [42] and is valid for all targets. Quark density parameterisations have to be used, which are taken from other experiments, for example MRS(A) [56], GRV [57] or CTEQ [58] parameterisations. The fragmentation functions can then be extracted without further assumptions.

5.1 The Simple Way: Extraction Method I

Though this extraction method is restricted to a deuterium target, a set of general equations which are valid for all targets shall be derived first. This way, the major advantage of a deuterium compared to other targets can be illustrated: In the case of deuterium, the x-dependence reduces to a constant and the equation is suitable for the fragmentation function extraction. The approximations will however become important.

In the following, the quark momentum distributions are separated into valence and sea quark distributions, i.e.

$$\left.\begin{array}{rrcl} & q(x) & = & q_V(x)+q_S(x) \\ \text{where} & q_V(x) & = & q(x)-\bar{q}(x) \end{array}\right\} \quad \Leftrightarrow \quad q_S(x)=\bar{q}(x) \tag{5.1}$$

with $q(x) = u(x), d(x)$. The quark distributions are abbreviated $q \equiv q(x)$ with $q = u, d, s$ and charge symmetry of the sea will be implied, $q_S + \bar{q} = 2\bar{q}$.

The main QPM assumption of charge and isospin conjugation invariance concerns the fragmentation functions itself. As pointed out in Sec. 3.4.3, this assumption is necessary to combine unfavoured and favoured fragmentation functions $D^+(z)$ and $D^-(z)$ from the various fragmentation functions $D_f^{\pi^\pm}(z)$. It is the necessary prerequisite to extract the fragmentation functions from measured pion spectra. The impact of the QPM assumtion on the result is however large and will be determined to $2-10\%$ in Sec. 6.5.

Rewriting the differential normalised charged pion rates $(1/N_e)\, N_A^+ \equiv (1/N_e)\, \mathrm{d}N_A^{\pi^\pm}/\mathrm{d}z$ for a target of mass A with Z protons and N neutrons, $A = Z + N$, according to the QPM cross section formula (Eq. 2.7) yields

$$\frac{1}{N_e}\, N_A^+ \;=\; \frac{(1/9A)\Big[4(Zu_V + Nd_V)D^+ + (Zd_V + Nu_V)D^-\Big] + S^+}{(1/9A)\Big[(4Z+N)u_V + (4Z+N)d_V\Big] + S}\,, \tag{5.2}$$

$$\begin{aligned} \text{with} \quad S^+ &= (1/9)\,\Big[\,4(u_S D^+ + \bar{u}D^-) + (d_S D^- + \bar{d}D^+) + (s_S + \bar{s})D^-\Big] \\ &= (1/9)\,\Big[\,(4\bar{u} + \bar{d})(D^+ + D^-) + 2\bar{s}D^-\Big] \end{aligned} \tag{5.3}$$

$$\text{and} \qquad S \;=\; (2/9)(4\bar{u} + \bar{d} + \bar{s})\,, \tag{5.4}$$

where the sea quark distributions are averaged over the nucleus and assumed to be the same for all A. The quark distributions are always referring to the proton, i.e. the d quark distribution in the neutron is identical to the u quark distribution in the proton, $u \equiv u^p = d^n$ and $d \equiv d^p = u^n$. Additionally, the assumption $D^s = D^-$ has been made.

The normalised differential π^- rate $(1/N_e)\, N_A^-$ is the same as for π^+, except that D^+ and D^- are interchanged for all non-strange quarks. The fragmentation of the sea quarks into π^- is the same as into π^+. The denominator of Eq. 5.2 is just $(1/x)$ times the structure function F_2^A of a nucleus of mass A,

$$(1/9A)\,\Big[\,(4Z+N)u_V + (4Z+N)d_V\Big] + S \;=\; (1/x)\, F_2^A\,.$$

The sum and the difference of the charged pion rates are expressions of the sum and the difference of D^+ and D^- only:

$$\begin{aligned} \frac{1}{N_e}\,(N_A^+ + N_A^-) &= \frac{(1/9A)\,\Big[\,(4Z+N)u_V + (4Z+N)d_V\Big] + S}{(1/x)\, F_2^A}\,\Big((1-C_s)D^+ + D^-\Big) \\ &\approx (D^+ + D^-)\,, \end{aligned} \tag{5.5}$$

$$\text{with} \quad C_s \;=\; \frac{(2/9)\,\bar{s}}{(1/x)\, F_2^A} \ll 1 \quad \text{and} \tag{5.6}$$

$$\frac{1}{N_e}\,(N_A^+ - N_A^-) \;=\; \frac{(1/9A)\,\Big[\,(4Z-N)u_V + (4N-Z)d_V\Big]}{(1/x)\, F_2^A}\,(D^+ - D^-)\,. \tag{5.7}$$

Two remarkable properties of Eq. 5.5 and Eq. 5.7 can be observed. First, if the strange quarks are neglected, the sum of the charged pion rates and the sum of the favoured and unfavoured fragmentation functions are an equality and independent of any parton distribution. Second (as it has already been mentioned above), the sea quark fragmentation cancels in performing the difference of the pion rates.

The amount of the strange sea, $2s$, is less than 3.5% for $x \approx 0.15$ and falling rapidly with increasing x. However this "correction" enters the favoured (D^+) and unfavoured (D^-) fragmentation functions in a different way and thus has an impact on the fragmentation function ratio. This is caused by the fact that pions have no strange quark content, but the sea of the nucleus is (approximately) $SU(3)$ flavour symmetric. The integral influence on D^+ and D^- is 1% and on the ratio D^-/D^+ is $< 2.4\%$. In the following, the strange sea will be ignored for simplicity, but it will be taken into account as a correction when extracting the fragmentation functions with method (I).

With the neglect of strange quarks, D^+ and D^- can now be written as follows,

$$D^+ = \frac{1}{2N_e}\left[\,(1+F_A)N_A^+ + (1-F_A)N_A^-\,\right] \tag{5.8}$$

$$D^- = \frac{1}{2N_e}\left[\,(1-F_A)N_A^+ + (1+F_A)N_A^-\,\right], \tag{5.9}$$

$$\text{with} \quad F_A = \frac{\frac{1}{x}F_2^A}{(1/9A)\left[(4Z-N)u_V + (4N-Z)d_V\right]}\,. \tag{5.10}$$

In particular, F_A becomes in the case of

$$\text{hydrogen:} \quad F_p = \frac{\frac{1}{x}F_2^p}{(1/9)\,(4u_V - d_V)}\,, \tag{5.11}$$

$$\text{deuterium:} \quad F_D = \frac{\frac{1}{x}F_2^D}{(3/18)\,(u_V + d_V)} = \frac{5}{3} + \frac{S}{3/18\,(u_V+d_V)} \tag{5.12}$$

$$\text{and } {}^3\text{Helium:} \quad F_{^3He} = \frac{\frac{1}{x}F_2^{^3He}}{(1/27)\,(7u_V + 2d_V)}\,. \tag{5.13}$$

This shows directly the advantage of an isoscalar target, where $Z = N$. When neglecting sea quarks, the fragmentation functions become independent of the quark distributions which reduce to a factor independent of x, i.e. $F_D = 5/3$. Inserting this into Eq. 5.8 and Eq. 5.9, yields a simple, x-independent expression for D^+ and D^- on a deuterium target,

$$D^{\pm} = \frac{1}{N_e}\frac{1}{3}(\,4N^{\pm}\; - \;N^{\mp}\,)\,. \tag{5.14}$$

The ratio $D^-(z)/D^+(z)$ is just a function of N^+/N^-,

$$D^-/D^+ = \frac{4\; - \;N^+/N^-}{4N^+/N^-\; - \;1}\,. \tag{5.15}$$

This shows, that the fragmentation functions of the light quarks can be extracted without further knowledge of the quark distributions. However, gluons and sea quarks distort this simple picture. Experimentally, the sea quarks can be suppressed by applying a lower cut on x. A cut at $x = 0.15$ for example reduces the amount of sea quarks in the cross section to less than 10%.

The influence on the fragmentation function is larger, as it can be seen from Eq. 5.8 and Eq. 5.9, where the factor F_D conributes with opposite sign to D^+ and D^-. Since the impact on the favoured and unfavoured fragmentation functions is also different, it has a significant impact on the ratio $D^-(z)/D^+(z)$. The necessary correction will be determined from a detailed Monte Carlo simulation (see Sec. 5.3).

To summarise, the following assumptions and approximations have been made in the derivation of method (I) (Eq. 5.14):

The Simple Way: Method I	
Approximations/assumptions:	Systematic influence on D^+ and D^-:
All targets:	
Isospin symmetry between n and p:	No influence.
Charge and isospin symmetry of the fragmentation between u and d:	Between 2% ($z \approx 0.5$) and 10% ($z \to 1$).
Neglect of the strange quarks:	Impact on D^+ and D^- is $\approx 1\%$, for the ratio D^-/D^+ it is $< 2.5\%$.
Deuterium only:	
Neglect of all sea quarks:	Large impact, up to 25%. This has been corrected for (see Sec. 5.3).

For the estimate on the values in this table, the same kinematic limits as used for the extraction of the results of method (I) have been taken, i.e. $x > 0.15$ and $W^2 > 10\ \mathrm{GeV}^2$.

5.2 The Direct Way: Extraction Method II

A different method to extract fragmentation functions from the measured normalised pion spectra, here called extraction method (II), makes use of parameterisations of the parton density functions (PDF). The fragmentation functions can then directly be extracted from Eq. 5.8 and Eq. 5.9 by explicitly calculating the factors F_A (Eq. 5.10). This shall be done in a more general way below.

This second approach does not neglect any quark distributions, but the assumption of the validity of isospin symmetry between neutron and proton is made, as in method (I). Also, the isospin and charge conjugation invariance of the fragmentation functions is assumed. This has already been mentioned in the previous section and turned out to be the major contribution to systematic uncertainties besides the sea correction. Its influence will be estimated in Sec. 6.5.

The following general formula for the normalised differential pion rates $(1/N_e)\, N_A^+$ and $(1/N_e)\, N_A^-$ of the scattering on a target of mass A with Z protons and N neutrons can be derived from Eq. 5.2:

$$\frac{1}{N_e}\begin{pmatrix} N_A^+ \\ N_A^- \end{pmatrix} = \begin{pmatrix} b_{11}^A & b_{12}^A \\ b_{21}^A & b_{22}^A \end{pmatrix}\begin{pmatrix} D^+ \\ D^- \end{pmatrix} . \tag{5.16}$$

The above 2×2 matrix $\mathbf{B}_A$ has then the following elements:

$$\begin{aligned} b_{11}^A &= R_A\left(4Zu{+}4Nd{+}\ N\bar{u}{+}\ Z\bar{d}\right) \\ b_{12}^A &= R_A\left(\ Nu{+}\ \ Zd{+}4Z\bar{u}{+}4N\bar{d}+(Z+N)(s+\bar{s})\right) \\ b_{21}^A &= R_A\left(\ Nu{+}\ \ Zd{+}4Z\bar{u}{+}4N\bar{d}\right) \\ b_{22}^A &= R_A\left(4Zu{+}4Nd{+}\ N\bar{u}{+}\ Z\bar{d}+(Z+N)(s+\bar{s})\right) \end{aligned} \tag{5.17}$$

with $R_A = \dfrac{1}{9A}\,\dfrac{x}{F_2^A}$.

The equation system can be solved for D^+ and D^- by inverting $\mathbf{B}_A$:

$$\begin{pmatrix} D^+ \\ D^- \end{pmatrix} = \mathbf{C}_A\,\frac{1}{N_e}\begin{pmatrix} N_A^+ \\ N_A^- \end{pmatrix} , \tag{5.18}$$

$$\text{with}\quad \mathbf{C}_A = \mathbf{B}_A^{-1} = \frac{1}{|\mathbf{B}_A|}\begin{pmatrix} b_{22}^A & -b_{12}^A \\ -b_{21}^A & b_{11}^A\ . \end{pmatrix} \tag{5.19}$$

The matrix elements of $\mathbf{C}_A$ are for

Hydrogen:

$$\begin{aligned} c_{11}^H &= \ \ R'_A\left(4u{+}\ \bar{d}+s+\bar{s}\right) \\ c_{12}^H &= -R'_A\left(\ \ d{+}4\bar{u}\right) \\ c_{21}^H &= -R'_A\left(\ \ d{+}4\bar{u}+s+\bar{s}\right) \\ c_{22}^H &= \ \ R'_A\left(4u{+}\ \bar{d}\right) \end{aligned} \tag{5.20}$$

Deuterium:

$$\begin{aligned} c_{11}^D &= \ \ R'_A\left(4u{+}4d{+}\ \ \bar{u}{+}\ \bar{d}+2(s+\bar{s})\right) \\ c_{12}^D &= -R'_A\left(\ \ u{+}\ \ d{+}4\bar{u}{+}4\bar{d}\right) \\ c_{21}^D &= -R'_A\left(\ \ u{+}\ \ d{+}4\bar{u}{+}4\bar{d}+2(s+\bar{s})\right) \\ c_{22}^D &= \ \ R'_A\left(4u{+}4d{+}\ \ \bar{u}{+}\ \bar{d}\right) \end{aligned} \tag{5.21}$$

^{3}Helium:

$$\begin{aligned} c_{11}^{^3He} &= R'_A\left(8u{+}4d{+}\ \bar{u}{+}2\bar{d}+3(s+\bar{s})\right)\\ c_{12}^{^3He} &= -R'_A\left(\ \ u{+}2d{+}8\bar{u}{+}4\bar{d}\right)\\ c_{21}^{^3He} &= -R'_A\left(\ \ u{+}2d{+}8\bar{u}{+}4\bar{d}+3(s+\bar{s})\right)\\ c_{22}^{^3He} &= R'_A\left(8u{+}4d{+}\ \bar{u}{+}2\bar{d}\right) \end{aligned} \tag{5.22}$$

with $R'_A = \dfrac{1}{9A}\dfrac{x}{F_2^A}\dfrac{1}{|\mathbf{B}_A|}$.

The quark distributions which have been chosen to calculate these matix elements are NLO parameterisations from M. Glück, E. Reya and A. Vogt (GRV) in the $\overline{MS}$ renormalisation scheme [57] and have been taken from the parton distribution function library PDFLIB [59]. The GRV parameterisation has been chosen because of its validity down to $Q^2_{min} = 0.4$ GeV^2 which is suitable for the HERMES data, where $Q^2_{min} =$ 1 GeV^2.

It is now interesting to compare these matrix elements and their x- and z-dependence to the equaivalent expressions derived for method (I), formulas 5.8 - 5.10.

The matrix elements c_{11} and c_{22}, as well as the elements c_{12} and c_{21} are forming pairs which differ only in the strange distributions. As discussed above, these amount to less than 3.5%. It is therefore sufficient to restrict the following study to the elements c_{11} and c_{12}.

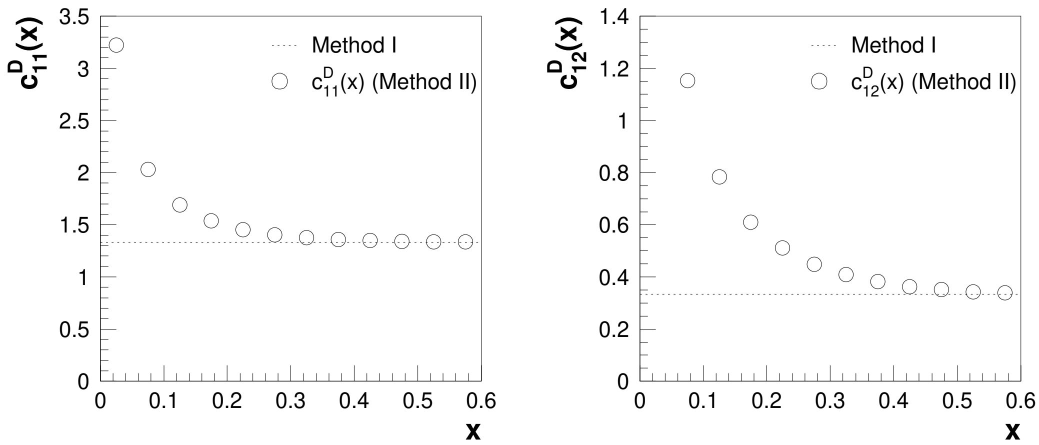

Figure 5.1: The x-dependence of the matrix elements c_{11} and c_{12} for deuterium. The dashed line corresponds to method (I), where the contribution of the sea quarks is neglected. For $x \approx 0.3 - 0.4$, this approximation is best.

In Fig. 5.1, the x-dependence of c^D_{11} and c^D_{12} is shown. The dashed line corresponds to the case without sea contribution, as it has been assumed in method (I). It is obvious, that this simple, first approach is only approximately fulfilled at $x > 0.2 - 0.3$, where the relative amount of sea quarks is small. It is thus possible to use method (I) by discarding semi-inclusive DIS events with $x < 0.15$. However, since the cross section is increasing with $1/x$, such a cut rejects a lot of the event statistics. If one wants to use the full statistics a large correction has to be applied. Even for $x > 0.15$ this correction is not negligible (see Sec. 5.3).

In order to discuss the impact of the x-dependence of the matrix elements c_{ij} on the fragmentation functions, the mean x of hadrons with fractional energy z has to be determined. The mean x from pions between 4 and 13.5 GeV for two different lower limits in x can be seen in Fig. 5.2. The cuts on x have been chosen in the way, that the lower value ($x > 0.02$) selects all DIS events, which are within the acceptance of HERMES. The higher cut ($x > 0.15$) is chosen as for method (I) to allow for a comparison. A correlation between the average x and z is seen for all events, i.e.

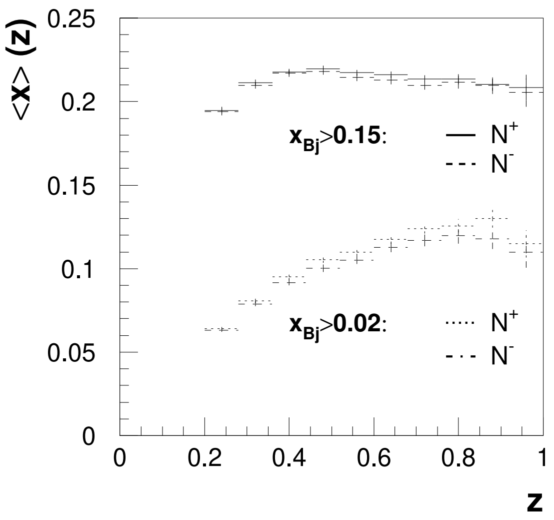

Figure 5.2: The mean x of the HERMES coincident pions, with $4 < P_\pi < 13.5$ GeV versus x. Two different samples are shown, having a lower x cut of $x > 0.02$ or $x > 0.15$, respectively.

for $x > 0.02$. This can be explained with the correlation of x and Q^2 in the HERMES acceptance. Due to $W^2 = M^2 + Q^1(1/x - 1)$, W^2 is correlated with x, too. A smaller value of x accounts for a higher W^2 and thus for a higher multiplicity. A higher multiplicity leads - on average - to smaller fractional energies z.

The weak z-dependence of the average x of semi-inclusive events above $x = 0.15$ leads to the weak z-dependence of the matrix elements c_{11} and c_{12} as shown in Fig. 5.3. In addition, the x-dependence of the matrix elements at $x \approx 0.2 - 0.25$ is weak, too. From this the approximate independence of the matrix elements with z can be understood.

The comparison with method (I) is denoted by the dashed line in the figure. This will be further discussed below (Sec. 5.4). The diagonal matrix elements c_{11} and c_{22} are both valence dominated, the elements c_{12} and c_{21} however are sea dominated. The discrepancy between the values of c_{12} and the dashed line denotes the correction factor for method (I).

As in the previous chapter, the impact of the approximations and assumptions on the result, by using method (II), are summarised in the following table:

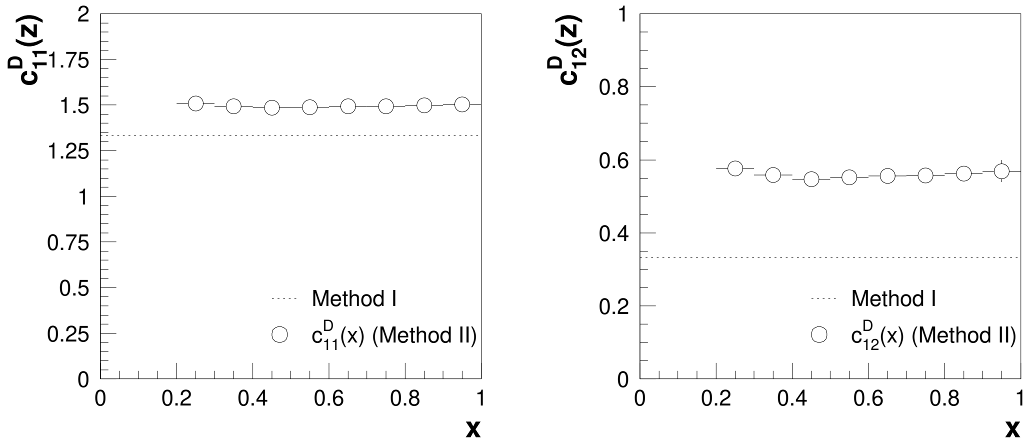

Figure 5.3: The z-dependence of the matrix elements c_{11} and c_{12} for deuterium, evaluated at the mean x of pions with fractional energy z. A cut of $x > 0.15$ has been applied. The dashed line corresponds to method I.

The Direct Way: Method II	
Approximations/assumptions:	Systematic influence on D^+ and D^-:
Isospin symmetry between n and p:	No influence.
Charge and isospin symmetry of the fragmentation between u and d:	Between 2% ($z \approx 0.5$) and 10% ($z \to 1$).
Strange quark fragmentation $D_s \approx D^-$:	Negligible influence ($\ll 1\%$).

The influences on method (II) are negligible except for the assumption of isospin- and charge conjugation invariance, which will be estimated in Sec. 6.5. The uncertainty of the parton density parameterisations will be evaluated there as well.

5.3 The Sea Quark Correction for Method I

In the derivation of extraction method (I), the contribution of the sea quarks to the pion fragmentation functions has been neglected. This is the only way to extract the D^+ and D^- fragmentation functions without any further (necessarily model dependent) input. The extracted fragmentation functions will however deviate from the "real" fragmentation functions due to the neglected sea quark contribution especially at low x.

Even with a reduction of the sensitivity to the quark sea by applying a lower cut on x a correction will be necessary. An analytical expression for the correction could be dervied and evaluated using PDFs. This is however equivalent to method (II). Therefore, the correction will be extracted with a Monte Carlo technique.

The correction is determined by comparing the fragmentation functions $D^{\pm}_{M1}(z)$ from a Monte Carlo simulation, extracted by using Eq. 5.14, with the "real", i.e. generated fragmentation functions $D^{\pm}_{Gen.}(z)$ as represented in the fragmentation model of the Monte Carlo generator:

$$C^{\pm}_{Sea}(z) = \frac{D^{\pm}_{Gen.}(z)}{D^{\pm}_{M1}(z)} \ . \tag{5.23}$$

In this way, the influence of the extraction method on the result can be determined. The dependence on the fragmentation model mostly cancels in performing the ratio. A remaining systematic dependence is estimated in Sec. 6.5.

In Fig. 5.4 the comparison between the generated ($D_{Gen.}(z)$) and extracted ($D_{M1}(z)$) fragmentation functions is shown. The ratio of the two fragmentation functions, i.e.

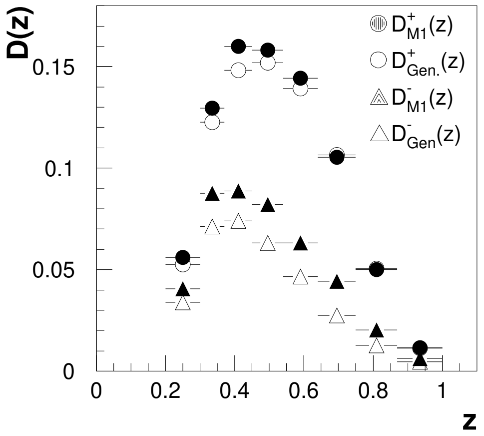

Figure 5.4: Comparison of the extracted and generated fragmentation functions.

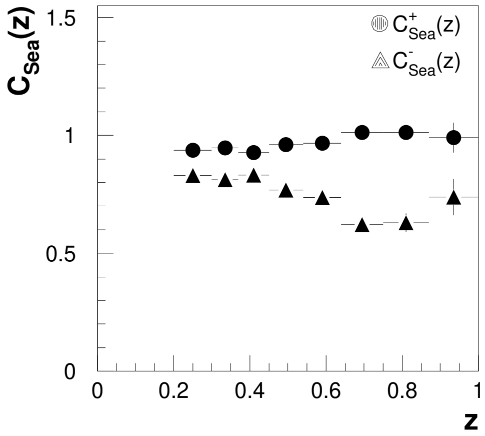

Figure 5.5: The ratio of the generated over the extracted fragmentation functions in Fig. 5.4 yields the sea correction factor $C_{Sea}(z)$.

the correction factor, is plotted in Fig. 5.5.

From the Eq. 5.8, Eq. 5.9 and Eq. 5.12, the contribution of the light quark sea ($\bar{u}$, $\bar{d}$) to the favoured and unfavoured fragmentation functions is about equal. However, in Fig. 5.5, the sea correction for the unfavoured fragmentation is significantly larger. The reason for the larger correction is the strange sea, which only contributes to $D^{-}(z)$.

5.4 Comparison of Method I and Method II

The two extraction methods derived above will be compared in this section. First, the equivalence between the two methods in the case of a deuterium target, where the sea quarks are neglected, is explicitly shown. Then, the differences after the consideration of sea quarks are quantified.

A comparison of Eq. 5.18 (method II) with Eq. 5.14 (method I) reveals the correspondance between

Method I	Method II
4/3	$\lvert c_{11}^{D}\rvert$, $\lvert c_{22}^{D}\rvert$
1/3	$\lvert c_{12}^{D}\rvert$, $\lvert c_{12}^{D}\rvert$.

Neglecting the sea quark densities in the case of the second method must yield $c_{11}^{v,D} = c_{22}^{v,D} = 4/3$ and $c_{12}^{v,D} = c_{21}^{v,D} = 1/3$, where the index v refers to the neglect of sea quarks. The equality $c_{11}^{v,D} = 4/3$ will be shown in the following:

$$c_{11}^{v,D} = \frac{R_D^v}{|\mathbf{B}_D^v|}\, 4\,(u+d)\,. \tag{5.24}$$

$$\text{With} \quad |\mathbf{B}_D^v| = (R_D^v)^2\,(b_{11}^{v,D} b_{22}^{v,D} - b_{12}^{v,D} b_{21}^{v,D}) = 15\,(R_D^v)^2\,(u+d)^2 \tag{5.25}$$

$$\text{follows} \quad c_{11}^{v,D} = \frac{R_D^v\, 4\,(u+d)}{(R_D^v)^2\, 15\,(u+d)^2} = \frac{4}{3}\,, \tag{5.26}$$

where $R_D^v = 1/(2 \cdot 9 \cdot (1/x) F_2^{v,D}(x)) = 1/(5(u+d))$. A good approximation for method (II) is to assume the matrix elements to be independent of z. This leads to the following table:

Different values for the elements of $\mathbf{C}_D$		
Element	Method I	Method II
c_{11}	1.67	1.49
c_{12}	0.33	0.56
c_{21}	0.33	0.53
c_{22}	1.67	1.52

It can be seen that another possibility to take sea quarks into account is to exchange the factors 1/3 and 4/3 in method (I) with the above quoted values from method (II). The uncertainties through the usage of parton density functions have to be evaluated by comparing the values gained from different PDF parameterisations. That way, the extraction will be equal to the second method.

In summary, the presented extraction methods are providing a feasible experimental access to the favoured and unfavoured pion fragmentation functions. Two methods are given which differ in the systematic error sources. Besides their systematic dependence on PDFs, both methods are based on the QPM assumption of charge and isospin conjugation invariance which introduces a non-negligible systematic error. All systematic errors are estimated in Sec. 6.5.

Method (I) provides simple formulas for the direct computation of the fragmentation functions in the case of a deuterium target without the direct usage of PDFs. Several approximations have however to be made, the most important of them is the neglect of any sea quark contribution. The correction by means of a Monte Carlo technique introduces new model dependences apart from the dependence on PDFs.

In contrast, method (II) does not make any assumptions on the quark densities. Besides the uncertainties of the used PDFs which are accurately measured nowadays, the main uncertainty originates from the above mentioned QPM assumption of charge and isospin conjugation invariance. Since this method does not depend systematically on the Monte Carlo like the sea correction in method (I) it is preferrable.

For the extraction with method (I) the criterion $x > 0.15$ has been applied to reduce the size of the sea correction. As far as method (II) is concerned, no such constraint has to be made, that is $x > 0.02$. For a consistent comparison between the methods the results where $x > 0.15$ have been compared as well as the results with $x > 0.02$. The latter result is a measure for the reliability of the sea correction for method (I).

6 Analysis

6.1 Data Processing

The detector output is a large data stream consisting of the signals of the detector channels (wires, photomultipliers) which belong to one trigger signal, i.e. one "event"[1]. In addition, a variety of control parameters like target temperature, luminosity or polarisation, called slow control data, is recorded every ten seconds. The data is stored, then further processed by a chain of different programs as diagrammed in Fig. 6.1.

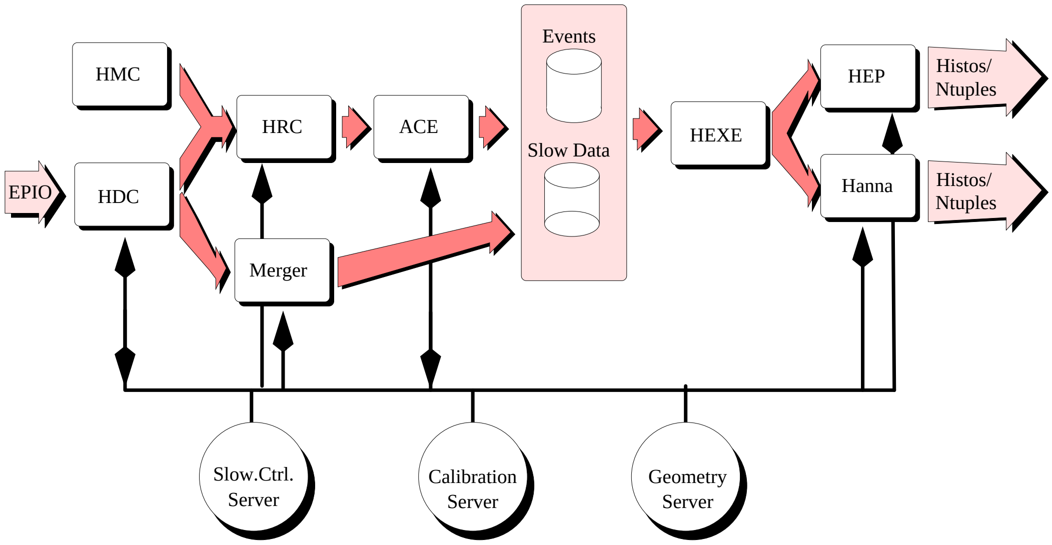

Figure 6.1: Scheme of the components taking part in the HERMES data analysis chain. HMC, the HERMES Monte Carlo, has a similar output as HDC, the HERMES decoder, which transforms the raw detector signals into hits in space.

The raw detector signal data in EPIO format is transformed by HDC, the HERMES decoder, into physical information. Wires of tracking chambers which fired are translated into lines in space, the signals of hodoscopes are transformed into deposited energy etc. The HERMES reconstruction program (HRC) then reconstructs from the given lines in space tracks of scattered particles by using a pattern matching algorithm [53].

[1]The event according to a trigger signal does not necessarily coincide with a real DIS event, for example if a background particle caused the trigger signal. This has to be checked "offline", i.e. in the data analysis.

HRC also assigns the momentum to a particle by using a momentum lookup table technique. The signals of the particle identification (PID) detectors, the preshower hodoscopes, the TRD, the Čerenkov detector, and the lead glass calorimeter, are grouped into clusters, which are assigned to each track. The probability of the track to be either a positron or a hadron is then calculated with the usage of a likelihood method: The detector response of the given track is compared to measured "parent" distributions of a particular particle type. The ratio of these probabilities is a sensitive measure for a particle to be either a positron or a hadron.

After the calculation of the track efficiencies by the ACE (Afficiency, Calibration and Alignment) program which are needed for normalisation purposes, the slow control information is added to the event data. These so called mDSTs[2], are then further reduced in size, which yield the μDST files (not shown in the above figure). The data contained in the μDSTs can then be analysed by an analysis program based on HANNA, a library of C routines for data analysis at HERMES, or by HEP, the HERMES Event Processor.

The entire data processing and analysis is realised in ADAMO [60], a data base which organises data according to the Entity-Relationship-Model, where data are stored together with the relationships between them. The access to the ADAMO database is however limited to a single process and computer, therefore DAD, the Distributed ADAMO Database, has been developed [61], to makes multiple accesses from different computers possible, even via TCP/IP, the Transmission Control Protocol/Internet Protocol. Several servers keep the necessary information on the experiment like geometry data, calibration constants etc., as shown in Fig. 6.1, which can be accessed from authorised client programs on any computer. The HEXE program, also based on DAD, serves for the event filtering.

For example, the HERMES Monte Carlo production (see Sec. 6.4) uses the DAD concept to create "pipes" between the Monte Carlo program, the reconstruction package and the μDST writing program. This saves large amounts of time and disk space.

6.2 Data Selection

In the following, the data selection criteria used in this analysis are described. The data from the 1996 data taking on unpolarised hydrogen, deuterium and ^{3}Helium targets have been used to derive the results in this thesis [3].

The same selection criteria are also applied to the Monte Carlo data, except for the slow control data, which do not exist in the case of the Monte Carlo. The analysis program is identical in both cases, but the generated ("true") information is accessible for Monte Carlo data, too.

The data can be structured in different levels according to different time scales. The largest time scale is a "fill", the period of one positron fill in the HERA storage ring

[2]The prefix m or μ of a Data Stream Tape (DST) indicates the level of data reduction due to processing and offline filtering.

[3]The HERMES internal version of the μDST files used is $b3$, 1996.

($\approx 5-10h$). A fill is subdivided into "runs" of 10 minutes length for better data handling[4], which are then processed in the above described manner. The time scale of the slow control information is a "burst" of 10 seconds length. After data processing, all events of that burst are stored in one "record" together with the slow control data.

Selection criteria (cuts) are applied in order to obtain a "clean" data sample. The cuts which are listed below are ordered according to the time scale they belong to run, burst and track sequentially. Until a track passes certain conditions which identify it as a DIS positron, the event kinematics cannot be calculated. Therefore event cuts follow track cuts.

Run Level Selection

The runs analysed in this thesis have been preselected according to general criteria like target functionality, clean target gas (no contamination), and working detectors. Out of a total of 522 deuterium runs, 510 runs have been selected. For all targets, 1069 runs have been taken out of 1212 runs. Since the applied cuts are loose in order not to lose runs with a large fraction of good data, more stringent cuts have to be applied at the burst level.

Burst Level Selection

The burst level cuts are:

Slow control data selection:	loss	remaining
"raw" μDST	—	100.00 %
Data analysable	0.01 %	99.99 %
Target gas polluted, not unpolarised or unknown gas type	0.17 %	99.82 %
Track efficiency values available	0.05 %	99.77 %
First burst in each run skipped	1.46 %	98.31 %
DAQ deadtime too high	9.10 %	89.37 %
Luminosity out of limits	0.37 %	89.04 %
Proton background too high	0.84 %	88.29 %
TRD detector not working	0.06 %	88.24 %

The target mass has been determined by cross checking the gas type from three different sources: from the setting of the gas valves as stored in the slow control information, from the entry made in the electronic logbook, and from an offline analysis. This offline check is based on the deadtime[5] corrected luminosity rate which is measured via Bhabha scattering of the beam positrons off the electrons of the target atoms. This rate is therefore proportional to the target charge Z. In addition, the offline analysis

[4] A raw data file for one run has a size of about 500 MB.

[5] The deadtime is the fraction of triggers, which are not recorded to due a "busy" DAQ, compared to the total number of generated triggers.

can use the DIS positron yield N_e or the target density ρ_T, which are proportional to the target mass A. A comparison of ratios of these properties yields a sensitive measure for the target mass and could even point to a possible contamination during a target change. All three methods are required to coincide.

The Cuts on the Track Level

The selection of tracks mainly cuts "edge effects". These are, for example, the higher rate of multiple scattering near the edges of the tracking chambers, background particles, "ghost" tracks (an unphysical phenomenon of the reconstruction), or tracks which are too close to the outer edge of the calorimeter, where part of their energy is not measured. A minimum momentum is required and the track has to be in the geometric acceptance, i.e. $40 <= \theta_y <= 140$ mrad and $\theta_x <= 170$ mrad. The "vertex" of the positrons, i.e. the point of nearest approach of the scattered positron track with the beam is required to lie within the target area. For the hadron no such cut is applied, since decay products shall be kept.

For the pions, the requirement $x_F > 0.1$ accounts for the selection from the current fragmentation region (see Sec. 3.3.1).

Particle Identification

For particle identification purposes four detectors are used, as described in Sec. 4.3. The distributions of the detector responses for positrons and hadrons can be seen in Fig. 6.2.

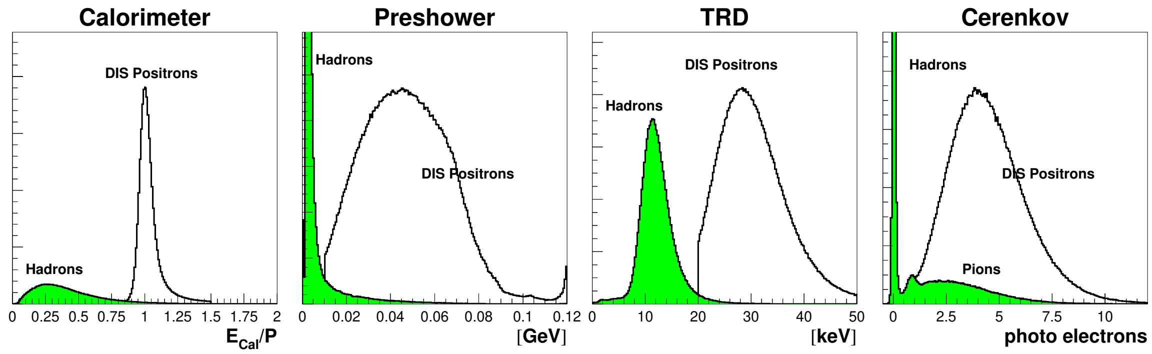

Figure 6.2: Detector responses of the different particle identification detectors.

There are two possibilities to identify the type of a particle, either to apply "hard" cuts on the individual detector responses at the minima between the distributions for hadrons and positrons, which has the disadvantage to be rather inefficient, or to use the likelihood method mentioned above. For the latter method the quantity *PID3* is calculated which denotes the logarithm of the ratio of the likelihoods for the track to be either a DIS positron e or a hadron h. The likelihood is the probability of the particle to be a positron or a hadron under the assumption that a positron or a hadron produced the signal. The ratio is thus a sensitive measure for the identity of the particle. The likelihoods are calculated as the product of the likelihoods for each detector $\mathcal{L}_D^{e/h}$, where $D \in \{Pre, Cer, Cal\}$, i.e.

$$PID3 \;=\; \log_{10} \frac{\mathcal{L}^e_{Pre}\mathcal{L}^e_{Cer}\mathcal{L}^e_{Cal}}{\mathcal{L}^h_{Pre}\mathcal{L}^h_{Cer}\mathcal{L}^h_{Cal}} \,. \tag{6.1}$$

Positrons have $PID3 > 0$ and hadrons accordingly $PID3 < 0$.

The PID method used in this analysis was the combination of $PID3$ with the probability ratio $PID5 = \mathcal{L}^e_{TRD}/\mathcal{L}^h_{TRD}$, where the lieklihoods of the individual TRD modules have been considered separately. The sum of $PID3$ and $PID5$ yields a positron identification efficiency $\geq 99\%$ and a hadron contamination $< 1\%$ [62].

As far as pions are concerned, the signal of the threshold Čerenkov counter above the π threshold of 3.8 GeV and below the K threshold (14.2 GeV) in conjunction with the above described likelihood method is used for the pion identification. In the analysis, the momentum of the pions is required to be in the range $4 \ldots 13.5$ GeV.

The hadron spectra for pions, protons and kaons can be seen in Fig. 6.3 and in Fig. 6.4. The spectra have been simulated with the HERMES Monte Carlo (HMC) which will be described in the next section. The lower limit in pion identification is denoted by the vertical line at 4 GeV in Fig. 6.3. The time-of-flight (TOF) method of hadron

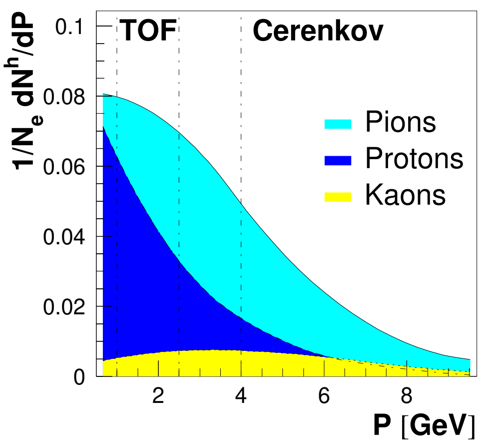

Figure 6.3: Normalised spectra of pions, protons and kaons in the HERMES geometric acceptance versus momentum, see text.

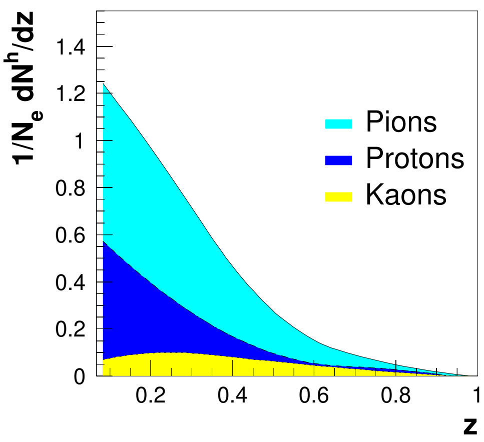

Figure 6.4: As in Fig. 6.3, but versus the fractional energy z.

identification which is possible at low momenta has not been used in this analysis.

Kinematic Cuts on the Event Level

From the momentum of a reconstructed positron, the kinematics are calculated according to Table 2.1. The following cuts were applied to identify deep-inelastic events:

The requirement $Q^2 > 1$ GeV^2 provides for an interpretation in the framework of the QPM, a cut on the relative transferred energy, $y < 0.85$, keeps the radiative corrections small, and a cut on the energy of the hadronic system W^2 suppresses resonances in the hadronic final state. For most of the results derived in this thesis, x has been restricted to $x > 0.15$ and $W^2 > 10$ GeV^2.

The x cut is necessary for extraction method (I), but is not necessary for method (II). It will be however applied to ensure consistency for comparisons. As far as the cut in W^2 is concerned, $W^2 > 4$ GeV^2 would be sufficient to suppress hadrons from resonance decays, but the used cut of $W^2 > 10$ GeV^2 has been found to be more safe to suppress pions from target fragmentation [63] without any significant loss of statistics for semi-inclusive events (see Fig. 4.4).

6.3 Statistics in this analysis

The statistics of the pion sample used in this analysis with $x_{Bj} > 0.15$ and $W^2 > 10$ GeV^2 are shown in Table 6.1. As already mentioned before, pions are taken as charged hadrons which produce a Čerenkov signal and have a momentum between 4 and 13.5 GeV. This already explains the small multiplicity of pions compared to hadrons, whose statistics is also shown.

$x_{Bj} > 0.15$:	Target:		
Particle type:	hydrogen	deuterium	^{3}Helium
DIS positrons	192240	325877	325877
Positive hadrons	31401	50781	15325
Negative hadrons	15429	28848	8153
Positive pions	9180	15020	4551
Negative pions	5312	10326	2858

Table 6.1: Multiplicity in the data sample, $x > 0.15$.

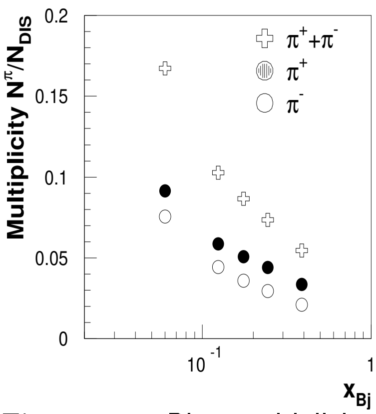

Figure 6.5: Pion multiplicity versus x

The decrease of the multiplicity with an increase of x follows from the correlation between x and Q^2 in the HERMES acceptance, which leads to a correlation between x and W^2 according to $W^2 = M^2 + Q^1(1/x - 1)$. A higher value of x accounts for a smaller W^2, see also Fig. 4.4. The multiplicity depends logarithmically on W^2, i.e. $\langle n \rangle \propto \ln W^2$, which follows from LLA QCD calculations [47]. Therefore, higher x leads to a lower multiplicity. This correlation between x and W^2 is shown in Fig. 6.5.

6.4 Monte Carlo Correction

Experiments in high energy physics employ highly complex devices, designed to reconstruct the tracks of scattered and produced particles of scattering events in space. The detectors have sensitive wires, strips or blocks and therefore finite resolution. Thus, the reconstructed track parameters deviate from the original "true" track parameters. In addition, the efficiencies of the detectors are $< 100\%$ which leads to tracks not being found sometimes. Other detector influences on the events are for example multiple coulomb scattering, energy loss and bremsstrahlung. All those effects lead to "smearing" of the kinematics, that is a difference between the reconstructed and the real kinematics of the process under investigation.

A measurement of absolute quantities like cross sections or fragmentation functions functions will be affected by the above mentioned effects. Therefore, the measured values have to be corrected, which is only possible by means of a simulation technique - the instrumental complexity makes an analytical description of the experiment unfeasible.

A Monte Carlo program divides the dynamics of a scattering event into many small subprocesses. The actual simulation of each subprocess depends on random decisions according to given probability distributions. For example, the kinematics of the scattered lepton is chosen randomly according to the differential cross section, the energy of a photon from bremsstrahlung is chosen randomly from the known energy distribution of bremstrahlung and a wire of a detector fires according to its efficiency function. The simulation of one event carries therefore as much information as one real event, and the precision obtained by this tool raises with the generated statistics. It is obvious, that in this way the physics and the detector environment can be simulated, in principle, as detailed as necessary. This depends however strongly on the understanding of the detector components and the parameters of the various subprocesses.

The output of Monte Carlo programs are "detector signals" whose format matches the experimental data after decoding, see Fig. 6.1, and which are processed, that is reconstructed, in the same way as data. In addition to data also the "true", that is the generated information, is accessible like the generated scattering angle of the lepton. Due to the above mentioned effects this will in general differ from the reconstructed value. Thus, the ratio of the generated over the reconstructed Monte Carlo information is the factor which corrects the measured data for e.g. detector effects.

In the following, the Monte Carlo program utilised for this analysis is briefly described before the correction factors needed for the analysis are discussed.

6.4.1 The Hermes Monte Carlo

The Hermes Monte Carlo (Hmc) [64] has been used to simulate the experiment. Hmc is based on the Lepto event generator [65] for the simulation of the deep-inelastic scattering process. Lepto uses first order QCD matrix elements for the calculation of the parton states after the hard-scattering subprocess occurred. In Hmc, no parton shower in Leading Logarithmic Approximation is simulated due to the low energies. Fragmentation and decay of the unstable primary hadrons is performed by Jetset [22] which is based on the LUND string model. Finally, the GEANT detector simulation package [66] undertakes the tracking and the detailed modelling of the detector response. The digitisation, that is the transformation of the detector signals, which are still perfect at this level, into "realistic" signals, which are smeared according to the experimental resolution and manipulated according to detector efficiency functions, is the last part in this simulation chain. The simulated events are reconstructed afterwards in the same way as real data.

In Fig. 6.6, the main parts of HMC are schematically drawn. As far as the fragmentation

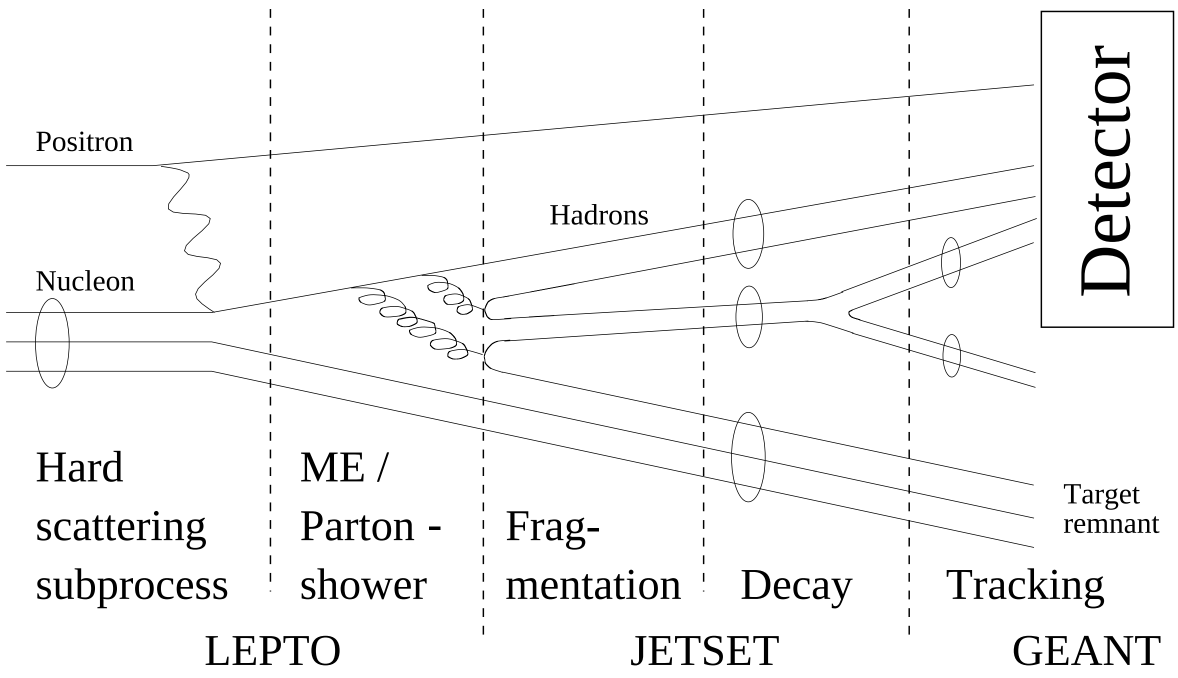

Figure 6.6: Sketch of the different parts which are realised in a Monte Carlo. The parton shower is not simulated in HMC due to the low energies, but from the matrix elements (ME) in first order QCD the parton evolution is calculated. The ovals denote states on mass shell.

simulation is concerned, three different models can be choosen, JETSET, independent fragmentation and HERWIG. The latter is based on the cluster fragmentation model and is used in comparison to the LUND string fragmentation model (JETSET), where independent fragmentation is only used in studies in Sec. 3.5.

An example for a scattering event can be seen in Fig. 6.7. Only full tracks, which pass through the whole detector are reconstructed. The deposited energy is denoted by the encircled crosses. Particles with low momenta are mostly scattered to larger angles and escape the geometric acceptance, defined by the inner dimension of the spectrometer magnet. Few tracks of low momenta are bent out of the spectrometer by the magnet. Others are not found due to detector effects.

To determine any correction to the data from the Monte Carlo simulation it is vital

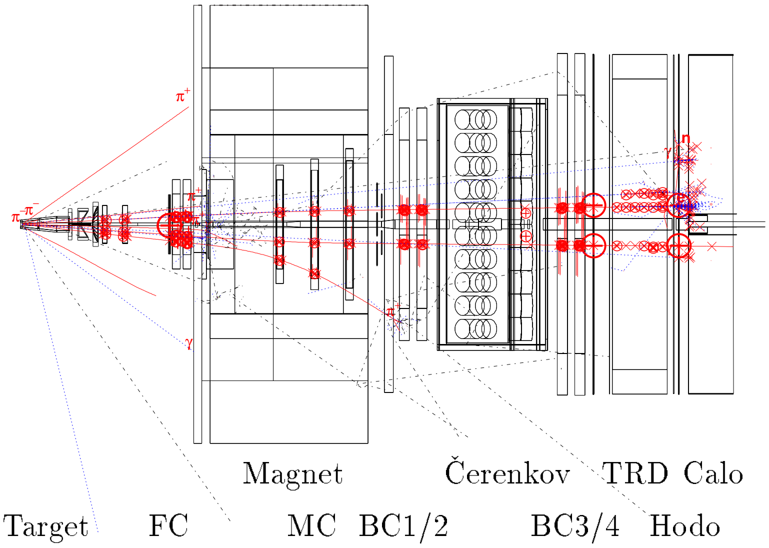

Figure 6.7: An example of a simulated scattering event, the detector is shown from top.

that the Monte Carlo models the experimental setup precisely. In Fig. 6.8 and Fig. 6.9 the momentum and x distributions of the scattered DIS positron can be seen. The agreement with data is very good which indicates that kinematics, acceptance, energy loss and resolution of the various detectors are well simulated.

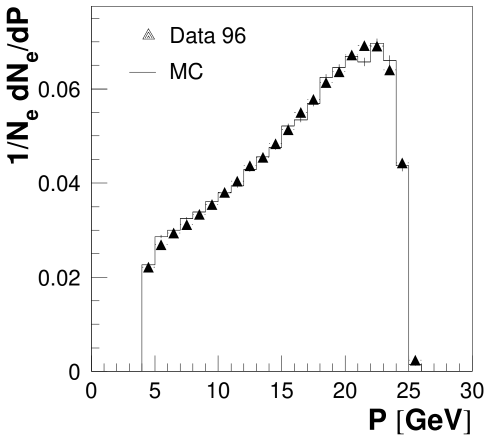

Figure 6.8: Momentum distribution of the scattered lepton, from data and Monte Carlo.

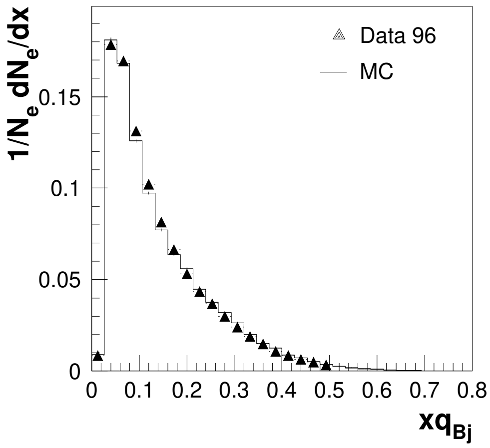

Figure 6.9: Distribution of x, from data and Monte Carlo.

The hadron distributions are more difficult to handle, because the fragmentation is described according to models where different interfering processes are involved. A tuning of the adjustable parameters of the fragmentation model is necessary, since the default parameter settings of the model are fitted to data at much higher energies, for example LEP data. This tuning will be described in the next section.

In Fig. 6.10, the normalised pion distributions from HMC are compared to measured spectra. The individual distributions are reasonably described for $z > 0.4$, the charged

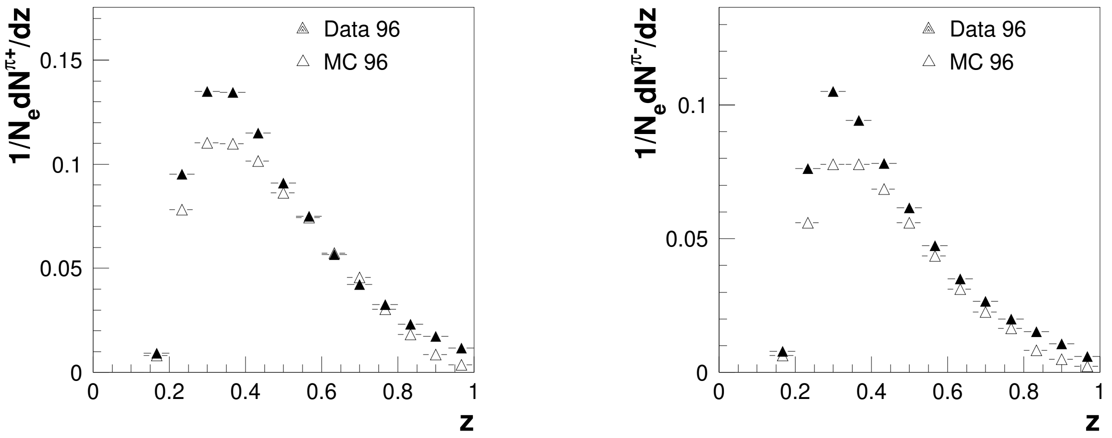

Figure 6.10: Distribution of the fractional energy z of the positive and negative pions (above) and the ratio N^{π^+}/N^{π^-} (right) for pions with momenta between 4 and 13.5 GeV in comparison to measured spectra. The discrepancy for $z \leq 0.4$ is due to the inaccurately simulated Čerenkov efficiency.

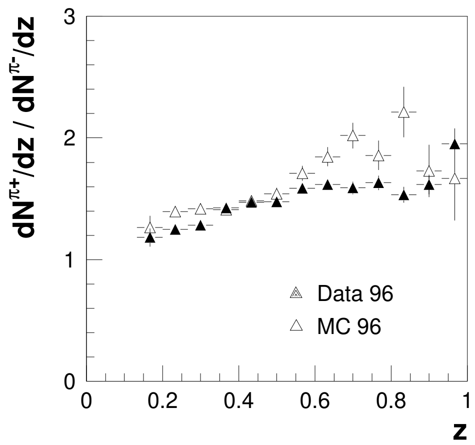

pion ratio agrees over almost the entire z region. When using the Monte Carlo for a correction of detector effects of the data, only the ratio of generated over reconstructed spectra is relevant. In performing the ratio, the model dependences cancel in first order and only the simulated detector influences remain. However, second order effects are expected from the relative fluxes of the different particle types which lead to a dependence of the ratio on the simulated spectra. This will be treated in Sec. 6.5.2.

6.4.2 Tuning of the Fragmentation Models

The different fragmentation models described in Sec. 3.2 have several free parameters which have to be adjusted to describe the measured spectra. In general, these the parameters depend on the accuracy of the QCD included in the Monte Carlo program. In case of the HERMES Monte Carlo the LUND model originally has been fitted to data at much higher energies [22] where the simulated parton showering, using the LLA approach, plays an important rôle. Because of the low energy of the HERMES experiment, in the simulation of the experiment the partonic final state is calculated by matrix elements of first order without further evolution of parton showers. Therefore, the parameters have to be readjusted to the measured spectra at HERMES.

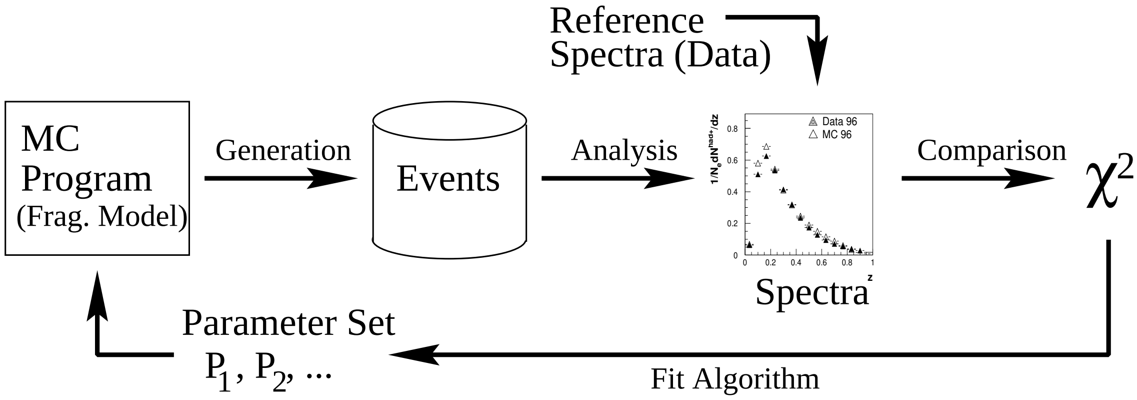

Figure 6.11: Iterative tuning procedure of the parameters of the fragmentation model. In each loop, 200 k Events are generated, analysed and compared to reference spectra from corrected, measured data.

The tuning procedure is an iterative process, where for each loop the Monte Carlo program with the to-be-tuned fragmentation model generates a certain number of events, see Fig. 6.11. The events are analysed using the same criteria as used in this fragmentation function analysis. The spectra from all hadrons, that is pions, protons and pions, are then compared to a reference spectra. This reference distribution from data is corrected for detector effects, that is reconstruction, absorption, multiple scattering etc. That way, the generated spectra do not have to be tracked through the virtual detector and reconstructed afterwards, which saves a huge amount of time[6]. For each loop, the χ^2 between the generated and the reference spectra is calculated as a measure for the agreement. The χ^2 is the sum of the squares of the differences of the generated to the reference spectra, $\chi^2 = \sum_i (N_i^{ref} - N_i^{model})^2$. The index i runs over all degrees of freedom, that is all bins of all spectra. Here, for five bins in Q^2 (1/2/4/6/10/20 GeV^2) the z and $p_\perp^2$ spectra for positive and negative hadrons were evaluated. The fit parameters which lead to a minimal χ^2 are taken.

Two different models have been fitted, the LUND and the Cluster model. The LUND model [23] is realised in the JETSET [22] program library and is the default fragmentation model of HMC. The parameters which define the longitudinal string breaking probability ("a" in Eq. 3.4), the tunneling probability ("b") and the mean $p_\perp^2$ were fitted (see also Sec. 3.2.2 and [67]). The default and the fitted values of these parameters are listed in Table 6.2. The result of the LUND fit can be seen in Fig. 6.12. A good

[6]The generation of 10^6 semi-inclusive events needs approximately 30 min on a 300 MHz *alpha* CPU, while the generation, radiative correction, tracking, digitisation and reconstruction of the same number of events needs 10 days.

Models:	LUND			HERWIG		
	a	b	$\langle p_\perp^2 \rangle$	Λ_{QCD} $[GeV]$	M_G $[GeV]$	$M^{max}_{Cluster}$ $[GeV]$
Default Value:	0.30	0.58	0.36	0.18	0.75	3.35
Fitted Value:	0.82	0.24	0.34	0.17	0.75	1.90

Table 6.2: Parameters of the LUND and HERWIG fragmentation model before and after the fitting.

agreement has been achieved. The main impact of the fit is a shifting of the spectra towards smaller z by increasing the string breaking probability at lower z.

The Cluster model is encoded in the HERWIG Monte Carlo program [27]. With HERWIG, the tuning procedure did not yield an equally satisfying agreement of the generated spectra to the measured data. The parameters of the model are described in Sec. 3.2.3: the scale parameter of the QCD for three flavours Λ_{QCD}, the mass of the gluons M_G and the maximal cluster mass. In Table 6.2 the values of the fit with lowest χ^2 are listed. The resulting spectra can be seen in Fig. 6.13. The cluster model produced too many hadrons at small z. This did not significantly change in the whole parameter space. Therefore, this model has only been used to obtain a rough estimate on the upper limits of the systematic dependence of the extracted fragmentation functions on the fragmentation model in the Monte Carlo program.

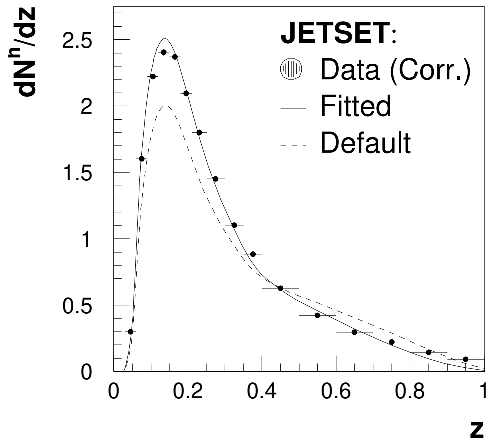

Figure 6.12: Charged hadron spectra (corrected for detector influences) in comparison with the simulated spectra from JETSET before (dashed line) and after (full line) the tuning procedure.

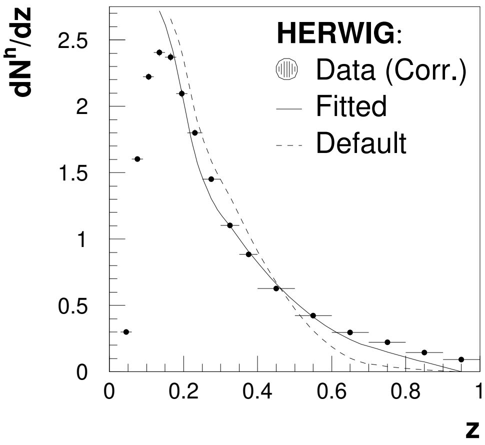

Figure 6.13: Charged hadron spectra as in Fig. 6.12. The simulated spectra from HERWIG is shown before (dashed line) and after (full line) the tuning procedure.

6.4.3 The Monte Carlo Correction to the Measured Spectra

The Monte Carlo correction is determined from the ratio of the generated over the reconstructed Monte Carlo data, which is then, bin by bin, multiplied to data:

$$\text{Corrected } \mathit{Spectrum}\,|_{\text{Acc.}} = \left(\frac{\text{Generated } \mathit{spectrum}\,|_{\text{Acc.}}}{\text{Reconstructed } \mathit{spectrum}} \right) \cdot \text{ Measured } \mathit{spectrum}\,, \tag{6.2}$$

with a given acceptance *Acc.*, which is discussed below.

There exist two different possibilities to correct the spectra in this way, depending on whether the quantity *spectrum* is $\mathrm{d}N^h/\mathrm{d}z$ or $1/N_e\,\mathrm{d}N^h/\mathrm{d}z$:

In the case, where $\mathit{spectrum} = \mathrm{d}N^h/\mathrm{d}z$, the hadron spectrum of reconstructed events is corrected. For all reconstructed DIS events, the ratio of generated over reconstructed hadrons determines the correction factor. This detector correction affects the hadron momentum only, and therefore depends almost only on the modelling of the detector (the event kinematics is slightly involved: since the generated fractional energy z of the hadron has to be calculated from the energy of the generated, scattered positron, the smearing of the positron is included). However, the events where no hadron is reconstructed could be distributed inhomogenously in phasespace. In this case, the detector effects could depend on the event kinematics and a bias would be introduced.

If $\mathit{spectrum} = (1/N_e)\,\mathrm{d}N^h/\mathrm{d}z$, the normalised (to the number of DIS events) hadron spectrum is corrected. DIS events both for the generated and reconstructed Monte Carlo events are selected independently from each other. In this way not only the hadron but also the positron distribution enters into the correction. Thus all detector effects on the event kinematics are considered, too, in addition to the effects on the momentum of the hadron. This method is, compared to the former one, a “physics” correction since it corrects a cross section, and has been chosen in this thesis.

The advantage of the latter method is, that it includes also those events, where no hadron has been reconstructed. The first method however depends (almost) only on the detector modelling and is therefore more transparent.

The confrontation of both methods can be seen in Fig. 6.14. The difference which causes the latter described correction to be higher is a superposition of two effects.

An overall shift is caused by the number of generated pions of those events, whose positrons are not reconstructed. This number is however not compensated by the increased number of generated events in the normalisation. The stronger rise at high z accounts for those detector effects, which reduce the momentum of the positron, like multiple scattering. Therefore, there are fewer reconstructed events near the upper limit in momenta which corresponds to low ν, since their energy is shifted slightly towards lower momenta. Since high z pions have low ν, there are more generated pions at high z in the first method than in the second method. The correlation of ν and z can be seen in Fig. 6.15, where the difference between the average ν of the generated pions of the DIS events without reconstructed positron, and all reconstructed pions is shown.

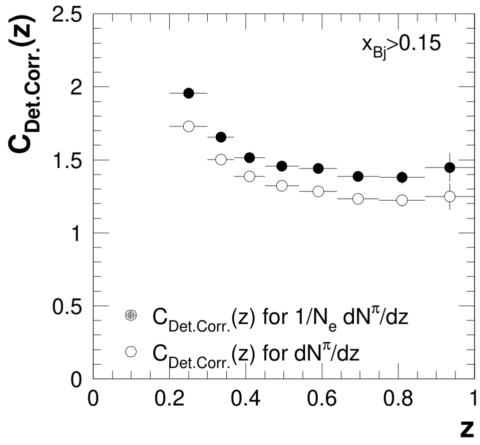

Figure 6.14: Comparison of two different correction methods. See text.

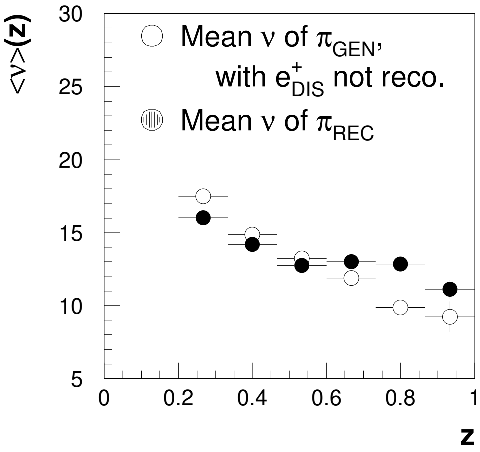

Figure 6.15: Mean value of ν for different pion samples, see text.

The effects, which lead to a loss of particles or a change of the kinematics of the particles, can be disentangled into different contributions. These are discussed separately in the following.

Detector effects:

The percentages of the particles which are lost by the different effects are listed in Table 6.3. The difference between the reconstructed and the generated distributions is thus the sum of all above effects.

	DIS Positrons		$1/N_e\cdot$ **Pions**	
Effect	loss (%)	remain. (%) (accumulative)	loss	remain. (%) (accumulative)
HERMES geometric acceptance	—	100.00	—	100.00
Absorption, Bending	2.62	97.38	7.06	92.94
Trigger	0.64	96.76	1.93	91.15
Reconstruction / Tracking eff.	13.67	83.53	0.87	90.35
Particle identification	1.08	82.63	18.88	73.30

Table 6.3: Impact of different detector effects on the distribution of positrons and normalised pions between 4 and 13.5 GeV. The "loss" is relative to the distribution "before" the effect, the "remaining" percentages are accumulative.

It is of some importance to be aware of the fact, that the correction factor of those effects which concern the tracking only (trigger, absorption, reconstruction ...), will be almost independent of the physics model which has been used to generate the events.

In this case, any remaining model dependent influences mostly cancel by performing the charge ratio. This is important for the ratio of the unfavoured over the favoured fragmentation function which only depend on the pion charge ratio.

However, as soon as the contamination of pions due to non-perfect PID is concerned, this independence does not hold anymore: the correction now includes the contamination with protons and kaons, which depends on the relative flux between the hadron types. This flux cannot be checked directly with data, because HERMES cannot distinguish between pions and kaons/protons. Different particle fluxes in conjunction with different (non-perfect) models of the PID detectors can lead to the same output in the Monte Carlo and thus contribute to a systematic uncertainty. This uncertainty can be reduced with the usage of a detailed Monte Carlo, which describes the kinematics and the PID detector signals very well. The comparison to data can best be performed with easy-to-identify particles like DIS positrons or pions from ρ^0 decays, if both decay pions are reconstructed. These pions are perfectly identified without any contamination.

An estimate of the remaining systematic dependence can be obtained by a comparison of the correction factors from different fragmentation models and for different "PID schemes". Here a PID scheme is defined by the algorithm which is used to determine the particle type from the PID detector signals. These studies are performed in Sec. 6.5.

In Fig. 6.16 and Fig. 6.17, the correction factor of the normalised positive pion rate and of the pion charge ratio can be seen. These corrections are determined within the HERMES geometric acceptance. The dominating detector effects are the Čerenkov inefficiency near the lower pion threshold and the tracking inefficiency at low momenta.

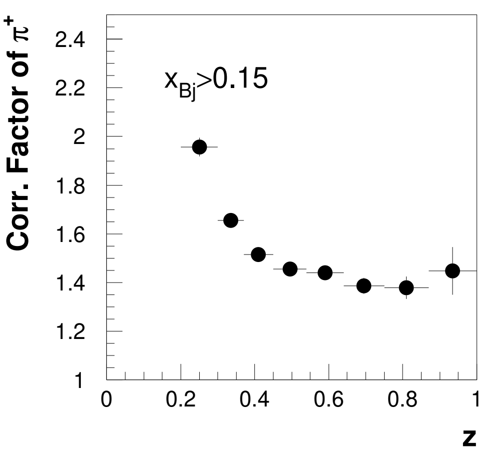

Figure 6.16: Detector correction of the normalised pion rate $1/N_e \mathrm{d}N^{\pi^+}/\mathrm{d}z$.

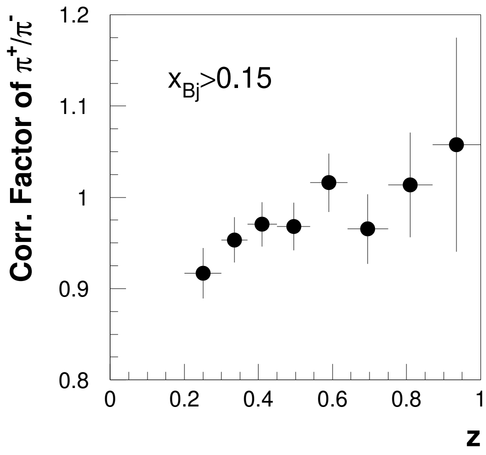

Figure 6.17: Detector correction of the charge ratio of the pion rate, $(\mathrm{d}N^{\pi^+}/\mathrm{d}z)/(\mathrm{d}N^{\pi^-}/\mathrm{d}z)$.

Radiation:

In semi-inclusive DIS, various radiative effects have to be taken into account:

- The emission of a radiative photon from the incoming or scattered lepton leads to a shift of the energy of the virtual photon and thus to a shift in the fractional pion energy z. This effect, called external radiation, has to be corrected. This is done by simulating the radiation in the Monte Carlo for each event in detail [68, 69] and using the "true" transferred energy ν_{true} to calculate z instead of using $\nu = E - E'$. This radiative correction can be included into the detector correction factor which affects the correction mostly at high values of z, see Fig. 6.18. In the high z range, the momentum of the positron is also large and high energetic radiative photons can be emitted.
- The same effect influences the normalisation N_e. For a non-negligible fraction of reconstructed positrons which have been identified as deep-inelastic events, the emission of a radiative photon has reduced the transferred energy in such a way that no deep-inelastic scattering has occurred, even though it looks like due to the reconstructed value of ν. The normalisation N_e has thus to be changed accordingly. This is done by comparing the number of events which are weighted with the cross section under consideration of all radiative effects, with the one-photon-exchange cross section. It should be mentioned, that all semi-inclusive events are deep-inelastic events due to the formation of the coincident hadron, but the normalisation includes also non-semi-inclusive events.
- The internal radiative correction accounts for photon emission in the hadronic final state. This is a small correction which has not been applied here.

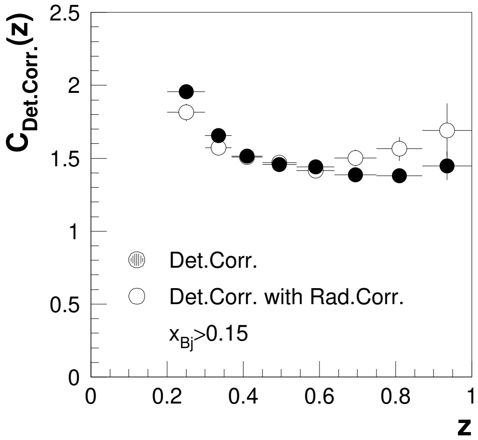

Figure 6.18: Influence of the radiative effects. Here, the difference between the correction factor of detector effects with and without the inclusion of a radiative effect correction is shown.

Acceptance correction:

An important parameter of the detector correction is the definition of the acceptance ("Acc." in Eq. 6.2) of the generated events. If the scattering angle of the generated hadrons is not limited, the corrected spectrum will look like a spectrum measured with a 4π detector. In this case, the correction factor and thus the systematic uncertainties will be large, since HERMES has a relatively small acceptance for the detection of events with more than one track, especially at low momenta. If the angular limitation of the generated events matches the HERMES geometric acceptance the correction includes only detector effects and will thus be almost model independent.

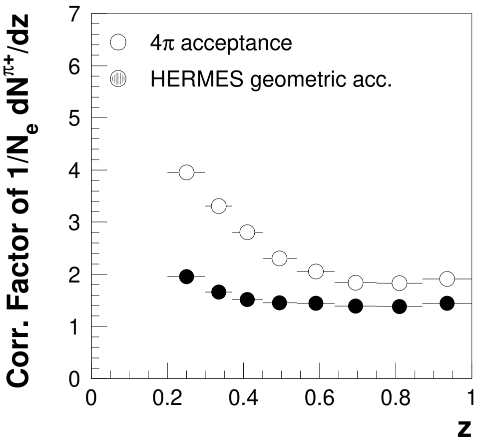

Figure 6.19: Comparison of the detector correction factor with the correction, where an acceptance correction to a 4π acceptance is included, for pions with momenta between 4 and 13.5 GeV.

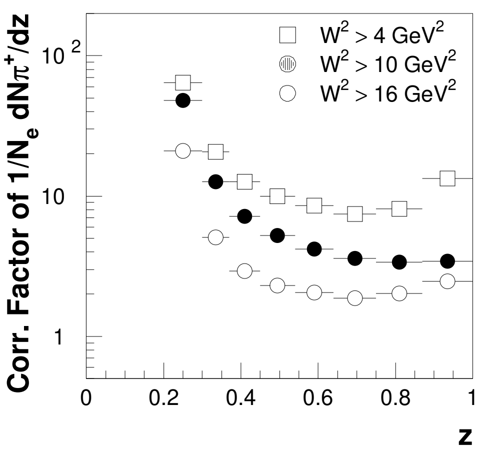

Figure 6.20: Detector and 4π acceptance correction factor for the normalised pion spectra of pions with a momentum between 4 and 13.5 GeV, to a normalised pion spectra of pions above 1 GeV as seen by a detector with a 4π acceptance, for different lower limits in W^2.

In Fig. 6.19, the comparison of the correction for 4π and HERMES geometric acceptance is shown for pions with momenta between 4 and 13.5 GeV. The detector correction factor is ≈ 1.5, the correction which includes the acceptance amounts to ≈ 2.5.

In Fig. 6.20, the detector and 4π acceptance correction is shown. In contrast to Fig. 6.19, all pions above 1 GeV are included in the generated sample, where the reconstructed sample is the same, i.e. consists of pions with momenta between 4 and 13.5 GeV as identified by the HERMES detector. This leads to a larger correction because the hadrons with such low momenta contribute significantly to the low z spectrum. For the comparison of absolute fragmentation functions with the results measured at other experiments, this correction has to be applied to the pion spectra in order to correct for the missing contribution of low momenta pions to the spectra at low z.

The differences between the corrected spectra for different cuts in W^2 are small. Therefore, the cut of $W^2 > 16\ \mathrm{GeV}^2$ has been applied. The correction for spectra with such a cut is significantly smaller than the correction for the spectra where $W^2 > 10\ \mathrm{GeV}^2$ and does not largely affect the statistics of the data but reduces the systematic influence on the Monte Carlo.

6.5 Systematic Error Evaluation

The uncertainties of a measurement are of various origins. Apart from purely statistic errors, other error sources exist which do not depend on the statistics and affect all measured points in a correlated way, i.e. have systematic character. These are for example approximations in the calculation or uncertainties in some input quantities. These systematic error sources have to be determined in order to obtain a quantitative estimate of all model dependences, approximations, assumptions and other non-statistical uncertainties which are introduced by the measurement and the analysis.

The error sources can be separated into various groups which are listed below. The specification of the errors is given in parantheses and the corresponding subsection where the influence is estimated is referenced at the right margin.

- Measurement
  - Target (Gas type determination) — Negligible (Sec. 6.2).
  - Reconstruction (Tracking effects) — MC corrected.
  - PID (Contamination) — MC corrected.
  - Contribution from diffractive ρ^0 decay — See text.
- Detector correction
  - Monte Carlo correction method — Sec. 6.5.1
  - Detector simulation (PID, Tracking) — Sec. 6.5.2
  - Fragmentation model used in simulation — Sec. 6.5.3
- Extraction method
  - QPM assumptions (Isospin-/charge conjugation invariance) — Sec. 6.5.4
  - PDF (Sea correction for method I) — Sec. 6.5.5
  - PDF (method II) — Sec. 6.5.6

In the following, the different influences are estimated as a functions of z. In the figures, ratios of correction factors or fragmentation functions are shown where the deviation from unity is a measure for the systematic influence. If the influences of the correction factors or the fragmentation functions inside the HERMES or in the 4π acceptance are different, they will be estimated separately.

If the systematic influences do not cancel when performing the charge ratio, then this influence is estimated as well and the impact on the fragmentation function ratio $D^-(z)/D^+(z)$ is shown in a separate figure.

The uncertainties of the measurement which are introduced by the apparatus and the data selection are small: The target gas type determination is sufficiently accurate (see Sec. 6.2). The reconstruction and PID effects are corrected with a Monte Carlo. The systematic effects introduced by this correction are discussed in Sec. 6.5.2. The influence from pions from the decay of diffractively produced ρ^0s has been estimated in [70] to be smaller than $3-4\%$, the impact on the ratio is very small. This influence has not been studied here.

6.5.1 Monte Carlo Correction Method

In Fig. 6.21 - Fig. 6.22, the comparison of the different correction methods as discussed in Sec. 6.4.3 is shown. For the detector correction, the impact of the method is 10% over the whole z range. The influence on the 4π correction amounts to 13%, while for the charge ratio it is negligible.

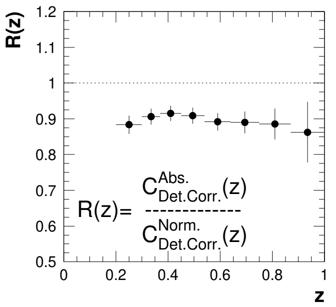

Figure 6.21: Comparison of the different correction methods as discussed in Sec. 6.4.3 for the detector correction $C_{Det.Corr.}(z)$.

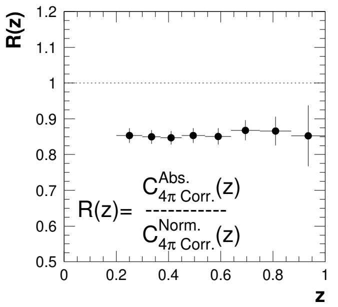

Figure 6.22: Comparison of the different correction methods as discussed in Sec. 6.4.3 for the 4π correction $C_{4\pi}(z)$.

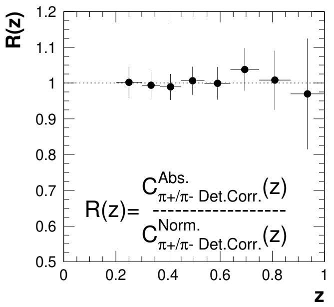

Figure 6.23: As in Fig. 6.21, but for the charged pion ratio.

6.5.2 PID Scheme

Particles are identified by applying a specific PID scheme (Sec. 6.2) on the reconstructed tracks. A PID scheme consists of several cuts on PID detector responses or related quantities (for example likelihoods), in order to separate the different particle types from each other. Since the detectors are not perfect, the PID can not be perfect either. This leads to an identification efficiency $< 100\%$ and to a contamination with particles of a different type. Different PID schemes will lead to a different subsample of particles, which are selected. These subsamples will be differently distributed, since the efficiencies and contaminations depend on the kinematics. Therefore, the kinematic distributions depend on the PID scheme.

The result on the fragmentation functions should however not depend on the PID, since the Monte Carlo is used to unfold all influences from non perfect detectors, including the influences from the PID scheme. However, in HMC the present simulation of the PID detectors does not agree sufficiently well with data to exclude influences on the results. The correction of the measured particle momentum distributions with such a Monte Carlo therefore depends on the PID scheme.

To estimate this effect, a comparison between the corrected, normalised pion distributions has been made, using the two mentioned PID schemes. The same method has been used both for data and Monte Carlo. However, in that way only the PID influence concerning detectors other than the Čerenkov can be estimated: in both cases the pions are separated from hadrons using the Čerenkov response in the same way.

The difference between the two PID schemes has been evaluated by performing the ratio $N^{\pm}_{like}/N^{\pm}_{hard}$, where the index *like* labels the spectra which are analysed and corrected using the likelihood method, where *hard* labels the spectra where the hard cuts have been applied. The results of this study are shown in Fig. 6.24 and Fig. 6.25. The

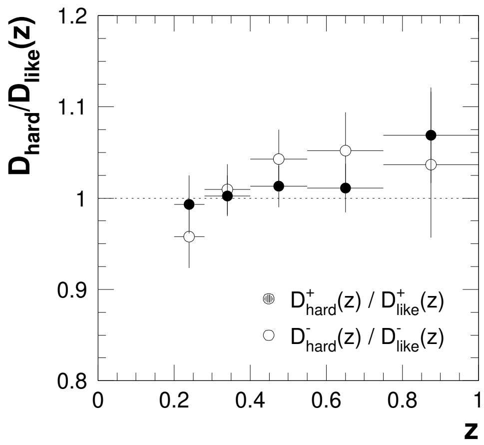

Figure 6.24: Influence of the PID scheme on the fragmentation functions. Shown are the ratios of the result with the *hard* PID scheme over the *like* PID scheme, see text.

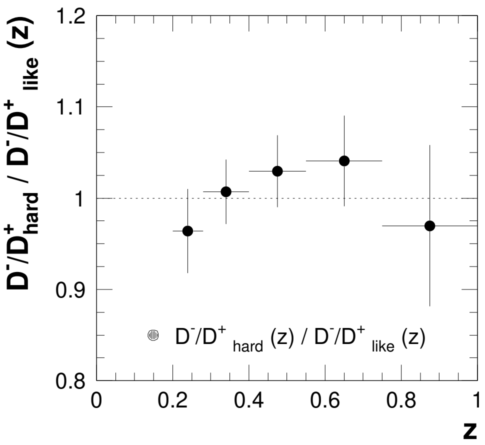

Figure 6.25: Impact of the different PID schemes on the fragmentation function ratio.

influence of the PID scheme for all PID detectors except for the Čerenkov detector varies between 1% and 5% for the unfavoured and favoured fragmentation functions, respectively, while the influence on the fragmentation function ratio with the present statistics is small. The influence of the Čerenkov digitisation is not included in the quoted error and has yet to be determined.

6.5.3 Fragmentation Model in the Monte Carlo

To estimate the influence of the fragmentation model as implemented in the Monte Carlo on the detector correction, a comparison of the corrections using two different fragmentation models has been performed. The LUND model has been used to derive the corrections, as it has been described in Sec. 6.4.1. For a comparison, the HERWIG fragmentation model has been implemented into HMC, where some attention has been payed to the consistency of the implementation. For example, the simulation of the cross section, the radiative effects and the decay mechanism of the produced hadrons are identical in both cases. However, as it has been described in Sec. 6.4.2, the HERWIG model could not be fitted sufficiently well to the HERMES data. This leads to large deviations of the simulated particle spectra from the measured data spectra.

The detector correction and the 4π corrections as determined from the LUND and from the HERWIG model are shown in Fig. 6.26. Due to the above mentioned deviation of

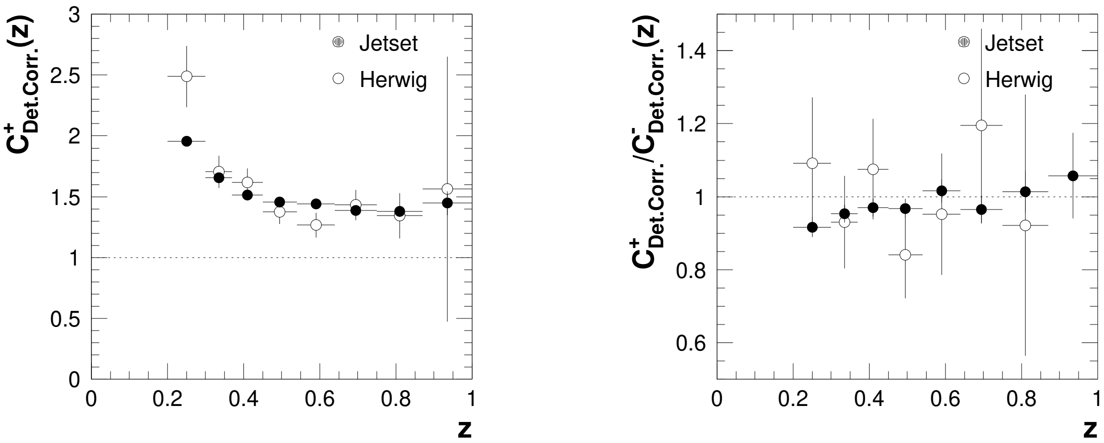

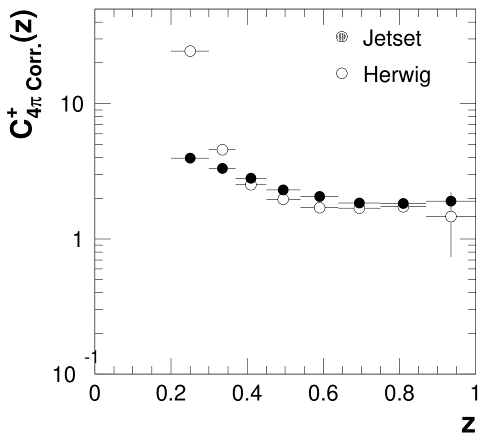

Figure 6.26: Monte Carlo correction from the LUND and the HERWIG fragmentation model for the detector effects of the normalised spectrum (upper left), the detector effects of the pionic charge ratio (upper right) and for the 4π correction of the normalised spectrum (lower right).

the HERWIG pion spectra to the measured pion distributions, the differences in the correction factors have been taken as upper limits. For the detector correction of the positive pion spectra inside the HERMES acceptance, the systematic error is 10% at the lowest z bin and 4% for the higher z range, while it is 5% for the negative pions and for the charge ratio. As far as the 4π correction is concerned, the error decreases from 100% at the lowest z bin to 5% for $z \geq 0.4$. This accounts for the uncertainty in the spectra of pions of low momenta which are not measured below the Čerenkov threshold. The low momenta correction therefore depends strongly on the fragmentation model as implemented in the Monte Carlo program.

6.5.4 Systematic Errors from QPM Assumptions

The influence of the assumption of isospin and charge conjugation invariance on the fragmentation functions according to the QPM has also been estimated using a Monte Carlo program. The result of the study can be seen in Fig. 6.27 and Fig. 6.28. The ratio of the fragmentation functions of valence quarks $D^{\pm}_{Val.}(z)$ over the fragmentation functions of valence plus sea quarks $D^{\pm}(z) = D^{\pm}_{Val.+Sea}(z)$ has been determined. This ratio is a measure for the validity of the assumption, since the valence fragmentation functions as realised in the Monte Carlo are satisfying the QPM assumption while the total fragmentation functions, i.e. valence and sea quark fragmentation function do not, cf. Sec. 3.4.3.

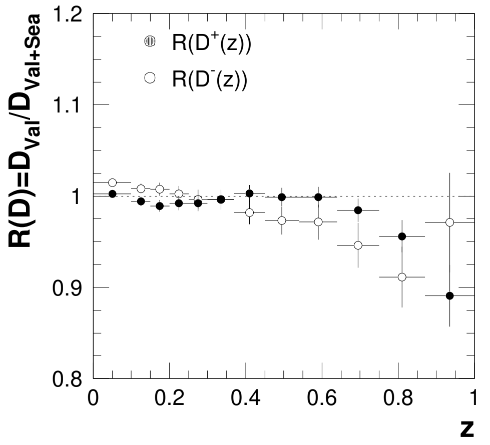

Figure 6.27: Influence of the isospin and charge conjugation assumption on the favoured and unfavoured fragmentation functions. Shown is the ratio of fragmentation function from valence over the fragmentation function from valence plus sea quarks, see text.

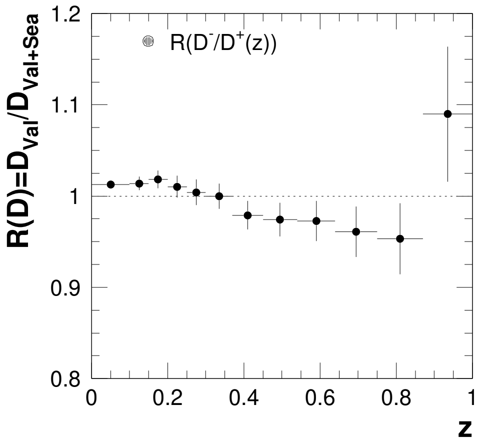

Figure 6.28: Same as in Fig. 6.27, for the ratio of unfavoured over favoured fragmentation function.

An error of 1% at low z up to 10% in the high z range has been taken as the systematic uncertainty for the favoured and unfavoured fragmentation functions. There is only a small difference between the uncertainty evaluated inside the HERMES acceptance compared to the 4π acceptance.

As far as the ratio of favoured over unfavoured fragmentation function is concerned, an uncertainty of 2% (small z) up to 5% (large z) has been determined from this study.

6.5.5 Dependence of the Sea Correction on the Parton Densities

The sea correction for method (I) as it has been determined with the Monte Carlo program is sensitive to the parton density parameterisation of the sea quarks. The influence of this dependence shall be estimated below.

The sea correction $C^{\pm}_{Sea}(z)$ is the ratio of the generated over the extracted fragmentation functions. In the generated fragmentation functions, the struck quark is tagged, where for the extraction no such tagging can be made. The difference, determined with the Monte Carlo, is thus sensitive to the used PDF, where mostly the quark sea densities are involved.

The ratio of the sea correction utilising two different PDFs can be seen in Fig. 6.29 and Fig. 6.30. In particular, the MRS(A) parameterisation [56] and the PDF of the GRV collaboration [57] are compared. A large influence of $\approx 15\%$ on the favoured and

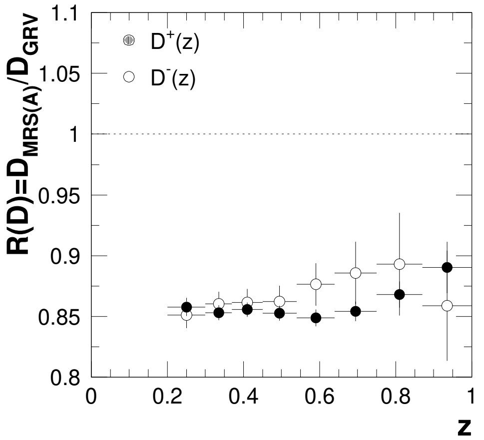

Figure 6.29: Influence of the PDF on the sea correction for favoured and unfavoured fragmentation functions extracted using method (I).

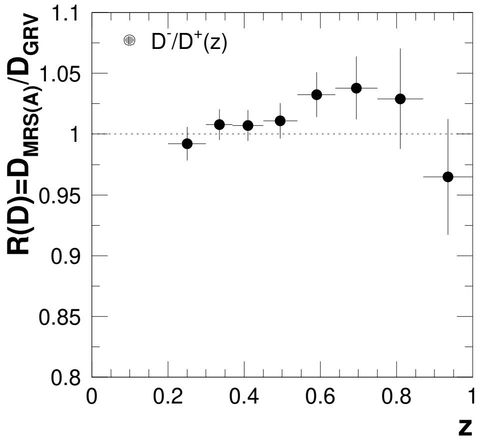

Figure 6.30: Influence of the PDF on the sea correction for the ratio of unfavoured over unfavoured fragmentation functions extracted using method (I).

$\approx 14\%$ on the unfavoured fragmentation functions is found. The influence on the ratio is estimated to be 1% for $z < 0.5$ and 3% for $z > 0.5$.

6.5.6 Dependence of the Result on the PDF (Method II)

The impact of different PDFs on the result of method (II) is estimated in the following. The ratio of the result for the favoured fragmentation function which is determined using the PDFs from the CTEQ collaboration [58] over the result derived using the GRV [57] parameterisation is shown in Fig. 6.31. An almost z-independent difference of $\approx 2.5\%$ can be observed.

The same study on the ratio of unfavoured over favoured fragmentation function yields a small z dependent correction of up to 2% at high z (Fig. 6.32).

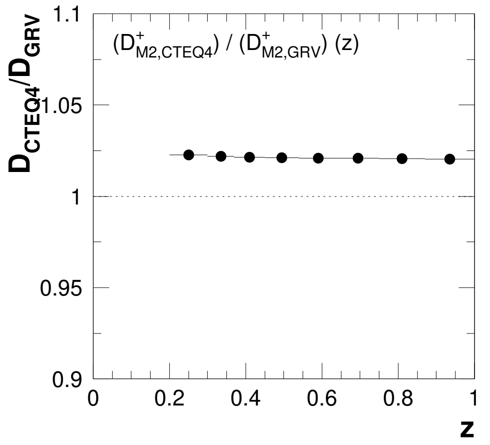

Figure 6.31: The impact of different parton distributions on the favoured fragmentation function, extracted using method (II).

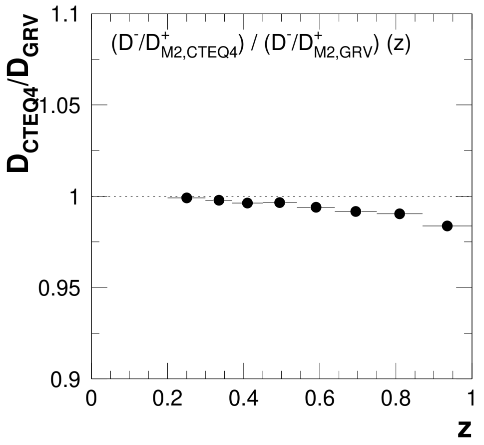

Figure 6.32: The impact of different parton distributions on the ratio of favoured over unfavoured fragmentation function, extracted using method (II).

6.5.7 The Total Systematic Error

The total fractional systematic errors as determined in the previous sections for the fragmentation functions inside the HERMES acceptance, the fragmentation function ratio and the fragmentation function in the 4π acceptance is shown in Fig. 6.33.

For the fragmentation functions inside the HERMES acceptance, the relative systematic uncertainties for the results of method (I) are almost twice as large as for method (II). This is the consequence from the large influence of the dependence on the PDFs for the sea correction. Both extraction methods suffer from the uncertainty of the correction method.

The relative systematic uncertainty for the fragmentation function ratio is below 5% except for the highest z bin where it is $\approx$ 11%. The large increase is a follow of the impact of the violation of isospin and charge conjugation invariance on the ratio at large z as implemented in the fragmentation function model of the Monte Carlo. The major influences for the ratio originates from this QPM assumption and from the dependence of the detector correction on the fragmentation model.

As far as the fragmentation functions in the 4π acceptance are concerned, the only difference to the result relative to the HERMES acceptance is for small z, where the dependence on the fragmentation model causes a large systematic error.

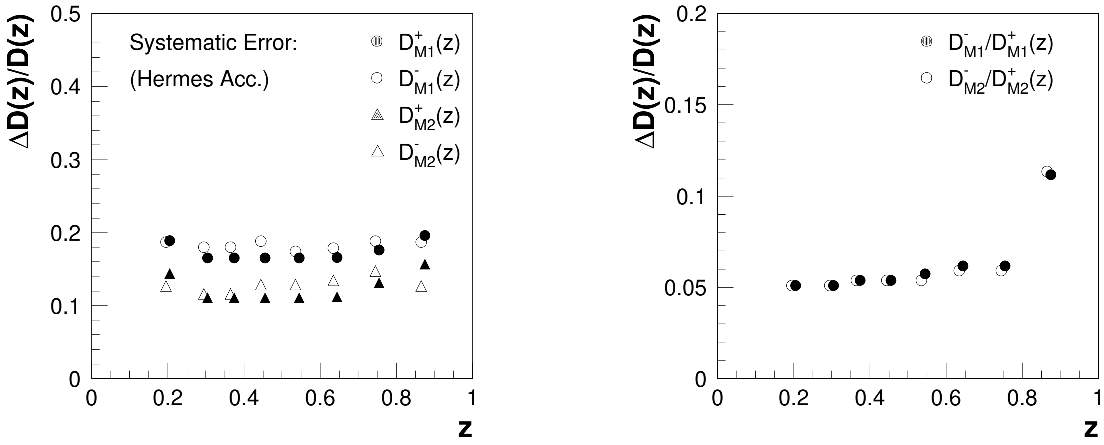

Figure 6.33: Total fractional systematic error on the fragmentation functions inside the HERMES acceptance (upper left), the fragmentation function ratio (upper right) and the fragmentation functions in the 4π acceptance (lower right).

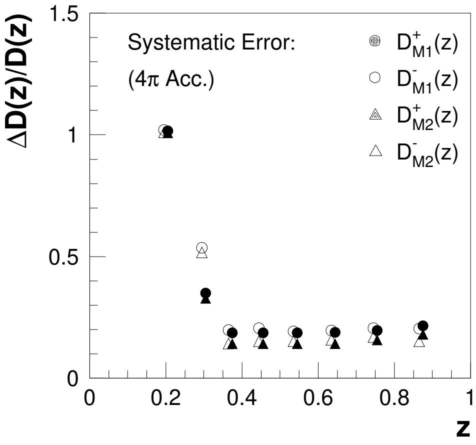

7 Results

7.1 The Pion Fragmentation Function (HERMES Acceptance)

The fragmentation functions inside the HERMES acceptance are extracted from detector corrected normalised pion spectra, measured on unpolarised deuterium in the case of method (I) and on hydrogen, deuterium and ^{3}Helium in the case of method (II). The determination of the detector corrected spectra is briefly summarised below, while the extraction of the fragmentation functions from the spectra will be separately treated in the next sections.

Measured Data:	**Monte Carlo Data:**
• (Sec. 6.2) Data selection of unpolarized data on a deuterium target, taken in 1996.	• (Sec. 6.2) Data selection.
• Determination of the normalized pion yield $N^{\pi^\pm}_{Meas.}(z)$.	• Determination of the normalized pion yields for generated and reconstructed pions.
	• (Sec. 6.4.3) Determination of the detector correction $C_{Det.}(z)$
• (Sec. 6.4.3) Detector correction of the normalized yield, $N^{\pi^\pm}_{Det.Corr.}(z) = C_{Det.}(z)\, N^{\pi^\pm}_{Meas.}(z)$.	

Again, the notation "pions" refers to pions with momenta between 4 and 13.5 GeV.

For the reason of better distinctness, the z values of two fragmentation functions which are shown on the same plot are slightly shifted. This is done in all comparisons of Sec. 7.

All results in this section are extracted with $x > 0.15$ and $W^2 > 10$ GeV^2, except if denoted differently.

7.1.1 Result from Method I

The extraction of the favoured and unfavoured fragmentation functions from normalised, detector corrected pion distributions inside the HERMES acceptance, using extraction method (I), will be presented in this section. For this, the steps of the extraction are summarised below.

Measured Data:

- (Sec. 5.1) Extraction of the fragmentation functions $D^{\pm}_{M1}(z)$ according to Eq. 5.14.
- (Sec. 5.3) Sea correction of the fragmentation functions $D^{\pm}_{M1,\,Sea\,Corr.}(z) = C_{Sea}(z)\,D^{\pm}_{M1}(z)$.

Monte Carlo Data:

- (Sec. 3.4.3) Determination of the generated fragmentation functions $D^{\pm}_{MC,\,Gen.}(z)$ according to Eq. 3.12.
- (Sec. 5.1) Extraction of the fragmentation functions $D^{\pm}_{MC,M1}(z)$ (Eq. 5.14).
- (Sec. 5.3) Determination of the sea correction factor $C_{Sea}(z)$ (Eq. 5.23).

The results for $D^{\pm}_{M1}(z)$ and $D^{\pm}_{M1,\,Sea\,Corr.}(z)$ are shown in Fig. 7.1. Due to the contribution of strange quarks, the sea correction for the unfavoured is clearly higher than for the favoured fragmentation function.

The pion Čerenkov threshold at 4 GeV leads to a minimum z of $z_{min} = 0.2$. The same momentum cutoff causes also the slow rise at $z > 0.2$: pions with fractional energies $z > 0.2$ but with momenta smaller than 4 GeV are not contributing and the fragmentation functions are thus decreasing towards low z. In the next section, after having discussed the fragmentation functions extracted with method (II), fragmentation functions from method (II) are presented which will also be corrected for these missing contributions. As it will be seen, the bending down towards lower z is vanishing in that case.

The ratio is not affected by this influence, since the ratio of unfavoured over favoured fragmentation function scales with energy and thus the influence of the lower limit in pion momenta cancels. The ratio will be discussed in more detail in Sec. 7.2.

7.1.2 Result from Method II

The results for the fragmentation functions for pions inside the HERMES acceptance, using extraction method (II), are presented in this section. No Monte Carlo simulation is involved in the extraction. However, the normalised pion spectra which are used are detector corrected as described in Sec. 7.1.

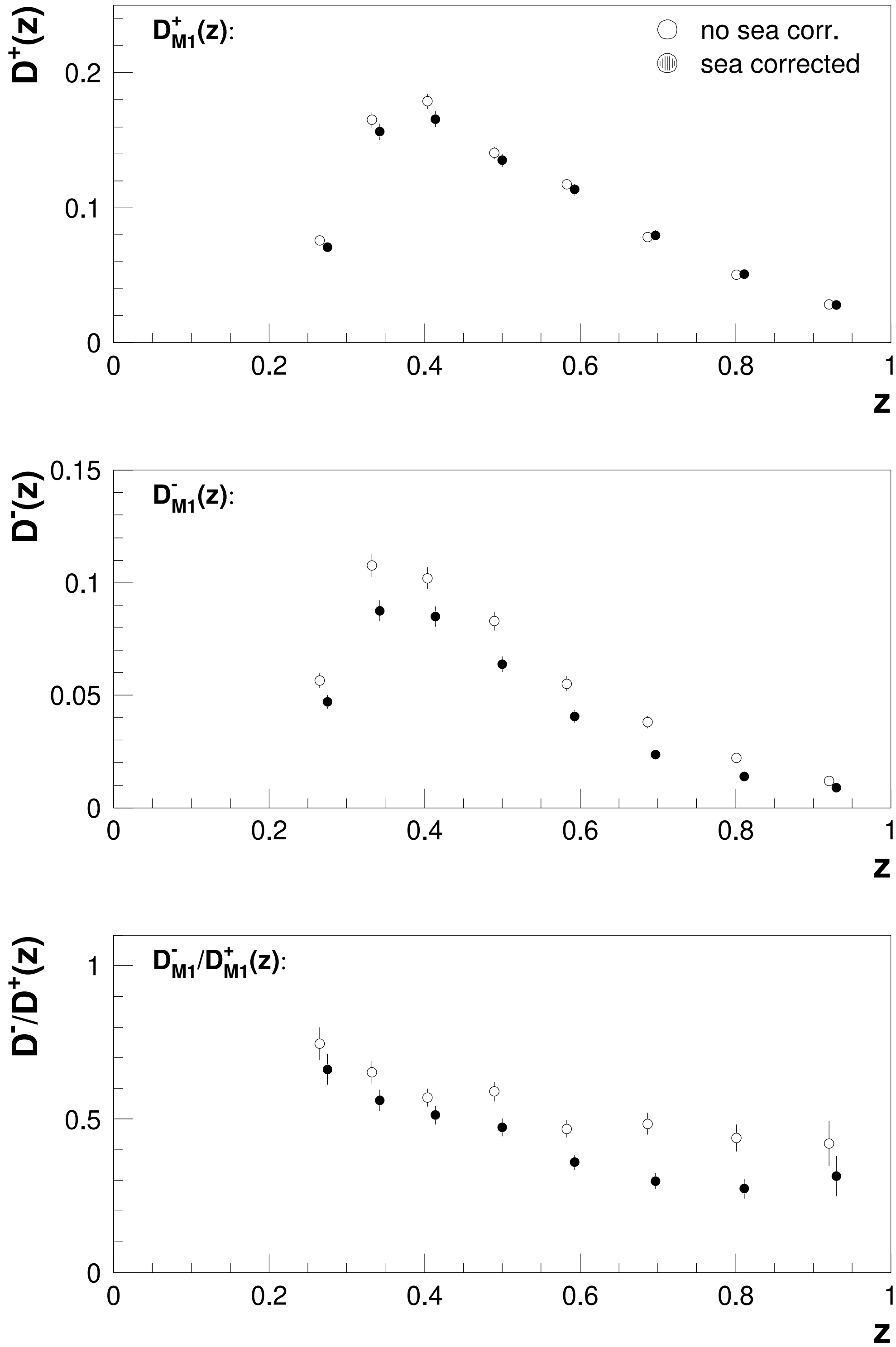

Figure 7.1: The pion fragmentation functions inside the HERMES acceptance, extracted by using Method (I). The impact of the sea correction is shown. $x > 0.15$ and $W^2 > 10$ GeV^2.

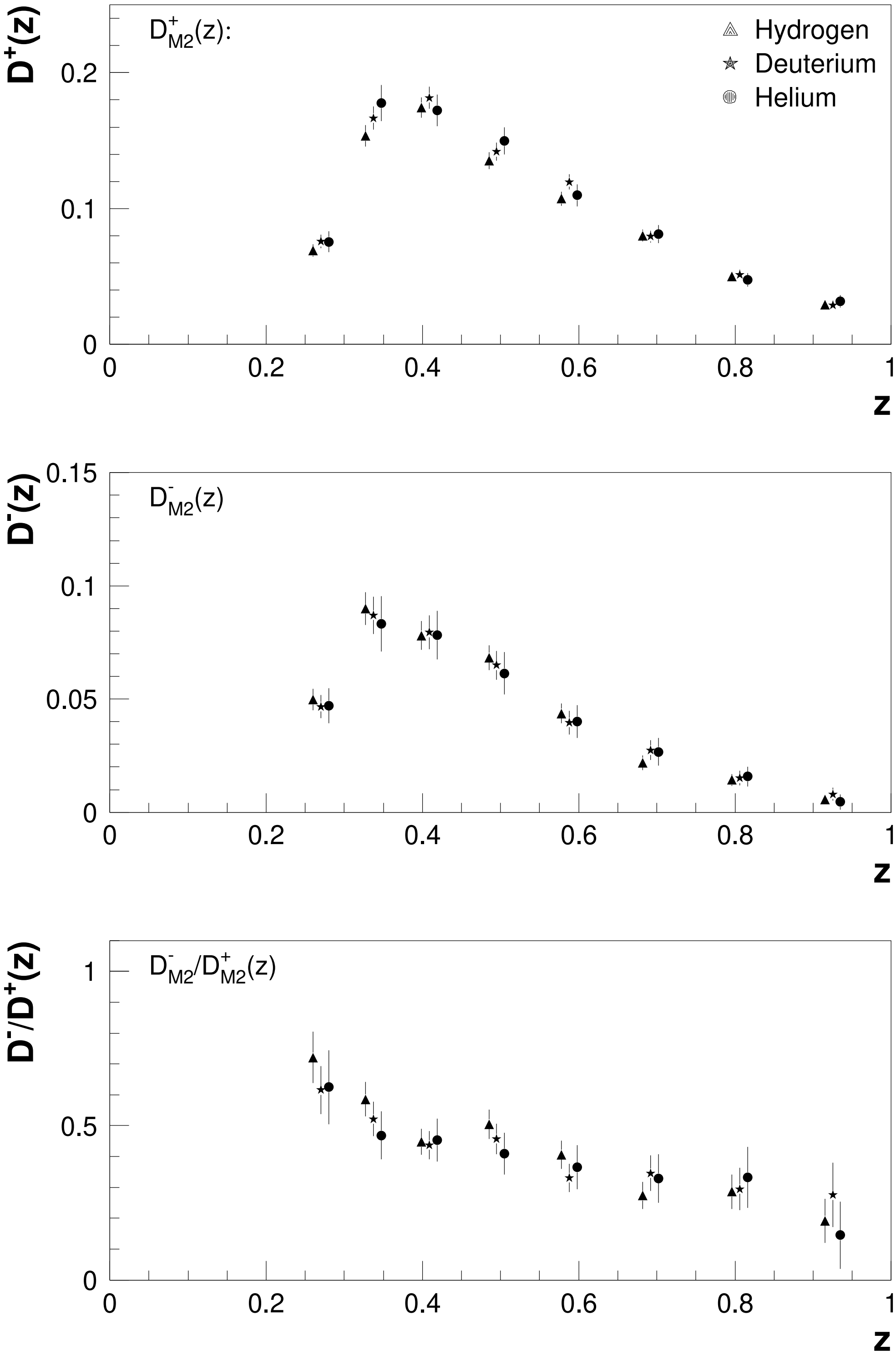

Figure 7.2: The pion fragmentation functions inside the HERMES acceptance, extracted using Method (II). The kinematic limits are the same as for method (I), i.e. $x > 0.15$ and $W^2 > 10$ GeV^2. The PDF parameterisation is from GRV, see text.

As in the previous section for method (I), the steps which have been undertaken to derive the results using method (II) are briefly summarised below. There are only two of them:

- (Sec. 5.2) Determine the elements of the matrix C_A at the mean value of x for all semi-inclusive events of targets $A \in \{H, D, {}^3He\}$ and for positive and negative pions separately. (Eq. 5.20-Eq. 5.22). The PDF used is from GRV [57].
- (Sec. 5.2) Multiplication of the normalized, corrected pion yields $N^{\pm}_{Det.Corr}$ with the matrix elements according to Eq. 5.18 to obtain the fragmentation functions $D^{\pm}_{M2}(z)$.

The results for the fragmentation functions extracted with method (II) are shown in Fig. 7.2 for different targets. With the statistics of the available data sample no systematic differences between the results for the various targets are observed. Thus the results of the different targets have been averaged and then compared to the first extraction method (see next section).

The impact of the momentum threshold in pion identification on the absolute pion fragmentation functions relative to the HERMES acceptance is shown in Fig. 7.3 and Fig. 7.4. The fragmentation functions marked with open circles would be measured, if all pions above 1 GeV were contributing with 100% efficiency. For this, a correction has been determined with the Monte Carlo which corrects for the pions below 4 GeV and above 13.5 GeV, which are scattered into the HERMES geometric acceptance but not reconstructed and/or identified as pions. For a comparison, the filled circles in Fig. 7.3 and Fig. 7.4 denote the fragmentation functions from pions between 4 and 13.5 GeV as in Fig. 7.2. Above $z \approx 0.5$, the fragmentation functions are approximately equal, while for the highest z bin a small deviation indicates the impact of the upper limit in pion momentum of 13.5 GeV due to the kaon Čerenkov threshold.

7.1.3 Comparison of Method I and Method II

The comparison of the two extraction methods for the favoured and unfavoured pion fragmentation functions is shown in Fig. 7.5. For the both the favoured fragmentation function, the unfavoured fragmentation function and the ratio, the sea corrected result from method (I) and the averaged result from method (II) are in agreement within the statistic errors.

For this comparison, the x range has been restricted to $x > 0.15$ to keep the sea correction small which is needed for method (I). It is however interesting to study the behaviour of the two methods at lower values of x as well. As the sea contribution increases towards low x, this will give a sensistive measure on the reliability of the sea quark correction.

In Fig. 7.6, the range in x has been expanded down to $x > 0.02$ which corresponds to the total available x-range of HERMES. It is seen that the fragmentation functions are

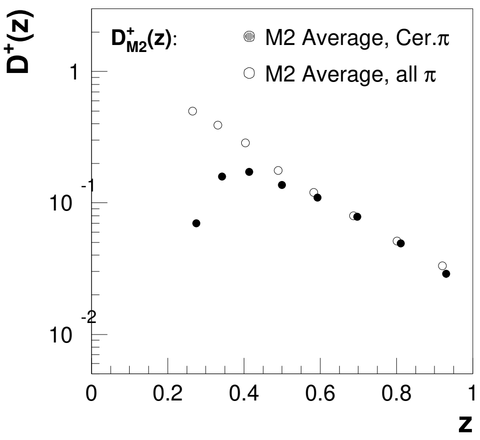

Figure 7.3: Favoured pion fragmentation function for all pions (open circles) compared to the fragmentation function from pions between 4 and 13.5 GeV (filled circles) as in Fig. 7.2.

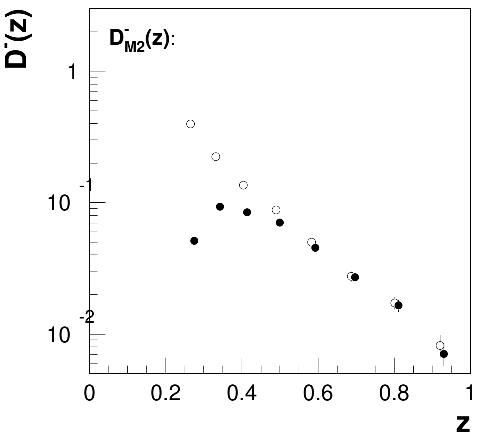

Figure 7.4: As in Fig. 7.3 but for the unfavoured fragmentation function.

no longer strongly bending down at low z. This can be understood by the correlation of x and z at small x as shown in Fig. 5.2: with decreasing x the average W^2 increases which causes a higher multiplicity and thus leads on average to more pions at low z. This affect is charge symmetric and the ratio is therefore not affected.

In the case of $x > 0.02$, the favoured fragmentation function as obtained with method (I) is always slightly larger than the result from method (II), for the unfavoured fragmentation functions this is true for $z < 0.7$. As far as the ratio is concerned, no systematic trend can be observed. As the sea quarks for these low values of x are dominating the cross-section and the sea correction is becoming large, this confirms the reliability of the sea correction for method (I).

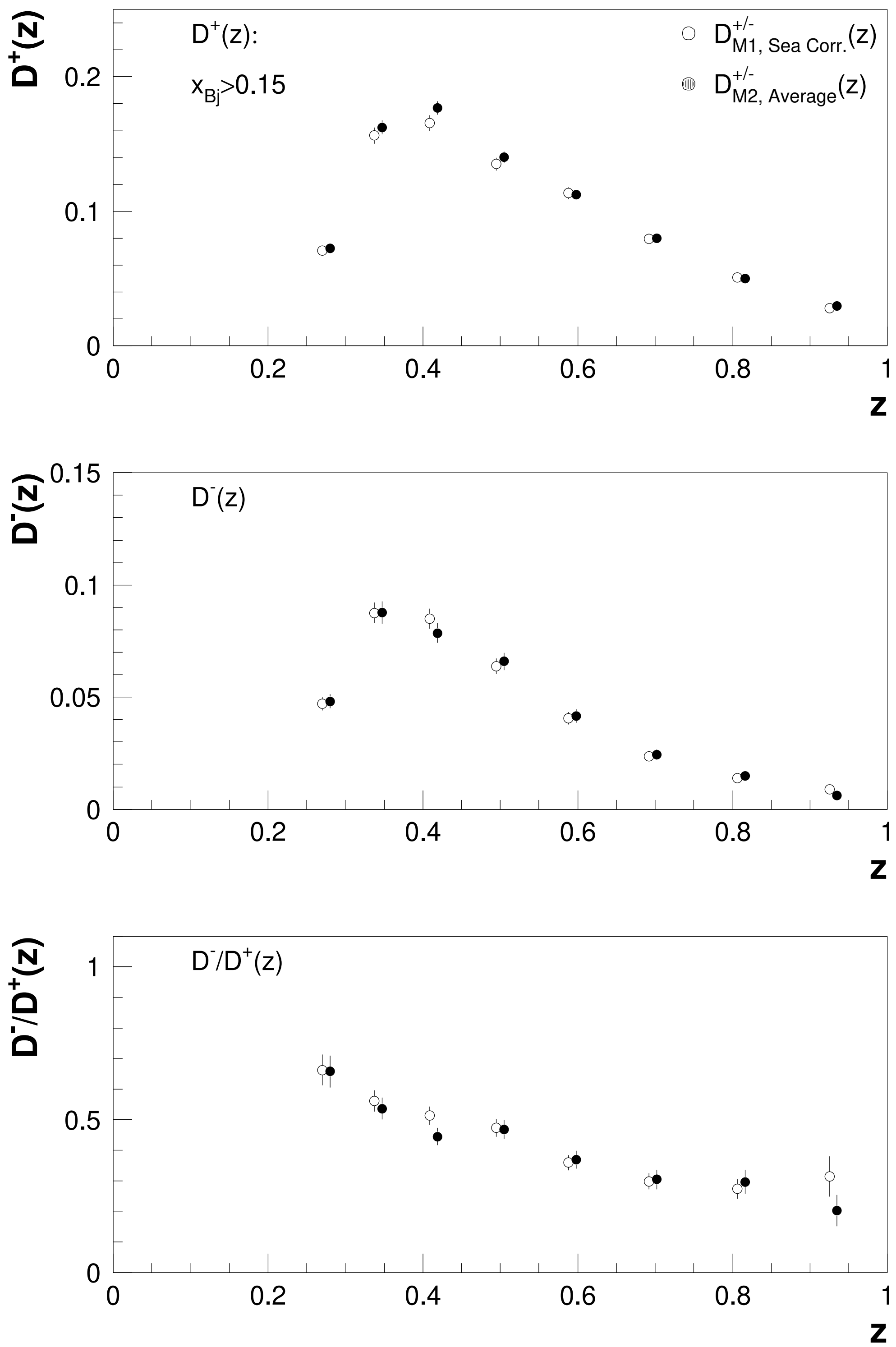

Figure 7.5: Comparison of the HERMES pion fragmentation functions from sea corrected method (I) and from method (II), for $x > 0.15$ and $W^2 > 10$ GeV^2.

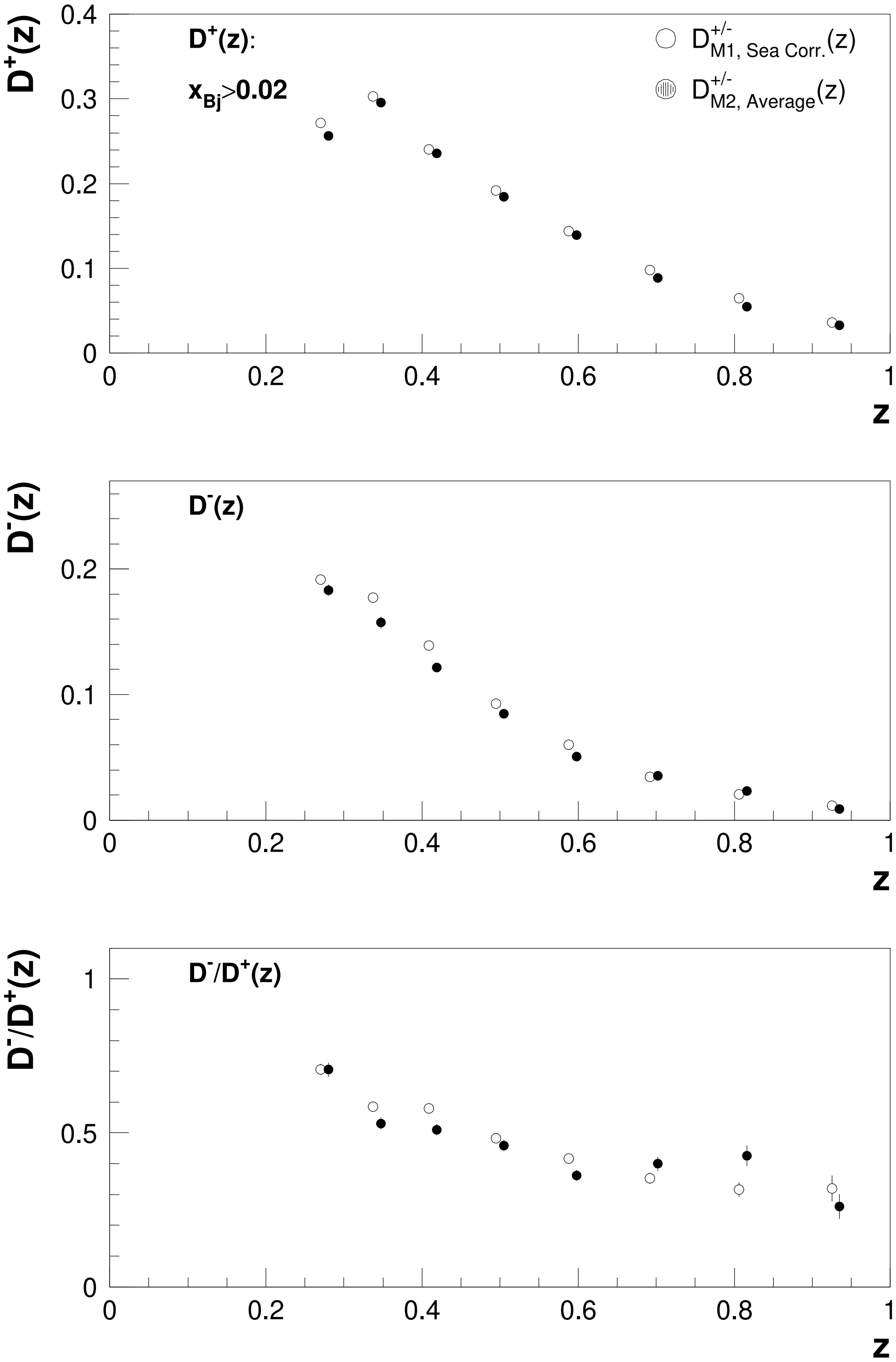

Figure 7.6: Comparison of the HERMES pion fragmentation functions from sea corrected method (I) and from method (II), for $x > 0.02$ and $W^2 > 10$ GeV^2.

7.1.4 Comparison to a Monte Carlo Simulation

For completeness, the extracted fragmentation functions are compared to the fragmentation functions as realised in the LUND string model of the HERMES Monte Carlo. Method (I) depends systematically on the fragmentation model as implemented in the Monte Carlo (this does of course not imply that the results of method (I) and the Monte Carlo are equal). A possible deviation to the fragmentation functions in the Monte is nevertheless best studied with the results from method (II) since method (II) is not using any Monte Carlo correction besides the detector correction.

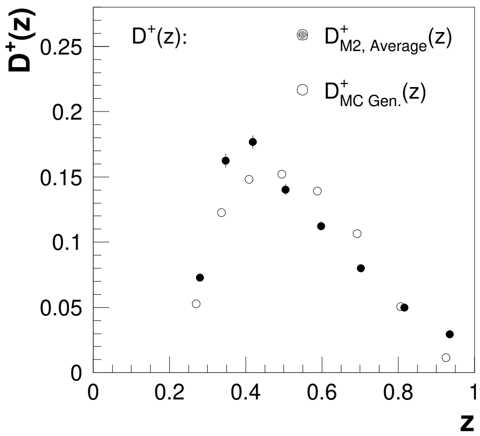

Figure 7.7: Comparison of the favoured fragmentation function extracted with method (II) to a Monte Carlo simulation.

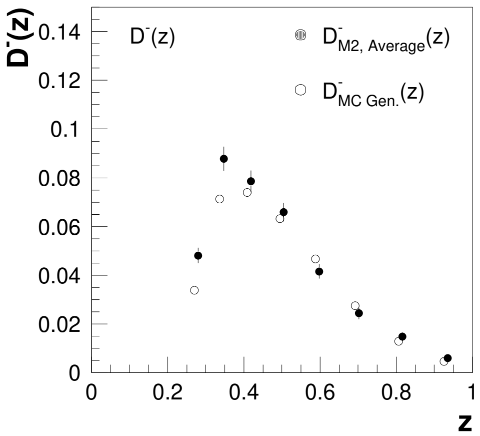

Figure 7.8: As in Fig. 7.7, but for the unfavoured fragmentation function.

The comparison of the favoured and unfavoured fragmentation functions is shown in Fig. 7.7 and Fig. 7.8, respectively (the ratio will be discussed in the next section). Significant deviations are observed. Remarkable is the large difference for both favoured and unfavoured fragmentation functions below $z = 0.4$, while the favoured fragmentation function disagrees also for higher z.

The detector correction influences the extracted result mostly via the assumed incorrect Čerenkov simulation. The deviations are however mostly caused by the description of the pion fragmentation in the Monte Carlo: The parameters of the fragmentation model have only be tuned to hadron spectra, that is the combined spectra for pions, kaons and protons, but not for pions separately (see Sec. 6.4.2). The pion spectra deviate largely for $z < 0.5$ as it could be seen in Fig. 6.10 which is caused by the fragmentation model.

7.2 The Fragmentation Function Ratio $D^-(z)/D^+(z)$ (HERMES Acceptance)

The fragmentation function ratio $D^-(z)/D^+(z)$ is especially interesting due to its independence from large detector and acceptance corrections. In addition, the consideration of energy conservation leads to the expectation for the ratio for independent fragmentation to tend from one at $z = 0$ to zero at $z = 1$. This has been discussed in Sec. 3.5.

The fragmentation function ratio is extracted from pion spectra inside the HERMES acceptance, since the systematic uncertainties from the 4π correction can be avoided in that case. An independent analysis [70] has shown that the result does not change when the full correction is applied which is expected.

In this section, the ratio of the unfavoured over the favoured fragmentation function as extracted from data is compared to this naïve expectation. The ratio is also compared to the Monte Carlo simulation and to the result from EMC. Then, its x-dependence is investigated. Finally, the impact of the rati oon the extraction of the light quark sea flavour asymmetry is shown.

7.2.1 Comparison to the Naïve Expectation

Comparing the ratio as already presented in Fig. 7.1 to the naïve expectation for independent fragmentation yields a situation as shown in Fig. 7.9. The ratios from both

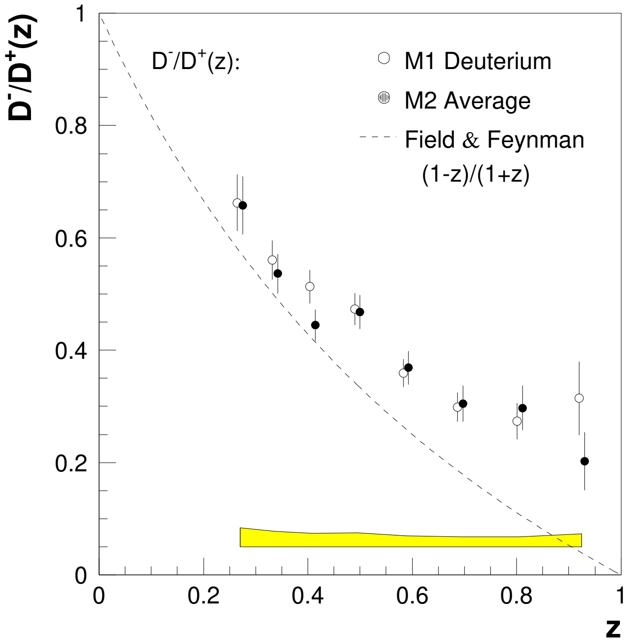

Figure 7.9: The ratio of unfavoured over favoured fragmentation function. The dashed line corresponds to a prediction from independent fragmentation [20] as given in Sec. 3.2.1. The error band denotes the systematic error as determined in Sec. 6.5 for method (II). It is approximately equal for both methods.

extraction methods lie significantly above the expectation for independent fragmentation over the entire z range. This deviation increases with z: the measured ratio

$D^-(z)/D^+(z)$ has a less steep z dependence and tends towards a value of ≈ 0.3. To understand this behaviour, pions originating from decays have been investigated using the Monte Carlo simulation. This attributes a tendency to the fragmentation function ratio to decrease less steeply. However, this does not hold at large z where only very vew pions are originating from decays.

7.2.2 Comparison to a Monte Carlo Simulation

The comparison of the extracted fragmentation function ratio $D^-(z)/D^+(z)$ to the Monte Carlo simulation is shown in Fig. 7.10. Since the result from method (I) includes the sea correction which is derived from the Monte Carlo simulation as well, only the result from method (II) is shown. Two characteristics are remarkable: First, in the

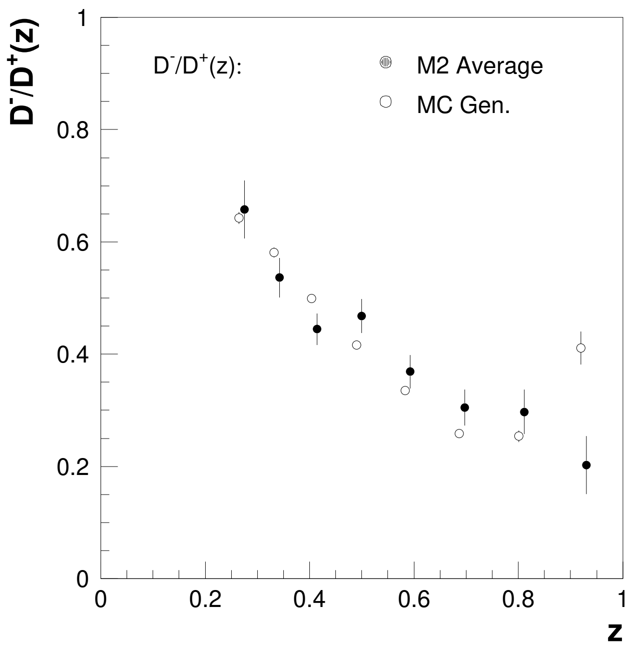

Figure 7.10: The ratio of unfavoured over favoured fragmentation function extracted using method (II) in comparison to a simulation from the Monte Carlo, based on the LUND model.

range $0.5 < z < 0.8$, the measured fragmentation function ratio is higher than the simulated ratio. This overhead might point, at least partly, to a deviating rate of decaying particles of the simulation compared to data as already mentioned in the previous section. Second, the significant increase of the simulated ratio in the last z bin does not describe the data. This increase at high z as simulated by string fragmentation in the Monte Carlo is not yet understood.

7.2.3 Comparison of the Ratio $D^-(z)/D^+(z)$ to EMC

The comparison of $D^-(z)/D^+(z)$ to the result from EMC [42] is shown in Fig. 7.11. Though the average value of Q^2 is 2.5 GeV^2 in the case of HERMES and 25 GeV^2 for the EMC result, the favoured and unfavoured fragmentation functions are expected to evolve similarly with Q^2 and thus a direct comparison of the ratios can be made.

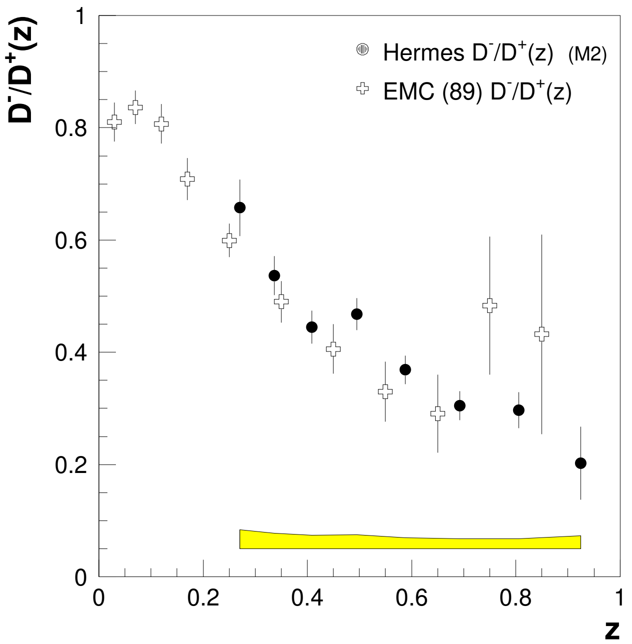

Figure 7.11: Comparison of the ratio of the unfavoured over the favoured pion fragmentation function as measured with HERMES to the result from the EMC [42]. The error band denotes the systematic error as determined in Sec. 6.5.

For almost the entire z range, the HERMES results from the second extraction method agrees within the errors with the EMC result. It is only slightly higher for the $z \approx 0.5$ which is not significant. In the previous section it could be seen that for intermediate z, the ratio as extracted from HERMES is also higher than naïvely expected, but also slightly higher than simulated. This has been explained with the contribution from decay products to the fragmentation functions. Since the fraction of pions from hadron decays are approximately the same in the case of HERMES and EMC [71, 72], this argument does not hold anymore.

7.2.4 The Dependence on x

The x-dependence of the ratio $D^-(z)/D^+(z)$ extracted with method (I) will be studied in this section. This behaviour is of particular interest, since the ratio is an important result of the fragmentation function analysis and is assumed to be x-independent. The detector correction for the ratio is expected to be x-independent as well, but the sea correction is x-dependent (Sec. 5.1). Since the realisation of the fragmentation process in the fragmentation model of the Monte Carlo is x-independent, the sea correction corrects only for the x-dependent neglect of sea quarks according to the extraction method. A possible x-dependence of the fragmentation process is not affected by the correction.

The x-dependence of fragmentation functions can be studied in performing the extraction for different "subranges" of x followed by an integration over z. Not only for the fragmentation function ratio, but also for the applied detector correction $C_{Det.Corr.}(z)$ and the sea correction $C_{Sea\,Corr.}(z)$ the x-dependence is studied in the described way. The results are shown in Fig. 7.12 and Fig. 7.13.

In the left plot of Fig. 7.12, the x-dependence of the detector correction for the charged pion ratio is shown. No x-dependence is observed which is expected since any dependence on the kinematics should cancel in performing the charge ratio. The x-dependence of the sea correction (Fig. 7.12, right plot) however decreases with decreasing x. This is caused by the rising contribution of sea quarks at small x: If the sea quarks are neglected, their contribution to the favoured and unfavoured fragmentation is averaged. The correction accounts for this averaging, i.e. reduces the unfavoured and increases the favoured fragmentation function. Therefore, the correction reduces the ratio at small x.

At higher values of x the sea correction should approach unity. According to Fig. 7.12 the correction still amounts to $\approx 10\%$ at $x = 0.3$. This is caused by the asymmetric contribution of the sea quarks to the fragmentation function ratio, where a relatively small amount of sea quarks leads to a significant contribution. In addition, the assumptions which lead to the extraction formula of method (I) like charge and isospin conjugation invariance are also considered in the correction.

As it can be seen in Fig. 7.13, the uncorrected fragmentation function ratio is x-dependent and the corrected ratio is independent of x. This confirms the reliability of the extraction method.

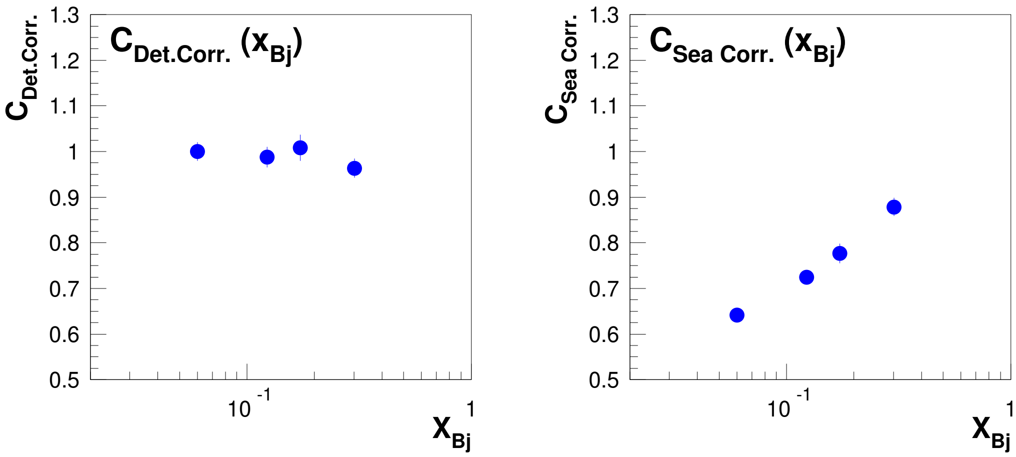

Figure 7.12: The x-depedence of the detector correction factor (left) and the correction factor which accounts for the neglected sea quark contribution (right) for the ratio of unfavoured over favoured pion fragmentation functions inside the HERMES acceptance, extracted using Method (I).

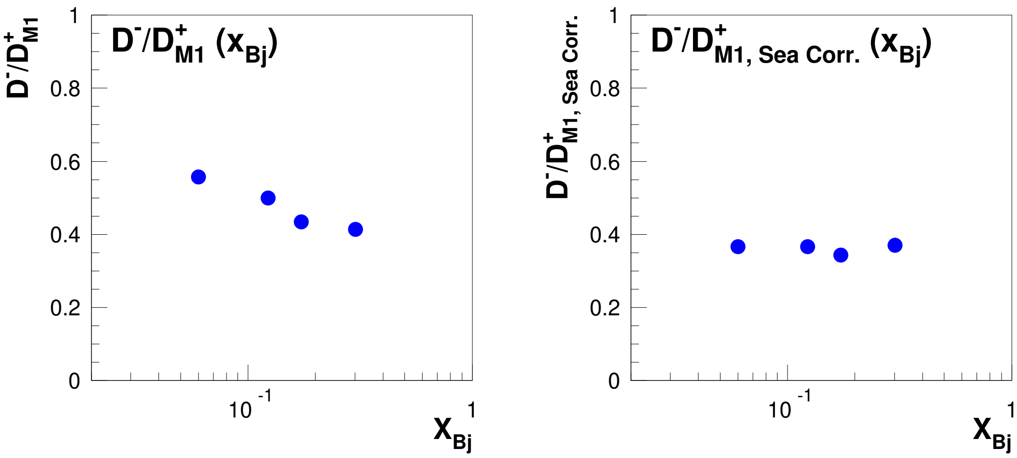

Figure 7.13: The x-depedence of the ratio of favoured over unfavoured pion fragmentation functions inside the HERMES acceptance, extracted using Method (I). The left plot shows the ratio without sea quark correction and the right plot the corrected ratio.

7.2.5 $D^-(z)/D^+(z)$ in the Extraction of the Sea Asymmetry

The light quark sea flavour asymmetry $(\bar{d}-\bar{u})/(u-d)$ can be extracted from semi-inclusive DIS by using the same formalism as for the extraction of fragmentation functions (see Sec. 2.5). However, the fragmentation function ratio $D^-(z)/D^+(z)$ has to be used (this corresponds to the usage of the PDFs when extracting fragmentation functions). The result should then become independent of z, assuming that factorisation holds. This is also a test for the fragmentation process at HERMES energies: The independence of z should occur by using the extracted result for $D^-(z)/D^+(z)$, in contrast to the usage of the ratio which is expected for independent fragmentation.

The extraction of the light quark sea asymmetry has been performed [73] using these two different fragmentation function ratios in comparison. In Fig. 7.14, the result based on the ratio as measured with HERMES is opposed to the result where the naïve expectation from independent fragmentation has been used. As it is seen, the

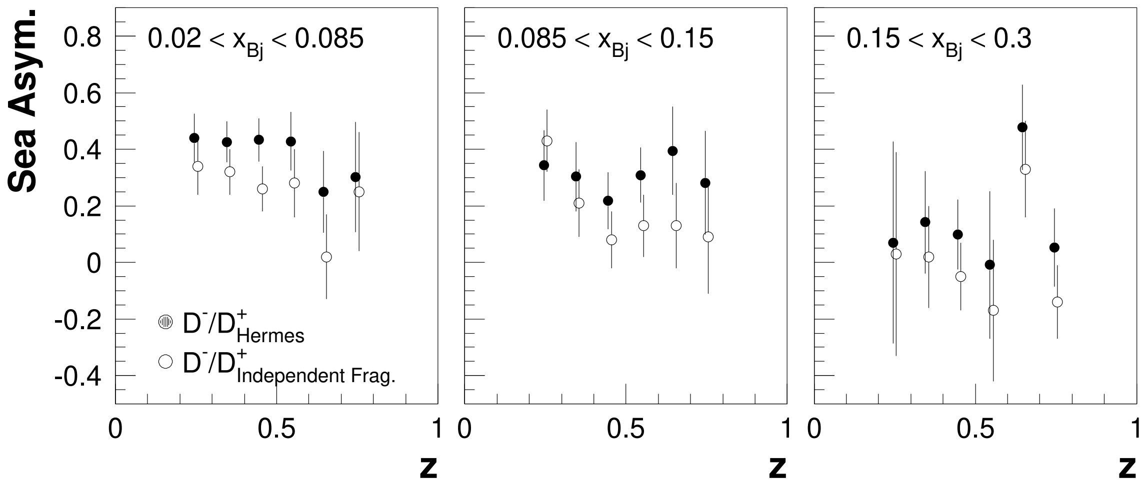

Figure 7.14: Light quark sea flavour asymmetry versus z for three different bins in x, from [73, 74]. The filled circles correspond to the result using the HERMES result for $D^-(z)/D^+(z)$, where the open circles denote the result where $D^-/D^+(z) = (1-z)/(1+z)$ is used.

extraction of a property $(N_p^- - N_p^+)/(N_n^- - N_n^+)$ (Eq. 2.14) leads to large statistic errors. However, the comparison of the χ^2-values of the results with a constant straight shows that the extracted fragmentation function ratio describes the fragmentation properties better than the naïve expectation: Using the HERMES result and the naïvely expected ratio, respectively, the $\chi^2/d.o.f.$ values are 0.37 (0.74), 0.23 (1.13) and 1.15 (1.11) for the three different x-bins.

This extraction of the light quark sea asymmetry leads also to a further extraction method for the fragmentation function ratio [75]: A simultaneous fit to the x- and z-dependence yields both the fragmentation function ratio and the asymmetry, if the asymmetry is required to be independent of z and the fragmentation function ratio accordingly independent of x. However, one bin of the result has to be fixed. The result for the ratio agrees within (large) errors [73] to the results extracted in this analysis.

7.3 The Pion Fragmentation Function (4π Acceptance)

The extraction of absolute fragmentation functions corrected for a 4π acceptance is the subject of this section. In contrast to the results of the previous sections where the fragmentation functions have been extracted inside the HERMES acceptance, here the measured pion spectra are corrected for the limited acceptance of the HERMES detector. The results thus appear as being measured with a detector with 4π acceptance. As for the previous results, the spectra are also corrected for detector effects.

The 4π acceptance correction does not only account for all pions above the Čerenkov threshold which are not measured with the spectrometer. It also includes a correction for all pions with momenta between 1 and 4 GeV and pions above 13.5 GeV. The pions with low momenta have a significant impact on the z distribution up to $z \approx 0.5$ and have to be included in the absolute fragmentation functions .

All results in this section are extracted with $x > 0.15$ and $W^2 > 16$ GeV^2. As already pointed out in Sec. 6.4.3, the results do not depend on the cut, but the corrections and hence the systematic errors are significantly smaller than those where $W^2 > 10$ GeV^2.

7.3.1 Result

The results for the 4π acceptance corrected fragmentation functions are shown in Fig. 7.15. The results obtained from both extraction methods are plotted and found to agree within the statistic errors. For the results from method (II), the differences between different targets are small and thus only the average values are shown.

The 4π correction is target independent. The differences between the results of method (II) on different targets are therefore the same as for the results of the fragmentation functions inside the HERMES acceptance. Only the sea correction for method (I) is slightly different between the HERMES to the 4π acceptance which is below 5%.

7.3.2 Comparison of the Sum $\frac{1}{2}(D^+ + D^-)$ to a Fit in NLO

The result for the sum $(1/2)(D^+(z) + D^-(z))$ of the 4π fragmentation functions is compared to a recent fit in NLO of fragmentation functions measured in e^+e^--annihilation [41]. In e^+e^--annihilation, only the average fragmentation function is measured instead of favoured and unfavoured fragmentation functions separately as in DIS. Therefore, the parameterisation has been compared to $(1/2)(D^+(z) + D^-(z))$. This is shown in Fig. 7.16.

Two characteristics are remarkable. First, at low z ($z \leq 0.4$), the average of the extracted fragmentation functions is significantly higher than the fit. A comparison to Fig. 3.6 where the same parameterisation is compared to the EMC result shows good agreement for $0.15 < z < 0.7$. This may point to a possible systematic influence of

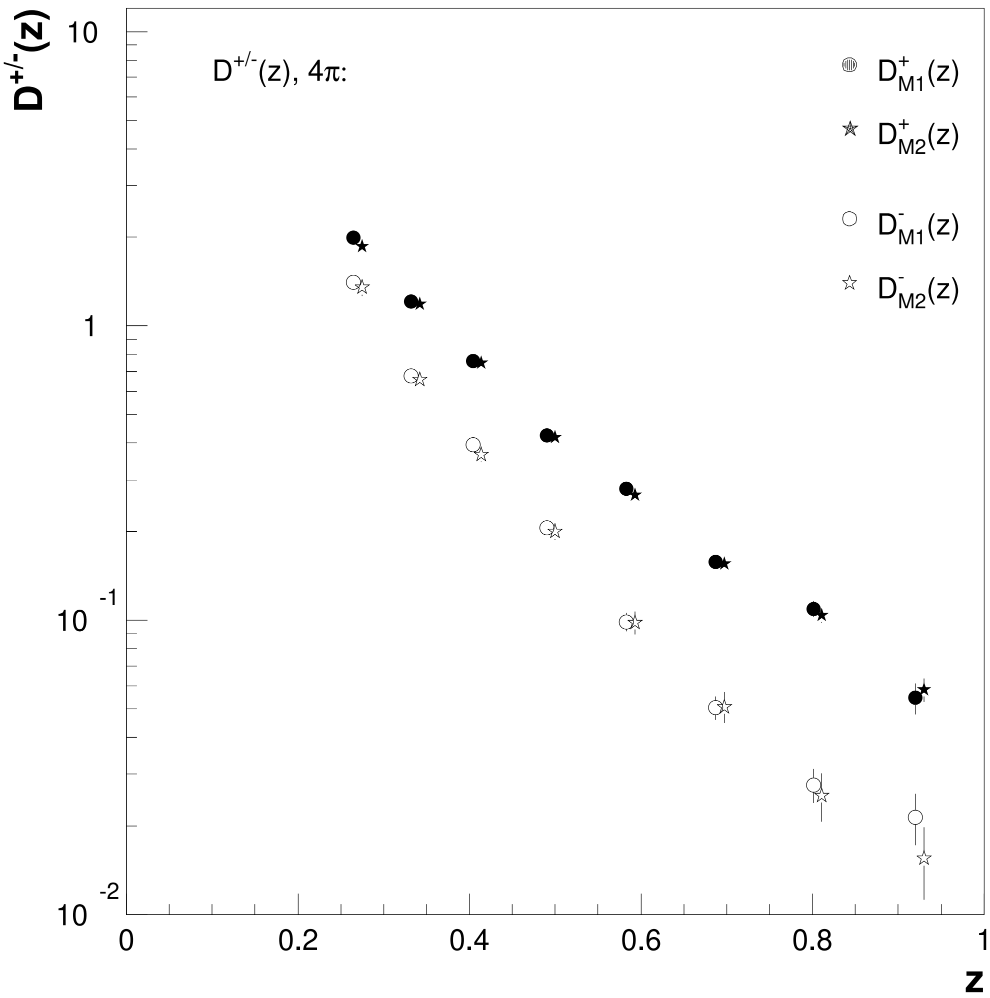

Figure 7.15: The favoured and unfavoured pion fragmentation functions in the 4π acceptance. Both results from method (I) and method (II) are shown. For method (II), the average of the results for the different targets is plotted. The kinematic limits are $x > 0.15$ and $W^2 > 16$ GeV^2.

the 4π correction or the Čerenkov digitisation as realised in the HERMES Monte Carlo program. If the pion rate for low momenta below the Čerenkov threshold as simulated by the Monte Carlo program is too high, this will lead to an over-correction of the pion spectra at low z. A too low Čerenkov efficiency in the Monte Carlo program will lead to a similar over-correction.

Second, also for $z \geq 0.75$ the average fragmentation function is larger than the fit. In Fig. 3.6 the result from the EMC has been compared to the same fit. It could be seen that for the high z range, the EMC result was also larger than the fit. Only a fraction of this difference could be explained by a deviation of the measured Q^2 values at high z from the average measured Q^2.

As far as the result extracted from HERMES data is concerned, the average Q^2 value

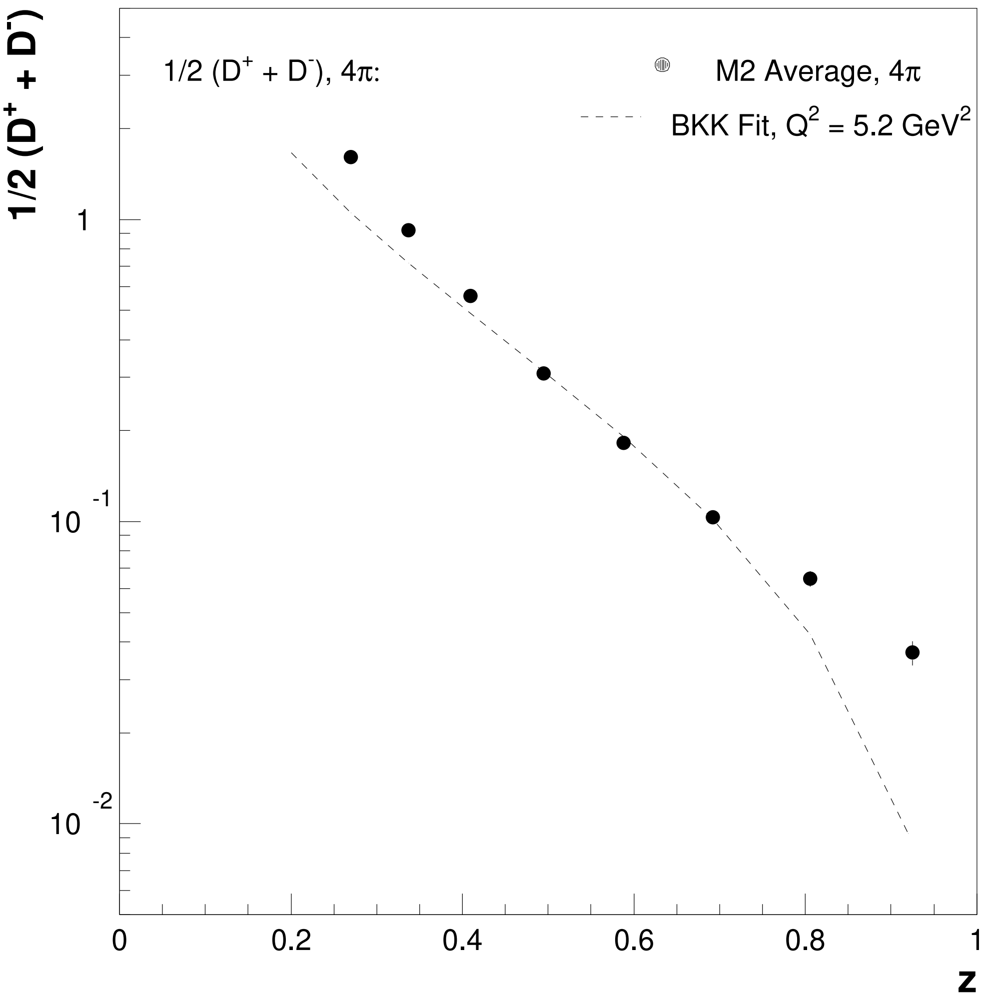

Figure 7.16: The average of favoured and unfavoured pion fragmentation functions in the 4π acceptance. Both results from method (I) and method (II) are shown. The dashed line corresponds to a recent parameterisation [41], which is evolved in NLO to $Q^2 = 5.2$ GeV^2. The kinematic limits are $x > 0.15$ and $W^2 > 16$ GeV^2.

of 5.2 GeV^2 is approximately independent of z. The difference between the extracted 4π fragmentation functions and the fit at high z could therefore have similar reasons than the difference between the EMC result and the fit. A comparison of the 4π corrected result from HERMES and from the EMC will elucidate this assertion. This is done in the next section.

7.3.3 Comparison to EMC

As the extracted fragmentation functions as presented above are corrected for a 4π acceptance, they can be compared to the results from the EMC. However, in contrast to the fragmentation function ratio, the absolute fragmentation functions have to be evolved to the same Q^2 in order to be compared consistently.

To evolve the extracted result to the average Q^2 of the EMC result, the EMC average value of Q^2 which depends on z has to be taken. These values are mentioned explicitly in the first of two publications on that subject [43] but not in the second one [42] which is used for this comparison. In the latter analysis, different kinematic selection criteria have been applied. The z-dependence of the average Q^2 in [42] has thus been estimated. The impact of the different Q^2 values on the evolution factor which is applied to the HERMES fragmentation functions is however small (see Fig. 7.17). The

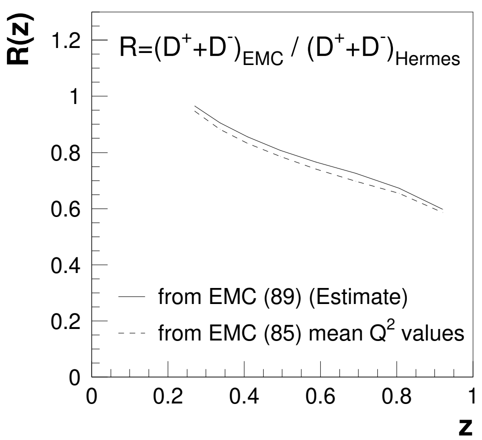

Figure 7.17: Evolution factor to the HERMES fragmentation functions, evolved to the average Q^2 of the EMC result. The dashed line corresponds to the values given in [43], while the full line is based on an estimate of the average Q^2 in [42].

comparison of the average fragmentation functions from the EMC and from HERMES (4π corrected) is shown in Fig. 7.18. In order to illustrate the impact of the evolution, also the HERMES result without the evolution to the average Q^2 of the EMC result is plotted. As presumed in the previous section, the average fragmentation function is similar to the EMC result for $z > 0.4$. At high z, both measurements differ from the parameterisation [41]. For $z < 0.4$, the result measured with HERMES differs from both the EMC result and from the parameterisation in a similar way. As already pointed out in the previous section, this could be explained by an inaccurate 4π or detector correction to the measured HERMES spectra.

The comparison of the favoured and unfavoured fragmentation functions to the EMC results is presented in Fig. 7.19. Both fragmentation functions show good agreement for $z \geq 0.4$. At smaller z, both the favoured and unfavoured fragmentation functions are larger than the result of the EMC. The deviation is larger for the unfavoured fragmentation function.

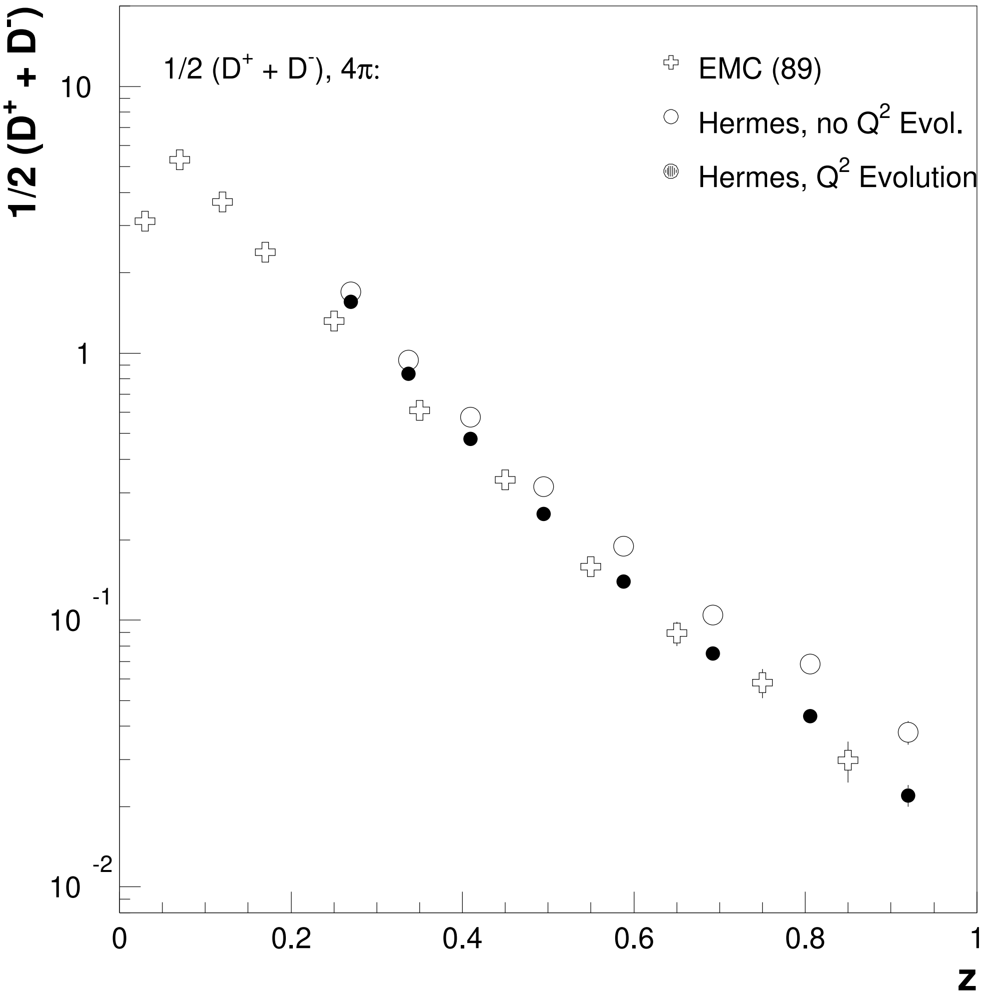

Figure 7.18: The sum of favoured and unfavoured pion fragmentation functions in the 4π acceptance is compared to the result from the EM Collaboration, without (open circles) and with (filled circles) an evolution of the HERMES data points to the specific mean Q^2 of the EMC result at each z value. The kinematic limits (HERMES) are $x > 0.15$ and $W^2 > 16$ GeV^2, the mean Q^2 of the EMC result is $\langle Q^2 \rangle = 25$ GeV^2.

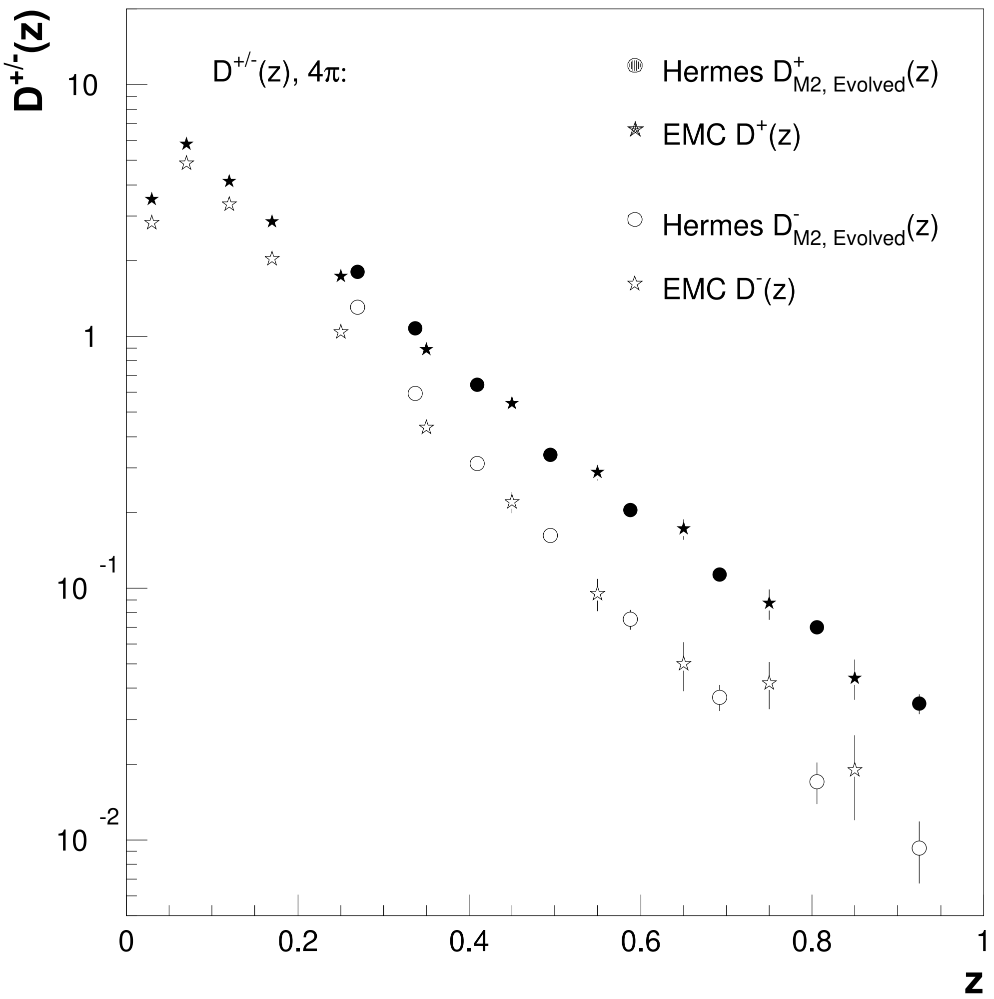

Figure 7.19: The favoured and unfavoured pion fragmentation functions in the 4π acceptance are compared to the result from the EMC. The results from HERMES are evolved to the mean Q^2 of the EMC result. The kinematic limits (HERMES) are $x > 0.15$ and $W^2 > 16$ GeV^2, the mean Q^2 of the EMC result is $\langle Q^2 \rangle = 25$ GeV^2.

7.3.4 Comparison to a Monte Carlo Simulation

For completeness, the extracted fragmentation functions will be compared to the simulation with the LUND model. In Fig. 7.20 the favoured and unfavoured fragmentation functions are shown for the 4π corrected result and the simulation.

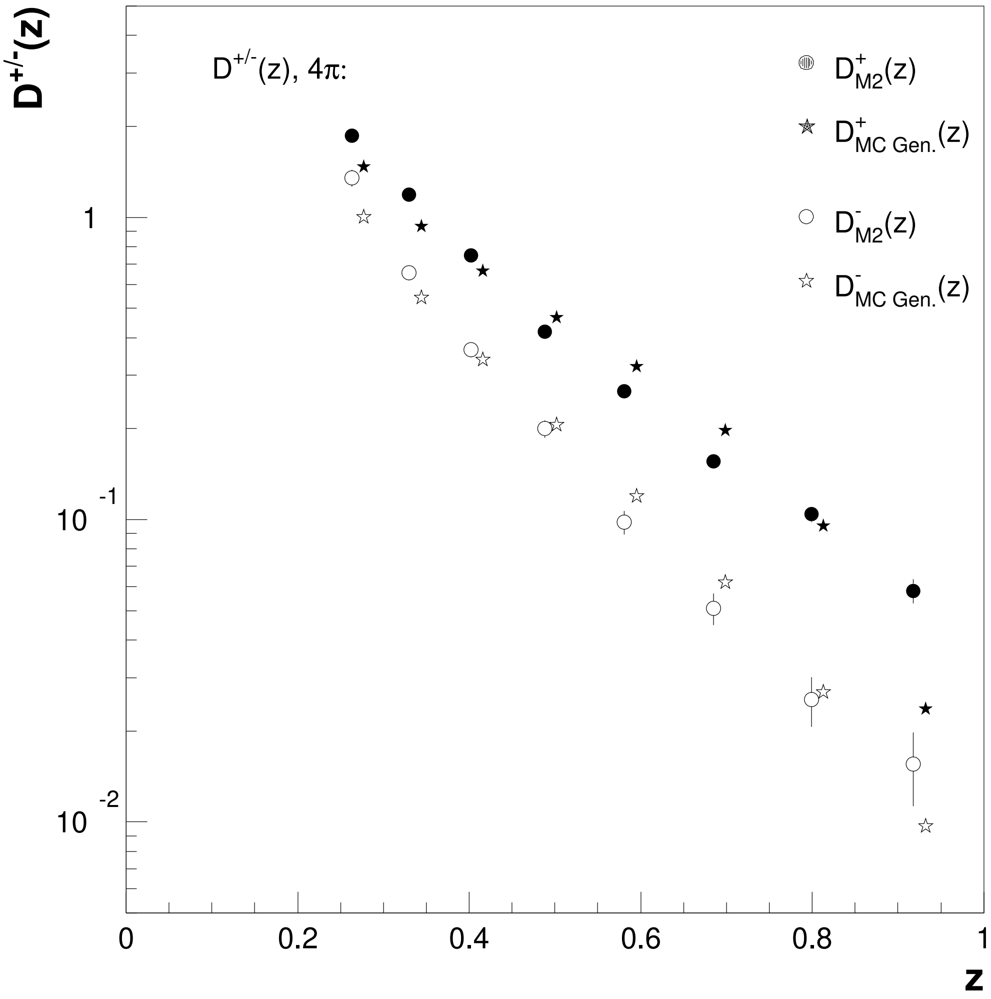

Figure 7.20: The favoured and unfavoured pion fragmentation functions in the 4π acceptance, compared to a simulation of the Monte Carlo based on the LUND model. The results are obtained by using method (II).

The extracted fragmentation functions deviate from the simulation over the entire z range. At small and at large z, the extracted fragmentation functions are larger than the simulation, while at intermediate z they are smaller. The deviations at low z have also been observed in the comparisons to a parameterisation [41] (Fig. 7.16) and to the result from the EMC [42] (Fig. 7.19). At high values of z the extracted fragmentation functions are larger than the simulation. This has been observed in the comparison to the parameterisation as well, but not in the comparison to the result from the EMC. The parameterisation has been performed to data from e^+e^--annihilation experiments. Also the LUND model has been created mostly in comparisons to hadron spectra from e^+e^--annihilation. A possible explanation might therefore be a difference of the DIS fragmentation process and the fragmentation in e^+e^--annihilation at high z.

The comparisons to fragmentation functions as simulated with independent fragmentation or with the Cluster model are not performed at this place because neither of them sufficiently describe the hadronic spectra measured with HERMES. Originally developped for higher energies, the tuning of the appropriate parameters of the fragmentation models failed. This has been interpreted as an indication that these models cannot be used to describe the spectra measured with HERMES.

8 Conclusion

In this analysis, the fragmentation functions of light quarks into charged pions as measured in semi-inclusive deep-inelastic scattering at HERMES have been extracted. In particular, the ratio of the unfavoured over the favoured fragmentation function which only weakly depends on detector effects has been determined for pions identified at HERMES, that is for pions with momenta between 4 and 13.5 GeV. Additionally, the measured favoured and unfavoured fragmentation functions have been corrected for the limited acceptance of the HERMES detector and compared to the results of other experiments.

For all results, the measured normalised pion spectra are corrected for detector effects using a Monte Carlo technique. The correction factor is ≈ 1.9 at the lowest fractional energies $z = 0.2$ and decreases to ≈ 1.4 at $z \approx 0.8$. The correction on the charge pion ratio N^{π^+}/N^{π^-}, important for the extraction of the ratio of unfavoured over favoured fragmentation functions, is small ($< 5\%$). A systematic error of the detector correction of $\approx 5\%$ has been estimated by comparing the corrections obtained from two different Monte Carlo fragmentation models.

Two different extraction methods have been used to determine the fragmentation functions from the measured pion spectra. Both methods are based on the quark-parton model formula of pion production in semi-inclusive deep-inelastic scattering. The first method exploits the x-independence of the expression for the fragmentation functions in case of a deuterium target, if the contribution of sea quarks is neglected. The necessary correction is determined with a Monte Carlo simulation resulting into a large systematic error in the fragmentation functions of ($\approx 15\%$).

The second extraction method relies on the knowledge of the quark density functions and allows the determination of the fragmentation functions from any target. The results obtained on hydrogen, deuterium and ^{3}Helium agree within the errors. The systematic error originating from the uncertainties in the parton density functions was estimated to be about 2.5%.

Special emphasis is put on the ratio of the unfavoured over the favoured fragmentation functions since it only depends on the charge pion ratio where detector and acceptance effects mostly cancel. The corrections and hence the systematic errors are small. In contrast to the naïve expectation for independent fragmentation, the extracted ratio does not decrease to zero as $z \to 1$, but decreases less steeply to a constant value of about 0.25 at high z. This behaviour is in agreement with a result of the European Muon Collaboration (EMC).

Finally, the measured pion spectra have been corrected for the limited acceptance of the HERMES detector. The correction factor to the pion spectra decreases from a large value of 20 at $z = 0.2$ to a value of 2 at $z \approx 0.8$. The corresponding systematic error has been obtained by comparing the corrections determined from two different fragmentation models. It has been estimated to 100% at $z = 0.2$ decreasing to about 5% for $z > 0.4$. The large uncertainty at low z accounts for the uncertainty in the description of the hadron spectra at low momenta where the present HERMES detector does not allow to separate pions from kaons and protons. From these acceptance corrected pion spectra the fragmentation functions have been extracted and compared to other measurements. First, the sum of the favoured and the unfavoured fragmentation functions has been compared to a next-to-leading order parameterisation of the pion fragmentation functions measured in e^+e^--annihilation, evolved to the Q^2 values of the HERMES result. At low values of z this fragmentation function measured at HERMES is higher than the parameterisation. This discrepancy is most probably due to an incorrect description of the pion spectra at low momenta in the present HERMES Monte Carlo simulation. For $0.4 < z < 0.7$ the result extracted from the HERMES data agrees well with the parameterisation while at high values of z, the result is again significantly higher than the parameterisation. This deviation at high z can not be attributed to any problem in the description of the HERMES detector.

Second, a comparison with the favoured and unfavoured fragmentation functions measured by EMC has been performed, where the HERMES result has been evolved to the Q^2 values of the EMC result. Good agreememt between the fragmentation functions of EMC and the HERMES results is observed for $z > 0.4$. Consequently, the EMC result for the sum of the favoured and the unfavoured fragmentation function also disagrees to the parameterisation in the high z range in the same way as the HERMES result. This might thus be interpreted as a deviation of the fragmentation properties measured in e^+e^--annihilation and in deep-inelastic scattering.

A Table of Results

	z	$D^+(z)$	$D^-(z)$	$D^-(z)/D^+(z)$
M1 (D)	0.270	$0.071 \pm 0.003 \pm 0.013$	$0.047 \pm 0.003 \pm 0.009$	$0.662 \pm 0.050 \pm 0.034$
	0.337	$0.156 \pm 0.006 \pm 0.026$	$0.088 \pm 0.005 \pm 0.016$	$0.561 \pm 0.035 \pm 0.029$
	0.409	$0.166 \pm 0.006 \pm 0.027$	$0.085 \pm 0.004 \pm 0.015$	$0.513 \pm 0.030 \pm 0.028$
	0.495	$0.135 \pm 0.005 \pm 0.022$	$0.064 \pm 0.004 \pm 0.012$	$0.473 \pm 0.029 \pm 0.025$
	0.588	$0.114 \pm 0.004 \pm 0.019$	$0.041 \pm 0.003 \pm 0.487$	$0.359 \pm 0.025 \pm 0.719$
	0.692	$0.079 \pm 0.004 \pm 0.013$	$0.024 \pm 0.002 \pm 0.284$	$0.299 \pm 0.026 \pm 0.598$
	0.806	$0.051 \pm 0.003 \pm 0.638$	$0.014 \pm 0.002 \pm 0.167$	$0.274 \pm 0.032 \pm 0.548$
	0.925	$0.028 \pm 0.003 \pm 0.351$	$0.009 \pm 0.002 \pm 0.123$	$0.314 \pm 0.065 \pm 0.035$
M2 (Average)	0.270	$0.073 \pm 0.003 \pm 0.010$	$0.048 \pm 0.003 \pm 0.006$	$0.658 \pm 0.052 \pm 0.034$
	0.337	$0.162 \pm 0.005 \pm 0.018$	$0.088 \pm 0.005 \pm 0.010$	$0.536 \pm 0.035 \pm 0.027$
	0.409	$0.177 \pm 0.005 \pm 0.020$	$0.079 \pm 0.004 \pm 0.009$	$0.445 \pm 0.028 \pm 0.024$
	0.495	$0.140 \pm 0.004 \pm 0.016$	$0.066 \pm 0.004 \pm 0.008$	$0.468 \pm 0.031 \pm 0.025$
	0.588	$0.112 \pm 0.004 \pm 0.012$	$0.042 \pm 0.003 \pm 0.005$	$0.369 \pm 0.030 \pm 0.020$
	0.692	$0.080 \pm 0.003 \pm 0.009$	$0.024 \pm 0.002 \pm 0.003$	$0.305 \pm 0.032 \pm 0.018$
	0.806	$0.050 \pm 0.002 \pm 0.007$	$0.015 \pm 0.002 \pm 0.002$	$0.297 \pm 0.040 \pm 0.018$
	0.925	$0.029 \pm 0.002 \pm 0.005$	$0.006 \pm 0.001 \pm 0.001$	$0.202 \pm 0.052 \pm 0.023$

Table A.1: Extracted fragmentation functions $D^+(z)$, $D^-(z)$ and $D^-(z)/D^+(z)$ for two different extraction methods, relative to the HERMES acceptance. The result of method (I) is sea corrected. The errors are statistic and systematic error, respectively.

	z	$D^+(z)$	$D^-(z)$
M1 (D)	0.270	$1.998 \pm 0.089 \pm 2.030$	$1.404 \pm 0.080 \pm 1.432$
	0.337	$1.208 \pm 0.043 \pm 0.423$	$0.677 \pm 0.034 \pm 0.363$
	0.409	$0.758 \pm 0.026 \pm 0.142$	$0.394 \pm 0.020 \pm 0.078$
	0.495	$0.424 \pm 0.016 \pm 0.079$	$0.207 \pm 0.012 \pm 0.043$
	0.588	$0.279 \pm 0.011 \pm 0.052$	$0.099 \pm 0.007 \pm 1.186$
	0.692	$0.158 \pm 0.008 \pm 0.030$	$0.050 \pm 0.005 \pm 0.606$
	0.806	$0.109 \pm 0.007 \pm 1.366$	$0.028 \pm 0.004 \pm 0.331$
	0.925	$0.054 \pm 0.007 \pm 0.681$	$0.021 \pm 0.004 \pm 0.300$
M2 (Average)	0.270	$1.866 \pm 0.081 \pm 1.883$	$1.350 \pm 0.084 \pm 1.364$
	0.337	$1.187 \pm 0.039 \pm 0.389$	$0.656 \pm 0.037 \pm 0.340$
	0.409	$0.748 \pm 0.023 \pm 0.106$	$0.366 \pm 0.021 \pm 0.052$
	0.495	$0.418 \pm 0.014 \pm 0.059$	$0.200 \pm 0.013 \pm 0.031$
	0.588	$0.266 \pm 0.010 \pm 0.038$	$0.098 \pm 0.009 \pm 0.015$
	0.692	$0.156 \pm 0.007 \pm 0.022$	$0.051 \pm 0.006 \pm 0.008$
	0.806	$0.104 \pm 0.006 \pm 0.016$	$0.025 \pm 0.005 \pm 0.004$
	0.925	$0.058 \pm 0.005 \pm 0.010$	$0.016 \pm 0.004 \pm 0.002$

Table A.2: Extracted fragmentation functions $D^+(z)$, $D^-(z)$ and $D^-(z)/D^+(z)$ for two different extraction methods, relative to the 4π acceptance. The result of method (I) is sea corrected.

Glossary

The most frequent abbreviations are expanded below, regardless their familiarity:

DIS	Deep-Indelastic Scattering
EMC	European Muon Collaboration
LO	Calculation in leading order of α_S
LPHD	Local Parton-Hadron-Duality
NLO	Calculation in next-to-leading order of α_S
PDF	Parton Density Function
PID	Particle Identification
QCD	Quantum Chromodynamics, field theory of the quarks and gluons
QED	Quantum Electrodynamics, field theory of electromagnetism
QPM	Quark-Parton Model
TRD	Transition Radiation Detector

The most frequent symbols used in this analysis are the following:

$(1/N_e)\, N^{\pm}_{ind}(z)$	The normalized pion yield, where $N^{\pm} \equiv \mathrm{d}N^{\pi^{\pm}}/\mathrm{d}z$, and	
where ind:	*Meas.*:	measured
	Det. Corr.:	measured and detector corrected
	4π *Corr.*:	4π acceptance corrected
	Gen.:	generated from Monte Carlo
	Rec.:	generated and reconstructed from Monte Carlo
$D^{\pm}_{ind1\, ind2}(z)$	The favoured (+) and unfavoured (−) pion fragmentation function,	
where $ind1$:	*M1*:	extracted from reconstructed spectra (method I)
	M1 Sea Corr.:	as *M1*, but corrected for the sea quark contribution
	M2:	extracted from reconstructed spectra (method II)
	M2 Average:	as *M2*, but the average of the fragmentation functions for all different target materials
	Gen.:	generated, i.e. as realised in the fragmentation model of the Monte Carlo
and $ind2$:	*Hermes*:	refers to fragmentation functions inside the HERMES acceptance
	4π:	refers to the unlimited 4π acceptance
$D^{\pi}(z)$	The average pion fragmentation function $D^{\pi}(z) = \frac{1}{2}(D^{+}(z) + D^{-}(z))$	
$D^{s}(z)$	The strange quark fragmentation function	
$C^{\pm}_{Det.Corr.}(z)$	The detector correction factor for the measured pion spectra	
$C^{\pm}_{4\pi}(z)$	The detector and acceptance correction factor for the measured pion spectra	
$C^{\pm}_{Sea}(z)$	The sea correction factor for the fragmentation functions extracted using method (I)	

References

[1] M. Anselmino, A. Efremov, and E. Leader. The Theory and Phenomenology of Polarized Deep-Inelastic Scattering. *Phys. Rep.*, **261** (1995) 1.

[2] F.E. Close. *An Introduction to Quarks and Partons*. Academic Press Inc., London, 1979.

[3] European Muon Collaboration. A Measurement of the Spin Asymmetry and Determination of the Structure Function g_1 in Deep-Inelastic Muon-Proton Scattering. *Phys. Lett.*, **B 206** (1988) 364.

[4] E143 Collaboration, K. Abe, et al. Measurement of the Q^2-Dependence of the Proton and the Deuteron Spin Structure Function g_1^p and g_1^d. *Phys. Lett.*, **B 364** (1995) 61.

[5] J.P. Nassalski. Spin Structure of the Nucleon. In *Proc. of XXVII Conf. on High Energy Physics*, Warsaw, Poland, 1996.

[6] J. Ellis and M. Karlinger. Nucleon Spin. In *Workshop on Deep-Inelastic Scattering and QCD (DIS 95)*, edited by J.F. Laporte and Y. Sirois, page 573, Paris, France, 1995.

[7] J.D. Bjorken. Inelastic Scattering of Polarized Leptons from Polarized Nucleons. *Phys. Rev.*, **D 1** (1970) 1376.

[8] J. Ellis and R. Jaffe. Sum Rule for Deep-Inelastic Electroproduction from Polarized Protons. *Phys. Rev.*, **D 9** (1974) 1444.

[9] M. Dueren. The HERMES Experiment: From the Design to the First Results. Habilitation thesis, Universität Erlangen, 1995.

[10] M. Strikman. Probing Polarized Nucleon Structure in Semi-Inclusive Deep-Inelastic Processes. In *Proc. of Symp. on the Internal Spin Structure of the Nucleon*, page 153, 1994.

[11] NM Collaboration, M. Arneodo, et al. Measurement of the u Valence Quark Distribution Function in the Proton and u Quark Fragmentation Function. *Nucl. Phys.*, **B 321** (1989) 541.

[12] A. Brüll. Die Strukturfunktionen des Nukleons und die Gottfried-Summe. Habilitation thesis, Ruprechts-Karls-Universität Heidelberg, 1995.

[13] R.D. Ball and S. Forte. Anomalous Evolution of the Gottfried Sum Rule. *Nucl. Phys.*, **B 425** (1994) 516.

[14] Y.L. Dockshitzer et al. *Basics of Perturbative QCD.* Editions Frontières, Gif-sur-Yvette, France, 1991.

[15] K. Gottfried and V.F. Weisskopf. *Concepts of Particle Physics*, volume II. Oxford University Press, New York, 1986.

[16] I.G. Knowles et al. QCD Event Generators. In *Proc. Workshop on Physics at LEP2*, edited by G. Altarelli, T. Sjöstrand, and F. Zwirner, page 103, CERN, Geneva, Switzerland, 1996.

[17] J. Binnewies. *Fragmentation Functions in Next-To-Leading Order QCD.* PhD thesis, Universität Hamburg, 1997.

[18] B.R. Webber. Hadronization. *hep-ph/9411384*, (1994).

[19] Y.I. Azimov, Y.L. Dockshitzer, et al. Similarity of Parton and Hadron Spectra in QCD Jets. *Z. Phys.*, **C 27** (1985) 65.

[20] R.D. Field and R.P. Feynman. A Parameterization of the Properties of Quark Jets. *Nucl. Phys.*, **B 136** (1978) 1.

[21] EM Collaboration, M. Arneodo, et al. Quark and Diquark Fragmentation into Neutral Strange Particles as Observed in Muon-Proton Interactions at 280 GeV. *Phys. Lett.*, **B 145** (1984) 458.

[22] T. Sjöstrand. High Energy Physics Event Generation with PYTHIA 5.7 and JETSET 7.4. *Comp. Phys. Comm.*, **82** (1994) 74.

[23] B. Andersson, G. Gustafson, et al. Parton Fragmentation and String Dynamics. *Phys. Rep.*, **97** (1983) 31.

[24] OPAL Collaboration, M.Z. Akrawy, et al. A Measurement of Global Event Shape Distributions in the Hadronic Decays of the Z^0. *Z. Phys.*, **C 45** (1990) 505.

[25] B. Andersson, G. Gustafson, et al. On High Energy Leptoproduction. *Z. Phys.*, **C 9** (1981) 233.

[26] J.W. Gary. *Tests of Models for Parton Fragmentation in e^+e^--Annihilation.* PhD thesis, Lawrence Berkely Laboratory (1985), University of California, 1985.

[27] G. Marchesi and B.R. Webber. HERWIG - *A Monte Carlo Generator for Simulating Hadron Emission Reactions with Interfering Gluons*, 1996. see also [28].

[28] G. Marchesi, B.R. Webber, et al. HERWIG 5.1 - a Monte Carlo Event Generator for Simulating Hadron Emission Reactions with Interfering Gluons. *Comp. Phys. Comm.*, **67** (1992) 465.

[29] P. Renton and W.S.C. Williams. Hadron Production in Lepton-Nucleon Scattering. *Annu. Rev. Nucl. Part. Sci.*, (1981) 193.

[30] EM Collaboration, M. Arneodo, et al. Charge and Transverse Momentum Correlations in DIS. *Z. Phys.*, **C 31** (1986) 333.

[31] EM Collaboration, M. Arneodo, et al. *CERN-EP/86-119*, (1985).

[32] EM Collaboration, J.J. Aubert, et al. Measurement of the Q^2, x and W^2 Dependence of Single Hadron Production in Deep-Inelastic Scattering. *Phys. Lett.*, **B 114** (1982) 373.

[33] R. Baier and K. Fey. Finite Corrections to Quark Fragmentation Functions in Perturbative QCD. *Z. Phys.*, **C 2** (1979) 339.

[34] S. Rolli. Fragmentation Functions Approach in pQCD Fragmentation Phenomena. *hep-ph/9607480*, (1996).

[35] J. Binnewies, B.A. Kniehl, and G. Kramer. NLO Fragmentation Functions for Pions and Kaons. *Z. Phys.*, **C 65** (1995) 471.

[36] TPC Collaboration, H. Aihara, et al. Charged-Hadron Inclusive Cross Sections and Fractions in e^+e^--Annihilation at $\sqrt{s} = 29$ GeV. *Phys. Rev. Lett.*, **61** (1988) 1263.

[37] ALEPH Collaboration, D. Buskulic, et al. Inclusive $\pi^\pm$, $K^\pm$ and $(p\bar{p})$ Differential Cross-Sections at the Z-Resonance. *Z. Phys.*, **C 66** (1995) 355.

[38] V.N. Gribov and L.N.Lipatov. Deep-Inelastic Scattering in Perturbation Theory. *Sov. J. Nucl. Phys.*, **15** (1972) 438.

[39] G. Altarelli and G. Parisi. Asymptotic Freedom in Parton Language. *Nucl. Phys.*, **B 126** (1977) 298.

[40] Y.L. Dockshitzer. Calculation of Structure Functions of Deep-Inelastic Scattering and e^+e^--Annihilation by Perturbative Theory in Quantum Chromodynamics. *Sov. Phys. JETP*, **46** (1977) 641.

[41] J. Binnewies, B.A. Kniehl, and G. Kramer. Pion and Kaon Production in e^+e^- and ep Collisions at NLO. *Phys. Rev.*, **D 52** (1995) 4947.

[42] EM Collaboration, M. Arneodo, et al. Measurements of the u-Valence-Quark Distribution Function in the Proton and u-Quark Fragmentation Functions. *Nucl. Phys.*, **B 321** (1989) 541.

[43] EM Collaboration, J.J. Aubert, et al. A Determination of the Fragmentation Functions of u-Quarks into Charged Pions. *Phys. Lett.*, **B 160** (1985) 417.

[44] E665 Collaboration, M.R. Adams, et al. Scaled Energy (z) Distributions of Charged Hadrons Observed in Deep-Inelastic Muon Scattering at 490 GeV from Xenon and Deuterium Targets. *Phys. Rev.*, **D 50** (1994) 1836.

[45] J. van Hunen. Private Communication.

[46] ALEPH Collaboration, G. Cowan, et al. Measurement of Scaling Violations in e^+e^--Annihilation. In *Proc. 27th. Int. Conf. on High Energy Physics*, volume 2, page 883, Glasgow, Scotland, 1994.

[47] TASSO Collaboration, M. Althoff, et al. Jet Production and Fragmentation in e^+e^--Annihilation at 12-43 GeV. *Z. Phys.*, **C 22** (1984) 307.

[48] HERMES Collaboration, K. Ackerstaff, et al. The HERMES Spectrometer, 1997. Submitted to Nucl. Instr. Meth.

[49] HERMES Collaboration, K. Ackerstaff, et al. Measurement of the Neutron Spin Structure Function g_1^n with a Polarized ^{3}He Internal Target. *Phys. Lett.*, **B 404** (1997) 383.

[50] R.L. Jaffe. Polarized Lambdas in the Current Fragmentation Region. *Phys. Rev.*, **D 54** (1996) 6581.

[51] S.F. Pate et al. The HERMES Polarized Internal Gas Target. In *Int. Workshop on Polarized Beams and Polarized Gas Targets*, page 39, London, 1996.

[52] B. Braun. Polarization of the HERMES Hydrogen Target. In *Proc. Conf. SPIN96*, Amsterdam/NL, 1996.

[53] W. Wander. *Rekonstruktion Hochenergetischer Streuereignisse bei* HERMES. PhD thesis, Universität Erlangen, Germany, 1996.

[54] HERMES Collaboration, K. Coulter, et al. Proposal, 1990. DESY PRC 90/01.

[55] HERMES Collaboration, K. Coulter, et al. Technical Design Report, 1993. DESY PRC 93/06.

[56] A.D. Martin, R.G. Roberts, and W.J. Stirling. Parton Distributions of the Proton. *Phys. Rev.*, **D 50** (1994) 6734.

[57] M. Glück, E. Reya, and A. Vogt. Dynamical Parton Distributions of the Proton and Small-x Physics. *Z. Phys.*, **C 67** (1995) 433.

[58] CTEQ Collaboration. Fourth Version of the CTEQ Parton Distribution Functions. *MSUHEP-60426, CTEQ-604*, (1996).

[59] H. Plothow-Besch. The Parton Distribution Function Library. *Int. J. Mod. Phys.*, **A 10** (1995) 2901.

[60] Programming Techniques Group. *ADAMO - An Entity-Relationship Programming System, Version 3.3.* ECP Division, CERN, Geneva, 1994.

[61] W. Wander et al. DAD - Distributed Adamo Database System at HERMES. In *Proc. of CHEP 95*, Rio de Janeiro, 1995.

[62] R. Kaiser. *Measurement of the Spin Structure of the Neutron using Polarised Deep-Inelastic Scattering.* PhD thesis, Simon Fraser University, Vancouver, Canada, 1997.

[63] E.L. Berger. Semi-Inclusive Inelastic Electron Scattering from Nuclei, 1987. ANL-HEP-PR-87-45.

[64] *The* HERMES *Monte Carlo documentation.* http://dxnhd1.mpi-hd.mpg.de/~herprod.

[65] G. Ingelman, A. Edin, and J. Rathsman. Lepto 6.5 - A Monte Carlo Generator for Deep-Inelastic Lepton Nucleon Scattering. *Comp. Phys. Comm.*, **101** (1997) 108.

[66] CERN Application Software Group. *GEANT - Detector Description and Simulation Tool.* CERN, Geneva, 1994.

[67] H. Tallini. *Extraction of Polarized Parton Distributions at* HERMES. PhD thesis, University of Liverpool, 1997.

[68] T.V. Kukhto and N.M. Shumeiko. Radiative Effects in Deep-Inelastic Scattering of Polarized Leptons by Polarized Nucleons. *Nucl. Phys.*, **B 219** (1983) 412.

[69] I.V. Akushevich and N.M. Shumeiko. Radiative Effects in Deep-Inelastic Scattering of Polarized Leptons by Polarized Light Nuclei. *J. Phys.*, **G 20** (1994) 513.

[70] J. Ouyang. HERMES Charged Pion Fragmentation Functions. HERMES *Internal Note*, **97-047** (1997).

[71] EM Collaboration, J.J. Aubert, et al. ρ^0 Production in Deep-Inelastic μ-p-Interactions. *Phys. Lett.*, **B 133** (1983) 370.

[72] H1 Collaboration, T. Carli, et al. Hadronic Final State in Deep-Inelastic Scattering at HERA. *hep-ph/9701395*, (1997).

[73] M. Vincter. Extraction of the Light Quark Sea Asymmetry from Pions Using the 1996 Unpolarized Data. HERMES *Internal Note*, **97-037** (1997).

[74] M. Vincter. Private Communication.

[75] M. Düren and M. Vincter. Extraction of the Flavor Asymmetry of the Light Quark Sea and of Fragmentation Function Ratios. HERMES *Internal Note*, **97-30** (1997).

Acknowledgements

It is a pleasure to thank Priv.-Doz. Antje Brüll for her support during the preparation of this thesis, for her critical spirit in attacking problems and her strong desire to understand and solve them all.

Thanks to Prof. Bogdan Povh for the possibility to work in his group at the Max-Planck-Institut.

I thank Prof. Otto Nachtmann for his efforts in correcting and valuating this thesis. I also thank him, Prof. Franz Eisele and Prof. Malte Faber in participating at the examination committee.

I want to express my special thanks to the collegues and friends of the working group at the Max-Planck-Institut. I am especially endebted to Dr. Christian Büscher who read the manuscript with great care and gave numerous critical suggestions. I highly estimate his precision, not only during the correction work but also during the last years by assisting in computer problems: they can always be either solved, or are bugs in the operating system (for which he certainly found a workaround already years ago).

I thank Dr. Eva Wittmann and Dr. Oliver Thilmann cordially for their friendship and support, the guys from the SELEX group for the humour they brought into the group, an essential prerequisite to meet the daily challenges in research. I also thank Priv.-Doz. Josef Pochodzalla, the FNC group, that is Thomas Nunnemann, Dr. Douglas Jansen and Dr. Ralf Todenhagen and the WA89 group for many helps, suggestions and discussions. Especially the heartpiece of our group, Claudia Schröder shall be mentioned at this place: Always helpful for all daily needs in organisation and always goodhumoured! Thanks!

The special flair in the HERMES collaboration was the basis for the motivation to this work, so I want to thank all collaborators for their contribution to this special spririt which renders pure work into the pursuit of an idea. Many thanks also to the spokesmen Prof. Richard Milner and Prof. Ed Kinney to make this idea conceivable. Of course, the "heart" of the collaboration, our secretaries Sabine Krohn and Ramona Matthes are playing a central rôle here!

Special thanks to my collaborators Dr. Holger Ihssen, Eric Volk, Marc-André Funk and Dr. Wolfgang Wander for the fruitful discussions and their assistance in acquiring the basics in attacking problems in research. I also want to thank Hugh Tallini, Wieland Hoprich, Dr. Manuella Vincter, Prof. Naomi Makins, Dr. Jin Ouyang, Dr. Ralph Kaiser and Prof. Michael Dueren for discussions and their help in case of questions. Many thanks to all collegues and friends of the collaboration!

I wish to thank also Prof. B. Kopeliovich, Prof. Hans Jürgen Pirner, Prof. Gunnar Ingelmann, Prof. Pete Mulders, Prof. Bryan Webber and Prof. Torbjörn Sjöstrand for their suggestions and assistance during this work.

I thank cordially Clint Cavanaugh and Benni von Heynitz for their help during the last corrections!

Meinen lieben Eltern Sissy und Günter seien an dieser Stelle umarmt für alles, was sie mir mit auf den Weg gegeben haben. Ihr steht mir immer zur Seite und setzt Euch für mich ein, dafür danke ich Euch ganz besonders.

Aber ohne Dich, liebe Constanze, wäre diese Arbeit Stückwerk. Danke Dir, daß Du mir den Rücken stärkst.